High order positivity-preserving discontinuous Galerkin schemes for radiative transfer equations on triangular meshes ☆

Min Zhang [a], Juan Cheng [b,c], Jianxian Qiu [d,*]

[a] *School of Mathematical Sciences, Xiamen University, Xiamen, Fujian 361005, PR China*
[b] *Laboratory of Computational Physics, Institute of Applied Physics and Computational Mathematics, Beijing 100088, PR China*
[c] *Center for Applied Physics and Technology, Peking University, Beijing 100871, PR China*
[d] *School of Mathematical Sciences and Fujian Provincial Key Laboratory of Mathematical Modeling and High-Performance Scientific Computing, Xiamen University, Xiamen, Fujian 361005, PR China*

ARTICLE INFO

ABSTRACT

It is an important and challenging issue for the numerical solution of radiative transfer equations to maintain both high order accuracy and positivity. For the two-dimensional radiative transfer equations, Ling et al. give a counterexample (Ling et al. (2018) [13]) showing that unmodulated discontinuous Galerkin (DG) solver based either on the P^k or Q^k polynomial spaces could generate negative cell averages even if the inflow boundary value and the source term are both positive (and, for time dependent problems, also a nonnegative initial condition). Therefore the positivity-preserving frameworks in Zhang and Shu (2010) [28] and Zhang et al. (2012) [29] which are based on the value of cell averages being positive cannot be directly used to obtain a high order conservative positivity-preserving DG scheme for the radiative transfer equations neither on rectangular meshes nor on triangular meshes. In Yuan et al. (2016) [26], when the cell average of DG schemes is negative, a rotational positivity-preserving limiter is constructed which could keep high order accuracy and positivity in the one-dimensional radiative transfer equations with P^k polynomials and could be straightforwardly extended to two-dimensional radiative transfer equations on rectangular meshes with Q^k polynomials (tensor product polynomials). This paper presents an extension of the idea of the above mentioned one-dimensional rotational positivity-preserving limiter algorithm to two-dimensional high order positivity-preserving DG schemes for solving steady and unsteady radiative transfer equations on triangular meshes with P^k polynomials. The extension of this method is conceptually plausible but highly nontrivial. We first focus on finding a special quadrature rule on a triangle which should satisfy some conditions. The most important one is that the quadrature points can be arranged on several line segments, on which we can use the one-dimensional rotational positivity-preserving limiter. Since the number of the quadrature points is larger than the number of basis functions of P^k polynomial space, we determine a k-th polynomial by a L_2-norm Least Square subject to its cell average being equal to the weighted average of the values on the quadrature points after using the rotational positivity-preserving limiter. Since the weights used here are the quadrature weights which are positive, then the cell average of the modified polynomial is nonnegative. And the final modified polynomial can be obtained by using the two-dimensional scaling positivity-preserving limiter on the triangular element. We theoretically prove that our rotational positivity-preserving

* Corresponding author.
E-mail addresses: minzhang2015@stu.xmu.edu.cn (M. Zhang), cheng_juan@iapcm.ac.cn (J. Cheng), jxqiu@xmu.edu.cn (J. Qiu).

limiter on triangular meshes could keep both high order accuracy and positivity. It is relatively simple to implement, and also does not affect convergence to weak solutions. The numerical results validate the high order accuracy and the positivity-preserving properties of our schemes. The advantage of the triangular meshes on handling complex domain is also presented in our numerical examples.

1. Introduction

The radiative transfer equation (RTE) describes the interaction of radiation with scattering and absorbing media, which has wide applications in the areas such as heat transfer, stellar atmospheres, optical molecular imaging, inertial confinement fusion, infrared and visible light in space and the atmosphere, and so on.

The RTE can be described as a hyperbolic-type integro-differential equation with six independent variables including three spatial variables, two solid angle variables and time. Due to the presence of complicated integral coupling term and the high dimension of the problem, it is a serious challenge to develop effective numerical methods for RTE, the topic of which attracted much attention in the past half century. The numerical methods used to solve this equations today include the discrete-ordinate method (DOM) [5], the Monte Carlo method (MCM) [9], the spherical harmonics method (SHM) [11], the finite volume method (FVM) [23], the finite element method (FEM) [24], the spectral method [30], and so on [8,20]. Among them, the DOM is widely applied to numerically solving the transport equation due to its relatively high accuracy, flexibility, and relatively low computational cost. The DOM uses a numerical integration rule to discretize the solid angle. The angle-discretized radiative transfer equation is then a system of linear hyperbolic equations coupled with a numerical integral term.

The discontinuous Galerkin (DG) method is known to be a particularly powerful numerical tool for the simulation of hyperbolic transport problems. Spatial DG finite element techniques applied to the radiative transfer equation have been pioneered by Reed and Hill [22] and theoretically studied in [12] by Lesaint and Raviart. Later, Cockburn and Shu extended it to nonlinear hyperbolic conservation laws [1–4], in which the authors have established a framework to easily solve nonlinear time dependent problems, such as the Euler equations, using explicit nonlinearly stable high order Runge-Kutta time discretizations and DG discretization in space described above. DG methods have the advantages of high order accuracy, geometric flexibility, suitability for handling h- and p-adaptivity, extremely local data structure, high parallel efficiency, and a good theoretical foundation for stability and error estimates. Over the last few decades, DG methods have been used widely in many areas of computational physics and computational engineering. In this paper, we will combine the discrete-ordinate method with the discontinuous Galerkin (DG) method to solve the radiative transfer equations on triangular meshes.

Physically and mathematically, the solution to the radiative transfer equation is non-negative, however this property is often lost in numerical approximations for a nonnegative source term and boundary condition (and, for time dependent problems, also a nonnegative initial condition), especially for high order methods. Especially in multidimensional problems, a negative solution in the numerical simulation may slow the convergence rate of the iterative processes, even lead to a failure in the simulation, and for time dependent problems, a negative solution may cause numerical instabilities. Furthermore, negative radiative intensity is non-physical which is difficult for physicists to accept. Several studies have been proposed to obtain positive intensities. The step scheme is proved to be positivity-preserving but is only first order accurate and introduces excessive numerical smearing [6]. The diamond scheme has second order accuracy, but negative intensities may appear [14]. And there are some other existing positivity-preserving schemes including the variable-weight scheme [10,19], the linear exponential discontinuous finite element method [25], step and linear adaptive methods [18], the step characteristic scheme [16], the linear characteristic scheme [15], and the linear DG finite element method with the set-to-zero fix-up technique [17]. These methods are only first or second order accurate, or use non-polynomial nonlinear procedures which require iterative procedures to obtain the solution even for the system inside each cell, or rely on the characteristic procedure and hence are difficult to generalize to multi-dimensions.

This paper focuses on the positivity-preserving property of the high order accuracy DG schemes for the two-dimensional radiative transfer equations on triangular meshes. In [27], Zhang and Shu have established a general framework to construct arbitrarily high order accurate DG schemes satisfying a strict maximum principle for one- and two-dimensional scalar conservation laws on rectangular meshes. The technique is generalized to the scaling positivity-preserving limiter for high order DG schemes solving compressible Euler equations in [28]. In [29], the authors extended the results [27,28] to a general framework of constructing maximum-principle-satisfying and positivity-preserving high order DG schemes for scalar conservation laws on triangular meshes. It is important to emphasize that the scaling positivity-preserving limiter [28,29] are achieved by a linear scaling around the positive cell average of the primitive DG polynomial. Unfortunately, a counterexample is given in [13] that even if the inflow boundary value and the source term are both positive (and, for time dependent problems, also a nonnegative initial condition), unmodulated DG solver for two-dimensional radiative transfer equations based either on the P^k or Q^k polynomial spaces could generate negative cell averages. Therefore the scaling positivity-preserving limiter cannot be directly used to obtain high order positivity-preserving DG schemes for two-dimensional radiative transfer equations. Very recently in [26], Yuan et al. construct an implicit high order positivity-

preserving DG scheme for the one-dimensional steady and unsteady radiative transfer equations with P^k polynomial space, which is achieved by using the scaling positivity-preserving limiter when the cell average is positive and a new rotational positivity-preserving limiter when the cell average is negative. And they have given a straightforward extension of the one-dimensional algorithm to the two-dimensional high order positivity-preserving DG schemes on rectangular meshes with Q^k polynomials (tensor product polynomials).

In this paper, we give an extension of the one-dimensional rotational positivity-preserving limiter [26] to the two-dimensional rotational positivity-preserving limiter on triangular meshes for DG schemes solving the radiative transfer equations with P^k polynomials. The extension is conceptually plausible but highly nontrivial. We first find a special quadrature rule on the triangular element which should satisfy four major conditions. The first is a basic condition that the quadrature rule must be exact for the integration of the DG polynomial on the triangular element. The second one is that all the quadrature weights should be positive. The third one is that the quadrature points should have the Gauss-Lobatto type distribution on each edge of the triangular element, so that we could use one-dimensional scaling positivity-preserving limiter on the edge. The fourth one, which is one of the keypoints of this paper, is that these quadrature points can be arranged on certain line segments, each of which starts with one quadrature point on one edge of the triangular element and ends with another quadrature point on another edge. Then along these certain line segments, we could use the one-dimensional rotational positivity-preserving limiter.

Our limiter is combined of the scaling positivity-preserving limiter and the rotational positivity-preserving limiter, which can be used to solve the radiative transfer equations on triangular meshes by the implicit or iterative DG method. To be specific, if the cell average is positive, we use the two-dimensional scaling positivity-preserving limiter [29] on the triangular element. If the cell average is negative, the limiting procedure consists of a one-dimensional scaling positivity-preserving limiter on the relevant cell boundary followed by the rotational positivity-preserving limiter around this cell boundary. Since the number of the quadrature points is larger than the number of basis functions of P^k polynomial space, the modified polynomial cannot be interpolated directly. To solve this problem, we first find a k-th polynomial by a L_2-norm Least Square subject to its cell average being equal to the weighted average of the values on the quadrature points after using the rotational positivity-preserving limiter. Since the weights used here are the quadrature weights which are positive, then the cell average of the modified polynomial is nonnegative. This is the other keypoint of this paper. And the final modified polynomial can be obtained by using the two-dimensional scaling positivity-preserving limiter on the triangular element. We theoretically prove that our rotational positivity-preserving limiter on triangular meshes could keep both high order accuracy and positivity. It is relatively simple to implement, and also does not affect convergence to weak solutions. Numerical results of the two-dimensional steady and unsteady radiative transfer equations also verify the high order accuracy and the positivity-preserving properties of our schemes. The advantage of the triangular meshes on handling complex domain is also presented in our numerical examples.

This paper is organized as follows. In Section 2, we introduce the radiative transfer equations and their DOM-DG schemes. In Section 3, we construct a special quadrature rule on the triangle satisfying four major conditions for the design of the positivity-preserving DG schemes. In Section 4, we construct our high order positivity-preserving DG schemes on triangular meshes. Some numerical experiments have been carried out to demonstrate the good performance of our limiters in Section 5. Section 6 concludes the paper.

2. The radiative transfer equations and their DOM-DG schemes

2.1. The radiative transfer equations

The radiative transfer equation is the mathematical statement of the conservation of photons [21]. We consider a unsteady-state, isotropically scattering transfer equation

$$\frac{1}{c}\frac{\partial I(\boldsymbol{r}, \Omega, t)}{\partial t} + \Omega \cdot \nabla I(\boldsymbol{r}, \Omega, t) + \sigma_t I(\boldsymbol{r}, \Omega, t) = \frac{\sigma_s}{4\pi}\int_S I(\boldsymbol{r}, \Omega, t)d\Omega + q(\boldsymbol{r}, \Omega, t), \tag{2.1}$$

where c is the speed of photon, $I(\boldsymbol{r}, \Omega, t)$ is the radiative intensity in the direction Ω, the spatial position $\boldsymbol{r}$ and the time t, S is the unit sphere, $\sigma_s \geq 0$ is the scattering coefficient of the medium, $\sigma_t \geq \sigma_s$ is the extinction coefficient of the medium due to both absorption and scattering, total solid angle is 4π spherical degree and $q(\boldsymbol{r}, \Omega, t)$ is a given source term. The vector $\boldsymbol{r}$ is described by the Cartesian coordinates x, y, z. The vector Ω is usually described by a polar angle β measured with respect to a fixed axis in space (such as the z axis) and a corresponding azimuthal angle φ. If we introduce $\mu = \cos\beta$, $\zeta = \sin\beta\cos\varphi$, $\eta = \sin\beta\sin\varphi$ then

$$d\boldsymbol{r} = dxdydz, \quad d\Omega = \sin\beta d\beta d\varphi = -d\mu d\varphi.$$

In all cases the essential point is to interpret $\Omega \cdot \nabla I(\boldsymbol{r}, \Omega, t)$ in Equation (2.1) as a directional derivative in the Ω direction. That is, we write

$$\Omega \cdot \nabla I(\boldsymbol{r}, \Omega, t) = \frac{\partial I}{\partial s}, \tag{2.2}$$
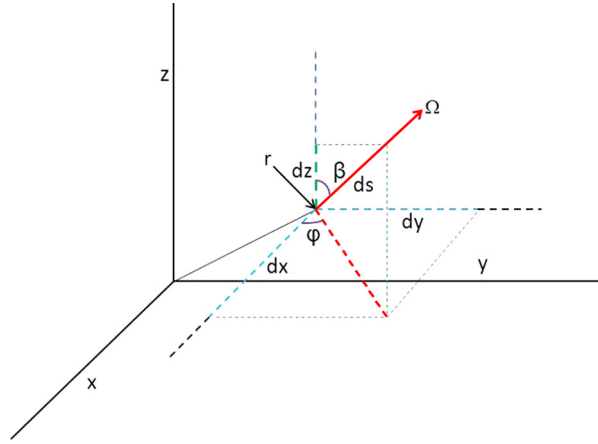
Fig. 1. Sketch of the geometry.

where s is a length along Ω.

If the x and y directions are infinite, the radiative intensity then depends only upon the single spatial coordinate z and the single angular coordinate β. This situation is shown in Fig. 1. Obviously, in this case, the directional derivative can be expressed as follows

$$\frac{\partial I}{\partial s} = \frac{\partial I}{\partial z}\left(\frac{dz}{ds}\right) + \frac{\partial I}{\partial \mu}\left(\frac{d\mu}{ds}\right). \tag{2.3}$$

From Fig. 1 we clearly see that

$$\frac{dz}{ds} = \cos\beta = \mu, \quad \frac{d\mu}{ds} = 0. \tag{2.4}$$

In the one-dimensional planar geometry, because $I(z, \mu, t)$ is independent of azimuthal angle φ, integral over the azimuthal angle φ is trivial. Hence in this geometry we have

$$\frac{1}{4\pi}\int_S I(\mathbf{r}, \Omega, t)d\Omega = \frac{1}{4\pi}\int_{-1}^{1}\int_0^{2\pi} I(z, \mu, t)d\mu d\varphi = \frac{1}{2}\int_{-1}^{1} I(z, \mu, t)d\mu, \tag{2.5}$$

and Equation (2.1) becomes

$$\frac{1}{c}\frac{\partial I(z, \mu, t)}{\partial t} + \mu\frac{\partial I(z, \mu, t)}{\partial z} + \sigma_t I(z, \mu, t) = \frac{\sigma_s}{2}\int_{-1}^{1} I(z, \mu, t)d\mu + q(z, \mu, t). \tag{2.6}$$

If we ignore the dependence of time, i.e., $\frac{\partial I}{\partial t} = 0$, then we have the general form of the one-dimensional steady radiative transfer equation

$$\mu\frac{\partial I(z, \mu)}{\partial z} + \sigma_t I(z, \mu) = \frac{\sigma_s}{2}\int_{-1}^{1} I(z, \mu)d\mu + q(z, \mu). \tag{2.7}$$

In the two-dimensional Cartesian coordinate, the radiative intensity depends on the spatial coordinate x and y and the angular coordinate ζ and η, then we have

$$\frac{\partial I}{\partial s} = \frac{\partial I}{\partial x}\left(\frac{dx}{ds}\right) + \frac{\partial I}{\partial y}\left(\frac{dy}{ds}\right) + \frac{\partial I}{\partial \zeta}\left(\frac{d\zeta}{ds}\right) + \frac{\partial I}{\partial \eta}\left(\frac{d\eta}{ds}\right). \tag{2.8}$$

Similarly, from Fig. 1 we can get

$$\frac{dx}{ds} = \sin\beta\cos\varphi = \zeta, \quad \frac{dy}{ds} = \sin\beta\sin\varphi = \eta, \quad \frac{d\zeta}{ds} = 0, \quad \frac{d\eta}{ds} = 0, \tag{2.9}$$

and

$$\frac{1}{4\pi} \int_S I(\mathbf{r}, \Omega, t)d\Omega = \frac{1}{4\pi} \int_{-1}^{1} \int_0^{2\pi} I(x, y, \sqrt{1-\mu^2}\cos\varphi, \sqrt{1-\mu^2}\sin\varphi, t)d\mu d\varphi. \tag{2.10}$$

Substitute (2.9) and (2.10) into (2.1), Equation (2.1) can be rewritten as

$$\frac{1}{c}\frac{\partial I(x, y, \zeta, \eta, t)}{\partial t} + \zeta\frac{\partial I(x, y, \zeta, \eta, t)}{\partial x} + \eta\frac{\partial I(x, y, \zeta, \eta, t)}{\partial y} + \sigma_t I(x, y, \zeta, \eta, t)$$

$$= \frac{\sigma_s}{4\pi} \int_{-1}^{1} \int_0^{2\pi} I(x, y, \zeta, \eta, t)d\mu d\varphi + q(x, y, \zeta, \eta, t), \tag{2.11}$$

where $\zeta = \sin\beta\cos\varphi = \sqrt{1-\mu^2}\cos\varphi$, $\eta = \sin\beta\sin\varphi = \sqrt{1-\mu^2}\sin\varphi$, and the two-dimensional steady radiative transfer equation is

$$\zeta\frac{\partial I(x, y, \zeta, \eta)}{\partial x} + \eta\frac{\partial I(x, y, \zeta, \eta)}{\partial y} + \sigma_t I(x, y, \zeta, \eta)$$

$$= \frac{\sigma_s}{4\pi} \int_{-1}^{1} \int_0^{2\pi} I(x, y, \zeta, \eta)d\mu d\varphi + q(x, y, \zeta, \eta). \tag{2.12}$$

2.2. The discrete ordinate method (DOM) for the radiative transfer equations

To solve the radiative transfer equation numerically, first we must discretize the angular variables to obtain a system of linear hyperbolic equations coupled with a numerical integral term. In this paper, we adopt the discrete-ordinate method. The radiative transfer equation (2.1) is solved for a finite number of directions spanning the total solid angle of the unit sphere around a point in space, and the integral over solid angle is replaced by a numerical quadrature.

We first consider a steady radiative transfer equation

$$\Omega \cdot \nabla I(\mathbf{r}, \Omega) + \sigma_t I(\mathbf{r}, \Omega) = \frac{\sigma_s}{4\pi} \int_S I(\mathbf{r}, \Omega)d\Omega + q(\mathbf{r}, \Omega), \quad \mathbf{r} \in \mathbb{D}. \tag{2.13}$$

Use $\mathbf{n}(\mathbf{r})$ to denote the unit outward normal vector at the point $\mathbf{r}$ on the domain boundary $\partial\mathbb{D}$ and define $\partial\mathbb{D}_{in} = \{\mathbf{r}|\mathbf{r} \in \partial\mathbb{D}, \mathbf{n}(\mathbf{r}) \cdot \Omega < 0\}$. The boundary condition is

$$I(\mathbf{r}, \Omega) = f(\mathbf{r}, \Omega), \quad \mathbf{r} \in \partial\mathbb{D}_{in}. \tag{2.14}$$

For each discrete direction $\Omega_m, m = 1, \cdots, M$, the equation (2.13) can be written as the following linear hyperbolic equations

$$\Omega_m \cdot \nabla I_m(\mathbf{r}) + \sigma_t I_m(\mathbf{r}) = \sigma_s \sum_{m'=1}^{M} w_{m'} I_{m'}(\mathbf{r}) + q_m(\mathbf{r}), \quad m = 1 \cdots M, \tag{2.15}$$

where $I_m(\mathbf{r}) = I(\mathbf{r}, \Omega_m)$ is the radiative intensity in the direction Ω_m and all the average of the radiative intensity $\frac{1}{4\pi} \int_S I(\mathbf{r}, \Omega)d\Omega$ is approximated by the Legendre-Chebyshev P_N-T_N quadrature $\sum_{m'=1}^{M} w_{m'} I_{m'}(\mathbf{r})$, i.e., $\frac{1}{4\pi} \int_S I(\mathbf{r}, \Omega)d\Omega \approx \sum_{m'=1}^{M} w_{m'} I_{m'}(\mathbf{r})$, the quadrature weights with $\sum_{m'=1}^{M} w_{m'} = 1$ and $w_{m'} > 0$, M is the number of directions on S.

Similarly, the discrete ordinate method for the unsteady radiative transfer equation reads

$$\frac{1}{c}\frac{\partial I_m(\mathbf{r}, t)}{\partial t} + \Omega_m \cdot \nabla I_m(\mathbf{r}, t) + \sigma_t I_m(\mathbf{r}, t) = \sigma_s \sum_{m'=1}^{M} w_{m'} I_{m'}(\mathbf{r}, t) + q_m(\mathbf{r}, t), \quad m = 1 \cdots M. \tag{2.16}$$

2.3. The DOM-DG method for the radiative transfer equations on triangular meshes

The angular discretization of the radiative transfer equation leads to a linear hyperbolic system of first-order partial differential equations in space. Now we discretize Equation (2.15) by the discontinuous Galerkin method.

Let's denote a triangulation of the computational domain $\mathbb{D}$ by $\mathcal{T}_h = \{K\}$ consisting of non-overlapping triangles covering completely the domain $\mathbb{D}$, where h is the maximum edge size of the triangular meshes. Assume the coordinates of the vertices $(\hat{x}, \hat{y})$ for the reference triangular element $\widehat{K}$ to be $\{(0, 1), (1, 0), (0, 0)\}$, and the area of $\widehat{K}$ to be $|\widehat{K}|$, then we can define the orthogonal basis functions $\{b_p(\hat{x}, \hat{y}), p = 0, 1, \cdots\}$ over $\widehat{K}$, the specific formulation of which can be found in
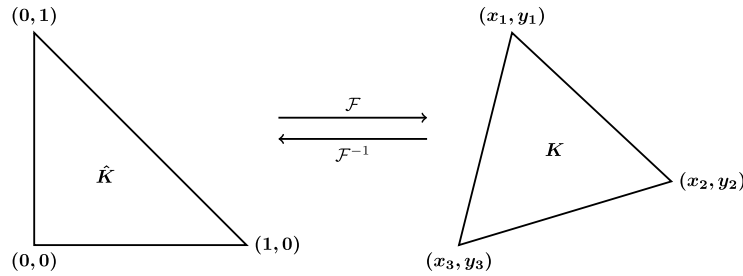
Fig. 2. Transformation between the reference element $\hat{K}$ and the arbitrary triangular element K.

Appendix A. For an arbitrary triangular element $K \in \mathcal{T}_h$, let its vertices be $\{(x_1, y_1), (x_2, y_2), (x_3, y_3)\}$, and its area be $|K|$, then there is an affine transformation $\mathcal{F} \colon \widehat{K} \to K$

$$\begin{bmatrix} x(\hat{x}, \hat{y}) \\ y(\hat{x}, \hat{y}) \end{bmatrix} = \begin{bmatrix} (x_2 - x_3) & (x_1 - x_3) \\ (y_2 - y_3) & (y_1 - y_3) \end{bmatrix} \begin{bmatrix} \hat{x} \\ \hat{y} \end{bmatrix} + \begin{bmatrix} x_3 \\ y_3 \end{bmatrix}, \tag{2.17}$$

and its inverse transformation $\mathcal{F}^{-1} \colon K \to \widehat{K}$

$$\begin{bmatrix} \hat{x}(x, y) \\ \hat{y}(x, y) \end{bmatrix} = \frac{1}{J} \begin{bmatrix} (y_1 - y_3) & -(x_1 - x_3) \\ -(y_2 - y_3) & (x_2 - x_3) \end{bmatrix} \begin{bmatrix} x - x_3 \\ y - y_3 \end{bmatrix}, \tag{2.18}$$

where $J = |\frac{\partial(x, y)}{\partial(\hat{x}, \hat{y})}| = (x_2 - x_3)(y_1 - y_3) - (y_2 - y_3)(x_1 - x_3) = |K|/|\widehat{K}|$. This transformation relation can be seen in Fig. 2. Therefore, we can define a series of orthogonal basis functions $\{\phi_p^{(K)}(x, y), \ p = 0, 1, \cdots\}$ over the arbitrary triangular element K by $\{b_p(\hat{x}, \hat{y}), \ p = 0, 1, \cdots\}$,

$$\phi_p^{(K)}(x, y) = b_p(\hat{x}(x, y), \hat{y}(x, y)), \quad p = 0, 1, \cdots. \tag{2.19}$$

Define the finite element space:

$$V_h^k = \{I_m^h(x, y) \in L^2(\mathbb{D}) : I_m^h(x, y)|_K \in P^k(K), \forall K\}, \tag{2.20}$$

where $P^k(K)$ is the set of all polynomials of degree at most k on the triangular element K and the dimension of $P^k(K)$ is $L = \dim(P^k(K)) = \frac{(k+1)(k+2)}{2}$.

For a given direction Ω_m, if we define the degrees of freedom as

$$I_{m,K}^{[p]} = \frac{1}{\int_K (\phi_p^{(K)}(x, y))^2 dxdy} \int_K I_m^h(x, y) \phi_p^{(K)}(x, y) dxdy, \quad p = 0, 1, \cdots, L - 1, \tag{2.21}$$

then the DG polynomial solution $I_m^h(x, y)$ in the space V_h^k can be expressed as

$$I_m^h(x, y) = \sum_{p=0}^{L-1} I_{m,K}^{[p]} \phi_p^{(K)}(x, y), \quad \forall (x, y) \in K. \tag{2.22}$$

We multiply Equation (2.15) by a test function $\phi(x, y) \in V_h^k$, then integrate it over the element K, and replace the exact solution $I_m(x, y)$ by its approximation $I_m^h(x, y)$, finally we have

$$\int_K \Omega_m \cdot (\nabla I_m^h(x, y)) \phi(x, y) dxdy + \int_K \sigma_t I_m^h(x, y) \phi(x, y) dxdy$$
$$= \int_K \sigma_s \Psi_K(x, y) \phi(x, y) dxdy + \int_K q_m(x, y) \phi(x, y) dxdy, \tag{2.23}$$

with

$$\Psi_K(x, y) = \sum_{m'=1}^{M} w_{m'} I_{m', K}(x, y).$$

Apply the Green's theorem on the gradient term, we have

$$\int_K \Omega_m \cdot (\nabla I_m^h(x,y))\phi(x,y)dxdy$$
$$= \int_{\partial K} \boldsymbol{n}_K^e \cdot (\Omega_m I_m^h(x,y)\phi(x,y))d\tau - \int_K (\Omega_m I_m^h(x,y)) \cdot (\nabla \phi(x,y))dxdy, \tag{2.24}$$

where $\boldsymbol{n}_K^e$ is the outward unit normal to the cell boundary ∂K.

It is noted that the function $I_m^h(x,y)$ may be discontinuous across the cell boundaries. For the particular direction Ω_m, we define the inflow boundary ∂K^{m-} and the outflow boundary ∂K^{m+} of the cell K by

$$\partial K^{m+} = \{e_{K^{m+}} \in \partial K | \Omega_m \cdot \boldsymbol{n}_{K^{m+}}^e \geq 0\},$$
$$\partial K^{m-} = \{e_{K^{m-}} \in \partial K | \Omega_m \cdot \boldsymbol{n}_{K^{m-}}^e < 0\}, \tag{2.25}$$

where $\boldsymbol{n}_{K^{m+}}^e$ and $\boldsymbol{n}_{K^{m-}}^e$ are the outward unit normal to ∂K^{m+} and ∂K^{m-}, respectively.

By applying the monotone upwind numerical flux at the cell boundaries, and use the notations $I_m^h(int(K))$ and $I_m^h(ext(K))$ to denote the approximations to the values on the edge $e_K \in \partial K$ obtained from the interior and the exterior of K, respectively. Then the DG scheme for solving the equation (2.15) on the triangular element K can be described as

$$\int_K \sigma_t I_m^h(x,y)\phi(x,y)dxdy - \int_K (\Omega_m I_m^h(x,y)) \cdot (\nabla\phi(x,y))dxdy$$
$$+ \int_{\partial K^{m+}} \boldsymbol{n}_{K^{m+}}^e \cdot (\Omega_m I_m^h(int(K)))\phi(x,y)d\tau$$
$$= \int_K \sigma_s \Psi_K(x,y)\phi(x,y)dxdy + \int_K q_m(x,y)\phi(x,y)dxdy \tag{2.26}$$
$$- \int_{\partial K^{m-}} \boldsymbol{n}_{K^{m-}}^e \cdot (\Omega_m I_m^h(ext(K)))\phi(x,y)d\tau.$$

Likewise, for the unsteady radiative transfer equation, we use the implicit backward Euler time discretization to solve Equation (2.16),

$$\int_K \hat{\sigma}_t I_m^h(x,y,t_n)\phi(x,y)dxdy - \int_K (\Omega_m I_m^h(x,y,t_n)) \cdot (\nabla\phi(x,y))dxdy$$
$$+ \int_{\partial K^{m+}} \boldsymbol{n}_{K^{m+}}^e \cdot (\Omega_m I_m^h(int(K),t_n))\phi(x,y)d\tau$$
$$= \int_K \sigma_s \Psi_K(x,y,t_n)\phi(x,y)dxdy + \int_K \hat{q}_m(x,y,t_n)\phi(x,y)dxdy \tag{2.27}$$
$$- \int_{\partial K^{m-}} \boldsymbol{n}_{K^{m-}}^e \cdot (\Omega_m I_m^h(ext(K),t_n))\phi(x,y)d\tau,$$

with $\hat{\sigma}_t = \frac{1}{c\Delta t_n} + \sigma_t$, $\hat{q}_m(x,y,t_n) = q_m(x,y,t_n) + \frac{1}{c\Delta t_n}I_m^h(x,y,t_{n-1})$, and the time step $\Delta t_n = t_n - t_{n-1}$.

Generally, the discrete set of algebraic equations in the DOM-DG schemes such as (2.26) and (2.27) is widely solved by the source iterative (SI) method [14] in an optimal sweeping order. This is usually referred to as the grid sweeping algorithm. More details can be found in [26]. The SI method is defined for solving the DOM-DG scheme (2.26) as follows: when the ℓ-th iteration solution $I_{m,K}^{(\ell)}(x,y)$ (for all $m = 1, \cdots, M$ and $\forall K$) is known, we compute $I_m^{(\ell+1)}(x,y)$ cell by cell in the sweeping direction [7], and for each fixed element K, we run through $m = 1, \cdots, M$ to solve (omitting the superscript h below for the sake of writing simplicity)

$$\int\limits_K \sigma_t I_m^{(\ell+1)}(x, y)\phi(x, y)dxdy - \int\limits_K (\Omega_m I_m^{(\ell+1)}(x, y)) \cdot (\nabla \phi(x, y))dxdy$$

$$+ \int\limits_{\partial K^{m+}} \boldsymbol{n}_{K^{m+}}^e \cdot (\Omega_m I_m^{(\ell+1)}(int(K)))\phi(x, y)d\tau$$

$$= \int\limits_K \sigma_s \Psi_K^*(x, y)\phi(x, y)dxdy + \int\limits_K q_m(x, y)\phi(x, y)dxdy \tag{2.28}$$

$$- \int\limits_{\partial K^{m-}} \boldsymbol{n}_{K^{m-}}^e \cdot (\Omega_m I_m^{(\ell+1)}(ext(K)))\phi(x, y)d\tau,$$

where

$$\Psi_K^*(x, y) = \sum_{m'=1}^M w_{m'} I_{m', K}^*(x, y),$$

and

$$I_{m', K}^*(x, y) = \begin{cases} I_{m', K}^{(\ell+1)}(x, y), & \text{if it is already available,} \\ I_{m', K}^{(\ell)}(x, y), & \text{otherwise.} \end{cases}$$

The initial iteration values $I_{m, K}^{(0)}$ can be determined arbitrarily. The SI iteration process continues until a prescribed convergence criterion is satisfied. In this paper we take the absolutely maximum residue $\max_m \|I_m^{(\ell+1)} - I_m^{(\ell)}\|_\infty \le 10^{-12}$ in our numerical experiments in Section 5.

Similarly, the SI method to solve the DOM-DG scheme (2.27) can be described as follows

$$\int\limits_K \hat{\sigma}_t I_m^{(\ell+1)}(x, y, t_n)\phi(x, y)dxdy - \int\limits_K (\Omega_m I_m^{(\ell+1)}(x, y, t_n)) \cdot (\nabla \phi(x, y))dxdy$$

$$+ \int\limits_{\partial K^{m+}} \boldsymbol{n}_{K^{m+}}^e \cdot (\Omega_m I_m^{(\ell+1)}(int(K), t_n))\phi(x, y)d\tau$$

$$= \int\limits_K \sigma_s \Psi_K^*(x, y, t_n)\phi(x, y)dxdy + \int\limits_K \hat{q}_m(x, y, t_n)\phi(x, y)dxdy \tag{2.29}$$

$$- \int\limits_{\partial K^{m-}} \boldsymbol{n}_{K^{m-}}^e \cdot (\Omega_m I_m^{(\ell+1)}(ext(K), t_n))\phi(x, y)d\tau.$$

Notice that the SI solver (2.29) is equivalent to (2.28) for solving the steady radiative transfer equation, thus, we only need to discuss (2.28) below.

3. The specific quadrature points on the triangle K for the design of the positivity-preserving DG schemes

In this section, we would like to find a special quadrature rule on the triangle K for the design of our two-dimensional rotational positivity-preserving limiter on triangular meshes by the idea of the one-dimensional rotational positivity-preserving limiter [26], which has been proven to maintain high order accuracy and positivity. The quadrature rule on the triangle K should satisfy:

(1) The quadrature rule is exact for the integration of the DG polynomial on the triangle K.
(2) All the quadrature weights should be positive.
(3) The quadrature points should have the Gauss-Lobatto type distribution on each edge e_K of the triangle K, so that we could use the one-dimensional scaling limiter on the edge.
(4) These quadrature points can be arranged on certain line segments, each of which starts with one quadrature point on one edge of the triangle K and ends with another quadrature point on another edge. Then on these certain line segments, we could use the one-dimensional rotational positivity-preserving limiter.

Let $P_K(x, y)$ be the DG polynomial of degree k on the triangle K, and $P_{\widehat{K}}(x(\hat{x}, \hat{y}), y(\hat{x}, \hat{y}))$ be the DG polynomial of degree k on the reference triangle $\widehat{K}$. For an arbitrary triangular element K, using the transformations (2.17) and (2.18), we have

$$\frac{1}{|K|}\int\limits_K P_K(x, y)dxdy = \frac{1}{|\widehat{K}|}\int\limits_{\hat{K}} P_{\widehat{K}}(x(\hat{x}, \hat{y}), y(\hat{x}, \hat{y}))d\hat{x}d\hat{y}. \tag{3.1}$$

Thus, we first discuss how to use quadrature to decompose the cell average as a convex combination of point values of the DG polynomial $P_{\widehat{K}}(x(\hat{x}, \hat{y}), y(\hat{x}, \hat{y}))$ on the reference triangle $\widehat{K}$ below.

Consider the quadrature rule on the unit square R with the vertices $S_1(-\frac{1}{2}, \frac{1}{2})$, $S_2(\frac{1}{2}, \frac{1}{2})$, $S_3(\frac{1}{2}, -\frac{1}{2})$, and $S_4(-\frac{1}{2}, -\frac{1}{2})$ in the u-v plane. Let N be the smallest integer such that $2N - 3 \geq k$, then the N-point Gauss-Lobatto quadrature rule is exact for a single variable polynomial of degree k. Let $\{\hat{v}^{\gamma_1} : \gamma_1 = 1, \cdots, N\}$ denote the Gauss-Lobatto quadrature points on $v \in [-\frac{1}{2}, \frac{1}{2}]$ with weights $\hat{w}_{\gamma_1}$, and $\{\hat{u}^{\gamma_2} : \gamma_2 = 1, \cdots, N\}$ denote the Gauss-Lobatto quadrature points on $u \in [-\frac{1}{2}, \frac{1}{2}]$ with weights $\hat{w}_{\gamma_2}$. For a two-variable polynomial, we can use the tensor product of N Gauss-Lobatto points for u and N Gauss-Lobatto points for v as the quadrature rule on the square R, then the quadrature points can be written as $R_k = \{(\hat{u}^{\gamma_2}, \hat{v}^{\gamma_1}) : \gamma_1 = 1, \cdots, N; \gamma_2 = 1, \cdots, N\}$. This quadrature is exact for a two-variable polynomial if its degree with respect to u is not larger than k and the degree with respect to v is also not larger than k.

Without loss of generality, we assume the orientation of the three vertices $\widehat{V}_1(0, 1)$, $\widehat{V}_2(1, 0)$ and $\widehat{V}_3(0, 0)$ of the triangular $\hat{K}$ is clockwise. We define the following three functions

$$g_1(u, v) = (\frac{1}{2} + v)\widehat{V}_1 + (\frac{1}{2} + u)(\frac{1}{2} - v)\widehat{V}_2 + (\frac{1}{2} - u)(\frac{1}{2} - v)\widehat{V}_3,$$

$$g_2(u, v) = (\frac{1}{2} + v)\widehat{V}_2 + (\frac{1}{2} + u)(\frac{1}{2} - v)\widehat{V}_3 + (\frac{1}{2} - u)(\frac{1}{2} - v)\widehat{V}_1, \qquad (3.2)$$

$$g_3(u, v) = (\frac{1}{2} + v)\widehat{V}_3 + (\frac{1}{2} + u)(\frac{1}{2} - v)\widehat{V}_1 + (\frac{1}{2} - u)(\frac{1}{2} - v)\widehat{V}_2.$$

Each of them is a projection from the square R to the reference triangle $\widehat{K}$, mapping the top edge of R into one vertex and the other three edges to the edges of $\widehat{K}$. We denote $\overline{S_1 S_2}$ as the line segment starts with the point S_1 and ends with the point S_2. Specifically, the function g_1 maps the top edge $\overline{S_1 S_2}$ of the rectangle R into the vertex $\widehat{V}_1$ and the edges $\overline{S_2 S_3}$, $\overline{S_3 S_4}$, $\overline{S_4 S_1}$ to the edges $\overline{\widehat{V}_1 \widehat{V}_2}$, $\overline{\widehat{V}_2 \widehat{V}_3}$, $\overline{\widehat{V}_3 \widehat{V}_1}$ of the triangle $\widehat{K}$, respectively. The function g_2 maps the top edge $\overline{S_1 S_2}$ of the R into the vertex $\widehat{V}_2$ and the edges $\overline{S_2 S_3}$, $\overline{S_3 S_4}$, $\overline{S_4 S_1}$ to the edges $\overline{\widehat{V}_2 \widehat{V}_3}$, $\overline{\widehat{V}_3 \widehat{V}_1}$, $\overline{\widehat{V}_1 \widehat{V}_2}$ of the triangle $\widehat{K}$, respectively. The function g_3 maps the top edge $\overline{S_1 S_2}$ of the rectangle R into the vertex $\widehat{V}_3$ and the edges $\overline{S_2 S_3}$, $\overline{S_3 S_4}$, $\overline{S_4 S_1}$ to the edges $\overline{\widehat{V}_3 \widehat{V}_1}$, $\overline{\widehat{V}_1 \widehat{V}_2}$, $\overline{\widehat{V}_2 \widehat{V}_3}$ of the triangle $\widehat{K}$, respectively. We will use the projects $g_i(u, v), i = 1, 2, 3$ and the quadrature points R_k to construct our quadrature points on the triangle $\widehat{K}$, then we have

$$\frac{1}{|\widehat{K}|} \int_{\widehat{K}} P_{\widehat{K}}(\hat{x}, \hat{y}) d\hat{x} d\hat{y} = \frac{1}{|\widehat{K}|} \int_R P_{\widehat{K}}(g_i(u, v)) \left| \frac{\partial g_i(u, v)}{\partial(u, v)} \right| du dv, \quad i = 1, 2, 3, \qquad (3.3)$$

where the Jacobian $\left| \frac{\partial g_i(u,v)}{\partial(u,v)} \right| = 2|\widehat{K}|(\frac{1}{2} - v)$. Notice that $P_{\widehat{K}}(g_i(u, v)) \left| \frac{\partial g_i(u,v)}{\partial(u,v)} \right|$ is still a two-variable polynomial and its degrees with respect to u and v are k and $k + 1$, respectively. Thus, the double integral in u and v is exact to the quadrature R_k if $2N - 3 \geq k + 1$. Here, we take $N = k + 1$ when $k \geq 2$. For the case of $k = 1$, we choose $N = k + 2$. Therefore, we have

$$\frac{1}{|\widehat{K}|} \int_R P_{\widehat{K}}(g_i(u, v)) \left| \frac{\partial g_i(u, v)}{\partial(u, v)} \right| du dv = \sum_{\gamma_1=1}^N \sum_{\gamma_2=1}^N \hat{w}_{\gamma_1} \hat{w}_{\gamma_2} 2(\frac{1}{2} - \hat{v}^{\gamma_1}) P_{\widehat{K}}(g_i(\hat{u}^{\gamma_2}, \hat{v}^{\gamma_1})), \quad i = 1, 2, 3. \qquad (3.4)$$

So we can obtain three different quadrature rules for $P_{\widehat{K}}(\hat{x}, \hat{y})$ over $\widehat{K}$. The quadrature points are $g_i(R_k), i = 1, 2, 3$ with nonnegative quadrature weights, see Figs. 3(b)(c)(d) for $k = 4$.

By combining the points of the three quadrature rules, we obtain the quadrature points $G_{\widehat{K}}^k$ on the reference triangle $\widehat{K}$

$$G_{\widehat{K}}^k = g_1(R_k) \cup g_2(R_k) \cup g_3(R_k). \qquad (3.5)$$

Let N_G be the number of $G_{\widehat{K}}^k$, then $N_G = 3(N - 1) + 3(N - 2)^2$. Clearly, the quadrature points $G_{\widehat{K}}^k$ have the Gauss-Lobatto type distribution on each edge of the reference element $\widehat{K}$, see Fig. 4 for $k = 4$. Using Equations (3.3) and (3.4), we can find a quadrature rule to decompose the cell average of $P_{\widehat{K}}(x, y)$ over the reference triangle $\widehat{K}$ as follows

$$\frac{1}{|\widehat{K}|} \int_{\widehat{K}} P_{\widehat{K}}(\hat{x}, \hat{y}) d\hat{x} d\hat{y} = \frac{1}{3} \sum_{i=1}^3 \sum_{\gamma_1=1}^N \sum_{\gamma_2=1}^N 2(\frac{1}{2} - \hat{v}^{\gamma_1}) \hat{w}_{\gamma_1} \hat{w}_{\gamma_2} P_{\widehat{K}}(g_i(\hat{u}^{\gamma_2}, \hat{v}^{\gamma_1}))$$

$$= \sum_{(\hat{x}^\alpha, \hat{y}^\alpha) \in G_{\widehat{K}}^k} \hat{w}_\alpha P_{\widehat{K}}(\hat{x}^\alpha, \hat{y}^\alpha). \qquad (3.6)$$

There are $3(N - 2)^2$ quadrature points laying in the interior of $\widehat{K}$, whose weights are

$$\frac{2}{3} \hat{w}_{\gamma_1} \hat{w}_{\gamma_2} (\frac{1}{2} - \hat{v}^{\gamma_1}), \quad \gamma_1 = 2, \cdots, N - 1; \; \gamma_2 = 2, \cdots, N - 1. \qquad (3.7)$$
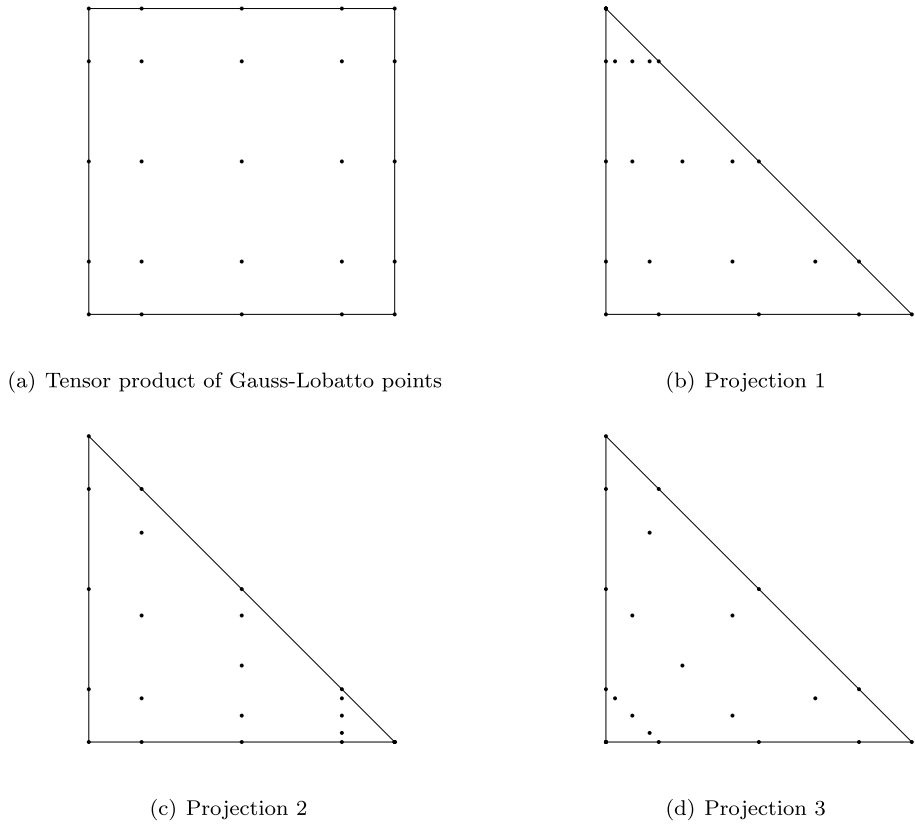
(a) Tensor product of Gauss-Lobatto points   (b) Projection 1

(c) Projection 2   (d) Projection 3

Fig. 3. Illustration of the three projections for $k = 4$.
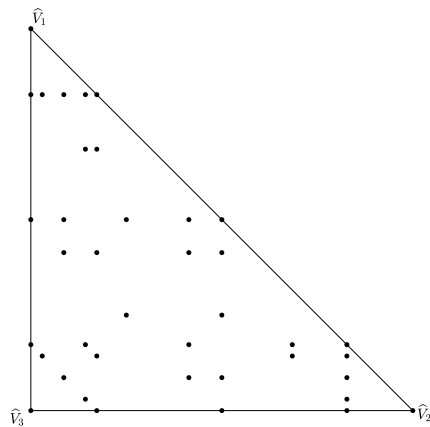
Fig. 4. The quadrature points $G_{\widehat{K}}^k$ on the triangle $\widehat{K}$ for $k = 4$.

We would like to find the quadrature weights $\hat{w}_\alpha$ in (3.6) for the quadrature points at three vertices and other Gauss-Lobatto points laying on each edge. Notice that $g_1(\hat{u}^{\gamma_2}, \hat{v}^N)$, $g_2(\hat{u}^1, \hat{v}^1)$ and $g_3(\hat{u}^N, \hat{v}^1)$ are the same point $\widehat{V}_1$; $g_1(\hat{u}^N, \hat{v}^1)$, $g_2(\hat{u}^{\gamma_2}, \hat{v}^N)$ and $g_3(\hat{u}^1, \hat{v}^1)$ are the same point $\widehat{V}_2$; $g_1(\hat{u}^1, \hat{v}^1)$, $g_2(\hat{u}^N, \hat{v}^1)$ and $g_3(\hat{u}^{\gamma_2}, \hat{v}^N)$ are the same point $\widehat{V}_3$. Using $\hat{v}^1 = -\frac{1}{2}$, $\hat{v}^N = \frac{1}{2}$ and $\hat{w}_1 = \hat{w}_N$, the quadrature weight of the vertex $\widehat{V}_1$ is

$$\frac{2}{3}(\frac{1}{2} - \hat{v}^N)\hat{w}_N \sum_{\gamma_2=1}^{N} \hat{w}_{\gamma_2} + \frac{2}{3}(\frac{1}{2} - \hat{v}^1)\hat{w}_1\hat{w}_1 + \frac{2}{3}(\frac{1}{2} - \hat{v}^1)\hat{w}_1\hat{w}_N = \frac{4}{3}\hat{w}_1\hat{w}_1. \tag{3.8}$$

Similarly, the weights for the vertices $\widehat{V}_2$ and $\widehat{V}_3$ are also $\frac{4}{3}\hat{w}_1\hat{w}_1$.

Remark 3.1. Notice that when $\hat{v}^N = \frac{1}{2}$, the quadrature weights of the points $g_i(\hat{u}^{\gamma_2}, \hat{v}^N), i = 1, 2, 3$, satisfy $\hat{w}_N \hat{w}_{\gamma_2} 2(\frac{1}{2} - \hat{v}^N) = 0$. Thus, the weights of the vertices $\widehat{V}_1$, $\widehat{V}_2$, $\widehat{V}_3$ are zero in the quadrature rules $g_1(R_k)$, $g_2(R_k)$, and $g_3(R_k)$, respectively. If we only choose one of the quadrature rules $g_i(R_k), i = 1, 2, 3$, the second and the third conditions in the beginning of this section are violated. That is why we combine the points of the three quadrature rules to obtain the quadrature points on the triangle. Moreover, the quadrature weights of the quadrature points are symmetric on the triangle in this way.

From the edge-mapping relationship of the projections, we easily find that for the projection g_1, the quadrature points $g_1(\hat{u}^N, -\hat{v}^\gamma)$, $g_1(-\hat{u}^\gamma, \hat{v}^1)$, $g_1(\hat{u}^1, \hat{v}^\gamma)$ lie on the edges $\overline{\widehat{V}_1 \widehat{V}_2}$, $\overline{\widehat{V}_2 \widehat{V}_3}$, $\overline{\widehat{V}_3 \widehat{V}_1}$, respectively. For the projection g_2, the quadrature points $g_2(\hat{u}^1, \hat{v}^\gamma)$, $g_2(\hat{u}^N, -\hat{v}^\gamma)$, $g_2(-\hat{u}^\gamma, \hat{v}^1)$ lie on the edges $\overline{\widehat{V}_1 \widehat{V}_2}$, $\overline{\widehat{V}_2 \widehat{V}_3}$, $\overline{\widehat{V}_3 \widehat{V}_1}$, respectively. And for the projection g_3, the quadrature points $g_3(-\hat{u}^\gamma, \hat{v}^1)$, $g_3(\hat{u}^1, \hat{v}^\gamma)$, $g_3(\hat{u}^N, -\hat{v}^\gamma)$ lie on the edges $\overline{\widehat{V}_1 \widehat{V}_2}$, $\overline{\widehat{V}_2 \widehat{V}_3}$, $\overline{\widehat{V}_3 \widehat{V}_1}$, respectively. Here $\gamma = 2, \cdots, N - 1$. After simple calculation, we can get

$$g_1(\ \hat{u}^N, -\hat{v}^\gamma) = (\frac{1}{2} + \hat{v}^\gamma, \frac{1}{2} - \hat{v}^\gamma), \quad g_1(-\hat{u}^\gamma, \ \hat{v}^1) = (\frac{1}{2} - \hat{u}^\gamma, 0), \quad g_1(\ \hat{u}^1, \ \hat{v}^\gamma) = (0, \frac{1}{2} + \hat{v}^\gamma),$$

$$g_2(\ \hat{u}^1, \ \hat{v}^\gamma) = (\frac{1}{2} + \hat{v}^\gamma, \frac{1}{2} - \hat{v}^\gamma), \quad g_2(\hat{u}^N, -\hat{v}^\gamma) = (\frac{1}{2} - \hat{v}^\gamma, 0), \quad g_2(-\hat{u}^\gamma, \ \hat{v}^1) = (0, \frac{1}{2} + \hat{u}^\gamma),$$

$$g_3(-\hat{u}^\gamma, \ \hat{v}^1) = (\frac{1}{2} + \hat{u}^\gamma, \frac{1}{2} - \hat{u}^\gamma), \quad g_3(\ \hat{u}^1, \ \hat{v}^\gamma) = (\frac{1}{2} - \hat{v}^\gamma, 0), \quad g_3(\ \hat{u}^N, -\hat{v}^\gamma) = (0, \frac{1}{2} + \hat{v}^\gamma).$$

Note that $\hat{u}^\gamma = \hat{v}^\gamma$, we substitute $\hat{u}^\gamma$ by $\hat{v}^\gamma$. Then $g_1(\hat{u}^N, -\hat{v}^\gamma)$, $g_2(\hat{u}^1, \hat{v}^\gamma)$, $g_3(-\hat{u}^\gamma, \hat{v}^1)$ are the same point $(\frac{1}{2} + \hat{v}^\gamma, \frac{1}{2} - \hat{v}^\gamma)$, and its weight is

$$\frac{2}{3}(\frac{1}{2} + \hat{v}^\gamma)\hat{w}_\gamma \hat{w}_N + \frac{2}{3}(\frac{1}{2} - \hat{v}^\gamma)\hat{w}_\gamma \hat{w}_1 + \frac{2}{3}(\frac{1}{2} - \hat{v}^1)\hat{w}_1 \hat{w}_\gamma = \frac{4}{3}\hat{w}_\gamma \hat{w}_1. \tag{3.9}$$

Similarly, the weights for $(\frac{1}{2} - \hat{v}^\gamma, 0)$, $(0, \frac{1}{2} + \hat{v}^\gamma)$ are $\frac{4}{3}\hat{w}_\gamma \hat{w}_1$.

Thus, the weights $\hat{w}_\alpha$ of all the quadrature points $(\hat{x}^\alpha, \hat{y}^\alpha) \in G_{\widehat{K}}^k$ on the reference triangular element are positive. We list the specific quadrature points on $\widehat{K}$ and the corresponding weights for the case of $k = 1, 2, 3, 4$ in Appendix B (Tables 10–12).

Obviously, the affine transformations between the reference triangle $\widehat{K}$ and the arbitrary triangle K only change the position of the quadrature points but do not change their weights. We denote quadrature points of the arbitrary triangle K as $G_K^k = \{(x_K^\alpha, y_K^\alpha), \alpha = 1, \cdots, N_G\}$, then we can find the quadrature rule on the triangle K as follows

$$\frac{1}{|K|} \int_K P_K(x, y) dx dy = \sum_{(x_K^\alpha, y_K^\alpha) \in G_K^k} \hat{w}_\alpha P_K(x_K^\alpha, y_K^\alpha). \tag{3.10}$$

Our quadrature points also satisfy the fourth condition presented in the beginning of this section. For convenience, for any $\gamma = 1, \cdots, N$, we use the notation Γ_v^γ to denote the line segment starts with the point $(\hat{u}^\gamma, \hat{v}^1)$ and ends with the point $(\hat{u}^\gamma, \hat{v}^N)$, Γ_{-u}^γ to denote the line segment starts with the point $(\hat{u}^N, \hat{v}^\gamma)$ and ends with the point $(\hat{u}^1, \hat{v}^\gamma)$, and Γ_u^γ to denote the line segment starts with the point $(\hat{u}^1, \hat{v}^\gamma)$ and ends with the point $(\hat{u}^N, \hat{v}^\gamma)$, see Figs. 5(a)(b)(c) for $k = 4$, respectively. Without loss of generality, here we only illustrate the edge $\overline{V_2 V_3}$ of the triangle K. Each of the transformations $g_i, i = 1, 2, 3$, maps the top edge $\overline{S_1 S_2}$ of the rectangle R into one vertex and maps the other three edges of R into the three edges of the reference triangle $\widehat{K}$, so that the edge $\overline{\widehat{V}_2 \widehat{V}_3}$ is corresponding to the edges $\overline{S_3 S_4}$, $\overline{S_2 S_3}$, $\overline{S_4 S_1}$ of the rectangle R in three transformations $g_i, i = 1, 2, 3$, respectively. The transformation g_1, g_2, g_3 map the line segments Γ_v^γ, Γ_{-u}^γ and Γ_u^γ on the rectangle R into the corresponding line segments $g_1(\Gamma_v^\gamma)$, $g_2(\Gamma_{-u}^\gamma)$ and $g_3(\Gamma_u^\gamma)$ on the reference triangle $\widehat{K}$, respectively. Let notations $\mathcal{T}_{g_1}^\gamma$, $\mathcal{T}_{g_2}^\gamma$ and $\mathcal{T}_{g_3}^\gamma$ on the arbitrary triangle K correspond to the line segments $g_1(\Gamma_v^\gamma)$, $g_2(\Gamma_{-u}^\gamma)$ and $g_3(\Gamma_u^\gamma)$ on the reference triangle $\widehat{K}$, respectively. See Fig. 5 for $k = 4$.

So for a given edge $\overline{V_2 V_3}$ of the arbitrary triangle K, which includes $N - 2$ Gauss-Lobatto points except for the vertices V_2 and V_3. We denote these points as $\{(x_e^\gamma, y_e^\gamma), \gamma = 2, \cdots, N - 1\}$, then we can arrange all the quadrature points on K on the certain line segments $\mathcal{T}_{g_1}^\gamma$, $\mathcal{T}_{g_2}^\gamma$ and $\mathcal{T}_{g_3}^{N+1-\gamma}$, on which there are N quadrature points including the point (x_e^γ, y_e^γ). See Figs. 5(g)(h)(i) for $k = 4$, respectively.

4. High order positivity-preserving DG schemes for radiative transfer equations on triangular meshes

Generally, higher order approximations for radiative intensity may provide more accurate solutions but artifacts might appear such as negativeness of the solutions. In Section 3, we have constructed the special quadrature points G_K^k on the arbitrary triangular K which satisfies four major conditions. One of the keypoints of this paper is these quadrature points can be arranged on the certain line segments, each of which starts with one quadrature point on one edge of the triangle K and ends with another quadrature point on another edge. On these certain line segments we can use the one-dimensional rotational positivity-preserving limiter [26]. In this section, we extend the one-dimensional rotational positivity-preserving
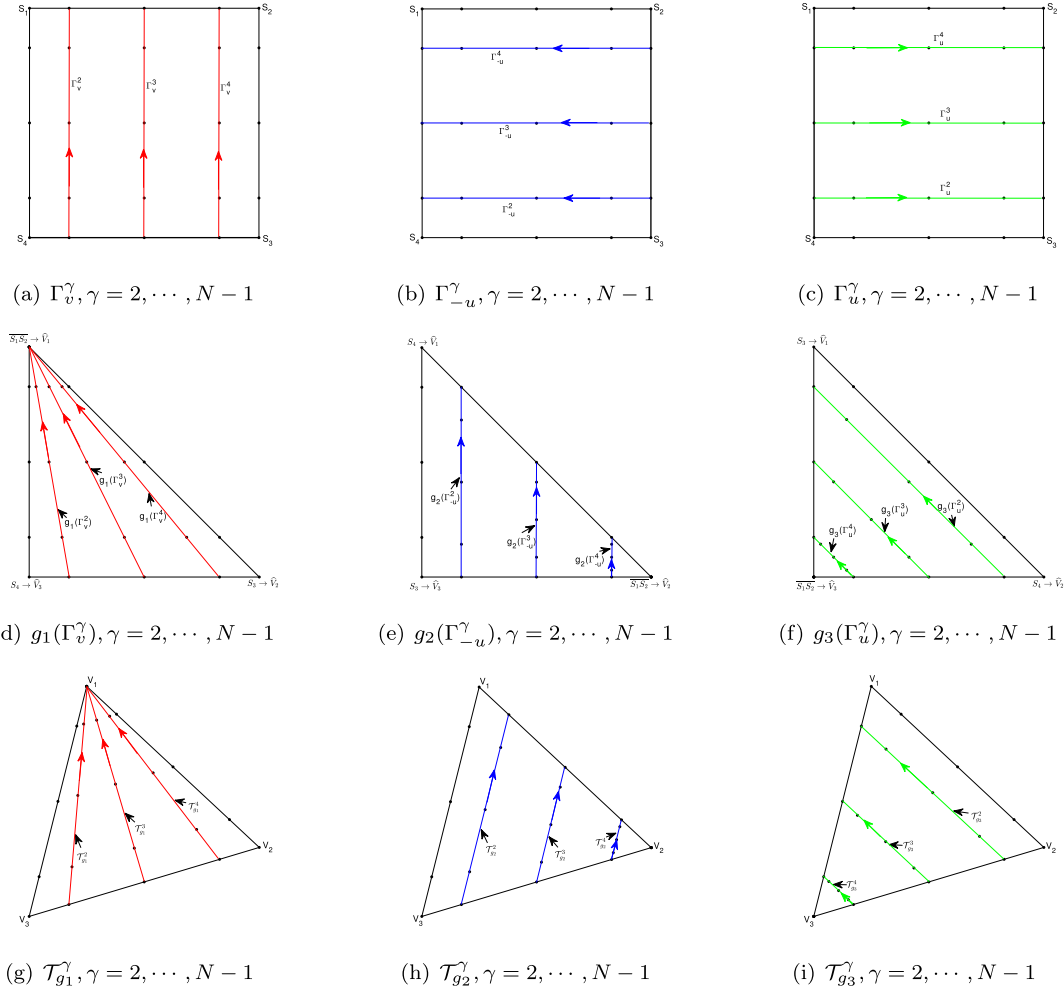
(a) $\Gamma_v^\gamma, \gamma = 2, \cdots, N-1$

(b) $\Gamma_{-u}^\gamma, \gamma = 2, \cdots, N-1$

(c) $\Gamma_u^\gamma, \gamma = 2, \cdots, N-1$

(d) $g_1(\Gamma_v^\gamma), \gamma = 2, \cdots, N-1$

(e) $g_2(\Gamma_{-u}^\gamma), \gamma = 2, \cdots, N-1$

(f) $g_3(\Gamma_u^\gamma), \gamma = 2, \cdots, N-1$

(g) $\mathcal{T}_{g_1}^\gamma, \gamma = 2, \cdots, N-1$

(h) $\mathcal{T}_{g_2}^\gamma, \gamma = 2, \cdots, N-1$

(i) $\mathcal{T}_{g_3}^\gamma, \gamma = 2, \cdots, N-1$

Fig. 5. All the quadrature points can be arranged on the line segments for $k = 4$.

limiter for DG method solving radiative transfer equations to the two-dimensional rotational positivity-preserving limiter on triangular meshes with P^k polynomials.

Taking the test function $\phi(x, y) = 1$ in Equation (2.28), the cell averages produced by the DG method satisfies

$$
\begin{aligned}
&\int_K \sigma_t I_m^{(\ell+1)}(x, y) dx dy + \int_{\partial K^{m+}} \boldsymbol{n}_{K^{m+}}^e \cdot (\Omega_m I_m^{(\ell+1)}(int(K))) d\tau \\
&= \int_K \sigma_s \Psi_K^*(x, y) dx dy + \int_K q_m(x, y) dx dy - \int_{\partial K^{m-}} \boldsymbol{n}_{K^{m-}}^e \cdot (\Omega_m I_m^{(\ell+1)}(ext(K))) d\tau.
\end{aligned}
\tag{4.1}
$$

For simplicity, we denote $\bar{(\cdot)}$ as the cell averaging operator over the triangle K, $\tilde{(\cdot)}$ as the edge averaging operator on the edge e_K, that is,

$$
\bar{P}_K = \frac{1}{|K|} \int_K P_K(x, y) dx dy, \quad \tilde{P}_{e_K} = \frac{1}{|e_K|} \int_{e_K} P_K(x, y) d\tau,
\tag{4.2}
$$

then Equation (4.1) can be rewritten as

$$
\begin{aligned}
&|K| \sigma_t \bar{I}_{m,K}^{(\ell+1)} + \sum_{e_{K^{m+}}} \left(|e_{K^{m+}}| (\boldsymbol{n}_{K^{m+}}^e \cdot \Omega_m) \tilde{I}_{m,e_{K^{m+}}}^{(\ell+1)} \right) \\
&= |K| \sigma_s \bar{\Psi}_K^* + |K| \bar{q}_{m,K} - \sum_{e_{K^{m-}}} \left(|e_{K^{m-}}| (\boldsymbol{n}_{K^{m-}}^e \cdot \Omega_m) \tilde{I}_{m,e_{K^{m-}}}^{(\ell+1)} \right).
\end{aligned}
\tag{4.3}
$$

We assume that the source term $q_{m,K}(x, y)$ and $I_{m,K}^{(\ell+1)}(x, y)$ at the domain boundary are nonnegative and the values of the DG polynomials $I_{m,K}^{(\ell)}$ and $I_{m,K}^{(\ell+1)}$ in the upstream cells (which have already been updated) at the quadrature points are also nonnegative (which is achieved by using the positivity-preserving limiter described below in the upstream cells), then we know that $\bar{\Psi}_K^*$, $\bar{q}_{m,K}$, $\tilde{I}_{m,e_{K^{m-}}}^{(\ell+1)}$ are all nonnegative. Notice that $\boldsymbol{n}_{K^{m+}}^e \cdot \Omega_m \geq 0$ and $\boldsymbol{n}_{K^{m-}}^e \cdot \Omega_m < 0$ in the equation (2.25), then on the triangular cell K, by the mean value theorem, there exists a point $q \in K$, such that

$$I_{m,K}^{(\ell+1)}(q) = \frac{|K|\sigma_t \bar{I}_{m,K}^{(\ell+1)} + \sum_{e_{K^{m+}}} \left((\boldsymbol{n}_{K^{m+}}^e \cdot \Omega_m) |e_{K^{m+}}| \tilde{I}_{m,e_{K^{m+}}}^{(\ell+1)} \right)}{|K|\sigma_t + \sum_{e_{K^{m+}}} \left((\boldsymbol{n}_{K^{m+}}^e \cdot \Omega_m) |e_{K^{m+}}| \right)} \geq 0. \tag{4.4}$$

Obviously, this equation implies that, at least one of $\bar{I}_{m,K}^{(\ell+1)}$ and $\tilde{I}_{m,e_{K^{m+}}}^{(\ell+1)}, \forall e_{K^{m+}} \in \partial K^{m+}$ is nonnegative.

Next, in order to keep the high order accuracy as well as the positivity preserving property of the radiative intensity on triangular meshes, we adopt either the scaling positivity-preserving limiter or the rotational positivity-preserving limiter on $I_{m,K}^{(\ell+1)}(x, y)$ depending on which is nonnegative among $\bar{I}_{m,K}^{(\ell+1)}$ and $\tilde{I}_{m,e_{K^{m+}}}^{(\ell+1)}, \forall e_{K^{m+}} \in \partial K^{m+}$.

4.1. The scaling positivity-preserving limiter on triangular meshes

If $\bar{I}_{m,K}^{(\ell+1)} \geq 0$, we will employ the scaling positivity-preserving limiter [29] to modify $I_{m,K}^{(\ell+1)}(x, y)$ as follows

$$\hat{I}_{m,K}^{(\ell+1)}(x, y) = \lambda \left(I_{m,K}^{(\ell+1)}(x, y) - \bar{I}_{m,K}^{(\ell+1)} \right) + \bar{I}_{m,K}^{(\ell+1)}, \tag{4.5}$$

with

$$\lambda = \min \left\{ \left| \frac{\bar{I}_{m,K}^{(\ell+1)}}{\bar{I}_{m,K}^{(\ell+1)} - z} \right|, 1 \right\}, \quad z = \min_{(x_K^\alpha, y_K^\alpha) \in G_K^k} \left(I_{m,K}^{(\ell+1)}(x_K^\alpha, y_K^\alpha), 0 \right). \tag{4.6}$$

Proposition 4.1. *[29]. Suppose $I_{m,K}^{(\ell+1)}(x, y)$ is a k-th degree polynomial defined on the triangular element K which approximates a smooth function $I(x, y) \geq 0$ to $(k+1)$-th order accuracy, and $\bar{I}_{m,K}^{(\ell+1)} \geq 0$, then the limited polynomial $\hat{I}_{m,K}^{(\ell+1)}(x, y)$ defined by (4.5) and (4.6) achieves positivity $\hat{I}_{m,K}^{(\ell+1)}(x_K^\alpha, y_K^\alpha) \geq 0$ for all $(x_K^\alpha, y_K^\alpha) \in G_K^k$ and guarantees the same $(k+1)$-th order accuracy for approximating $I(x, y)$.*

4.2. The rotational positivity-preserving limiter on triangular meshes

For a given discrete direction Ω_m, there are two different types of elements on triangular meshes. The first type has two inflow boundaries and one outflow boundary, and the second type has one inflow boundary and two outflow boundaries. If $\bar{I}_{m,K}^{(\ell+1)}$ is negative, then there exists at least one of outflow boundaries, denoted as $\tilde{e}_K \in \partial K^{m+}$, whose edge average $\tilde{I}_{m,\tilde{e}_K}^{(\ell+1)}$ should be nonnegative. In this case, the limiting procedure consists of the one-dimensional scaling positivity-preserving limiter on $\tilde{e}_K$ followed by the one-dimensional rotational positivity-preserving limiter around this cell boundary. In the second type, we only need to choose one of outflow boundaries denoted as $\tilde{e}_K$.

For the convenience of description, firstly we review the idea of the one-dimensional rotational positivity-preserving limiter algorithm proposed in [26]. To be specific, assume Γ to be a line segment which includes N Gauss-Lobatto points $\{\xi_j, j = 1, \cdots, N\}$, and $I(\xi)$ to be a k-th single variable polynomial defined on the cell Γ. For simplicity of notation, we denote the right end point ξ_N of Γ as ξ_c and its radiative intensity as I_c which satisfies $I_c \geq 0$. Similarly, for any points $\xi, \xi' \in \Gamma$ the values of the radiative intensity at these points are denoted as I and I', respectively. The rotational transformation can be written as follows:

$$\begin{bmatrix} \xi' - \xi_c \\ I' - I_c \end{bmatrix} = \begin{bmatrix} \cos\theta, & \sin\theta \\ -\sin\theta, & \cos\theta \end{bmatrix} \begin{bmatrix} \xi - \xi_c \\ I - I_c \end{bmatrix}, \tag{4.7}$$

where θ is the rotational angle, shown in Fig. 6. Suppose $I' = 0$, from Fig. 6 it is easy to compute $\theta = \theta_1 - \theta_2$, that is

$$\theta = \arcsin \frac{I_c - I}{\sqrt{(\xi_c - \xi)^2 + (I_c - I)^2}} - \arcsin \frac{I_c}{\sqrt{(\xi_c - \xi)^2 + (I_c - I)^2}}. \tag{4.8}$$

The algorithm for the one-dimensional rotational positivity-preserving limiter can be defined as follows:

1. Compute the rotational angle θ_j by (4.8) for each negative Gauss-Lobatto point ξ_j on the line segment Γ, so that the point $(\xi_j, I(\xi_j))$ is rotated around (ξ_c, I_c) clockwise to reach the new point $(\xi_j', 0)$. We set $\theta_j = 0$, if a particular ξ_j is a nonnegative Gauss-Lobatto point.
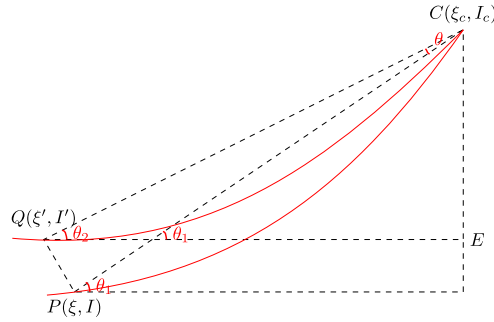
Fig. 6. Sketch of the rotational transformation.

2. Taking $\theta = \max_{j=1,\cdots,N-1} \theta_j$, for $j = 1, \cdots, N-1$, we rotate each point $(\xi_j, I(\xi_j))$ to the new point $(\xi_j', I_j^{(rot)})$ by the rotational transformation (4.7) with the rotational angle θ, where $I_j^{(rot)} = I_c + \cos\theta(I(\xi_j) - I_c) - \sin\theta(\xi_j - \xi_c)$, and $\xi_j' = \xi_c + \cos\theta(\xi_j - \xi_c) + \sin\theta(I(\xi_j) - I_c)$. Let $I_N^{(rot)} = I_c$, then it is easy to see that the value $I_j^{(rot)} \geq 0$ for all $j = 1, \cdots, N$.

This rotational positivity-preserving limiter has some properties proved in [26]. Here we only give the conclusion in the following lemma.

Lemma 4.2. [26]. *Suppose $I^{(\ell+1)}(\xi)$ is a k-th single variable polynomial defined on the cell Γ which approximates a smooth function $I(\xi) \geq 0$ to $(k+1)$-th order accuracy, and the right end point value $I^{(\ell+1)}(\xi_c)$ is nonnegative. By the procedure of the one-dimensional rotational positivity-preserving limiter algorithm above, we have the value $I_j^{(rot)} \geq 0$ and $\left| I_j^{(rot)} - I^{(\ell+1)}(\xi_j) \right| \leq Ch_1^{k+1}$ for all $j = 1 \cdots, N$, where h_1 is the length of Γ.*

Now, we modify the DG polynomial $I_{m,K}^{(\ell+1)}(x,y)$ on the triangular element K as follows. First, we apply the one-dimensional scaling positivity-preserving limiter on the outflow boundary $\tilde{e}_K$. We denote the Gauss-Lobatto points laying on this edge (anticlockwise order) as follows

$$G_e^k = \{(x_K^\alpha, y_K^\alpha)|_{\tilde{e}_K}\} = \{(x_e^\vartheta, y_e^\vartheta), \vartheta = 1, \cdots, N\}. \tag{4.9}$$

We determine the modified polynomial $\mathcal{I}_{m,K}^{(\ell+1)}(x,y)|_{\tilde{e}_K}$ at the outflow boundary $\tilde{e}_K$ of the triangle K as

$$\mathcal{I}_{m,K}^{(\ell+1)}(x,y)|_{\tilde{e}_K} = \lambda_e \left(I_{m,K}^{(\ell+1)}(x,y)|_{\tilde{e}_K} - \tilde{I}_{m,\tilde{e}_K}^{(\ell+1)} \right) + \tilde{I}_{m,\tilde{e}_K}^{(\ell+1)}, \tag{4.10}$$

with

$$\lambda_e = \min\left\{ \left| \frac{\tilde{I}_{m,\tilde{e}_K}^{(\ell+1)}}{\tilde{I}_{m,\tilde{e}_K}^{(\ell+1)} - z_e} \right|, 1 \right\}, \quad z_e = \min_{(x_e^\vartheta, y_e^\vartheta) \in G_e^k} \left(I_{m,K}^{(\ell+1)}(x_e^\vartheta, y_e^\vartheta), 0 \right). \tag{4.11}$$

This one-dimensional scaling positivity-preserving limiter (4.10) and (4.11) is proved in [28] to achieve positivity and maintain the original $(k+1)$-th order accuracy, i.e.,

$$\mathcal{I}_{m,K}^{(\ell+1)}(x_e^\vartheta, y_e^\vartheta)|_{\tilde{e}_K} \geq 0, \quad \vartheta = 1, \cdots, N, \tag{4.12}$$

and

$$\left| \mathcal{I}_{m,K}^{(\ell+1)}(x,y)|_{\tilde{e}_K} - I_{m,K}^{(\ell+1)}(x,y)|_{\tilde{e}_K} \right| = O(h^{k+1}). \tag{4.13}$$

We compute the difference d_e by

$$d_e = \max_\vartheta \left| \mathcal{I}_{m,K}^{(\ell+1)}(x_e^\vartheta, y_e^\vartheta)|_{\tilde{e}_K} - I_{m,K}^{(\ell+1)}(x_e^\vartheta, y_e^\vartheta) \right|. \tag{4.14}$$

Obviously, we have

$$d_e = O(h^{k+1}). \tag{4.15}$$

We modify the values of $I_{m,K}^{(\ell+1)}(x,y)$ at all the quadrature points by

$$\check{I}_{m,K}^{(\ell+1)}(x_K^\alpha, y_K^\alpha) = I_{m,K}^{(\ell+1)}(x_K^\alpha, y_K^\alpha) + d_e, \quad \forall(x_K^\alpha, y_K^\alpha) \in G_K^k. \tag{4.16}$$
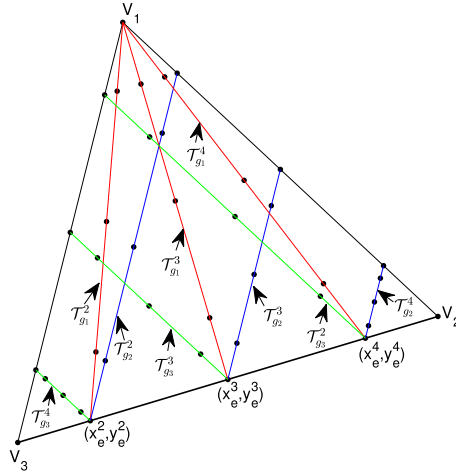
Fig. 7. Sketch of the line segments on which we perform rotational transformation. The red line segments represent $\mathcal{T}_{g_1}^{\vartheta}$, the blue line segments represent $\mathcal{T}_{g_2}^{\vartheta}$, and the green line segments represent $\mathcal{T}_{g_3}^{N-\vartheta+1}$. (For interpretation of the colors in the figure(s), the reader is referred to the web version of this article.)

Notice that $\{\phi_p^{(K)}(x, y), \ p = 0, 1, \cdots, L-1\}$ are the orthogonal basis functions on the triangular element K and $\phi_0^{(K)}(x, y) = 1$, then the k-th degree DG polynomial $I_{m,K}^{(\ell+1)}(x, y)$ can be written by

$$I_{m,K}^{(\ell+1)}(x, y) = \sum_{p=0}^{L-1} I_{m,K}^{[p]} \phi_p^{(K)}(x, y), \quad \forall (x, y) \in K, \tag{4.17}$$

where $I_{m,K}^{[p]} = \frac{\int_K I_{m,K}^{(\ell+1)}(x,y) \phi_p^{(K)}(x,y) dxdy}{\int_K (\phi_p^{(K)}(x,y))^2 dxdy}$, $\ p = 0, 1, \cdots, L-1$, are the degrees of freedom.

Thus, the k-th degree modified polynomial $\breve{I}_{m,K}^{(\ell+1)}(x, y)$ can be written as

$$\breve{I}_{m,K}^{(\ell+1)}(x, y) = (I_{m,K}^{[0]} + d_e) + \sum_{p=1}^{L-1} I_{m,K}^{[p]} \phi_p^{(K)}(x, y), \quad \forall (x, y) \in K. \tag{4.18}$$

Clearly, the modified polynomial $\breve{I}_{m,K}^{(\ell+1)}(x, y)$ maintains the $(k+1)$-th order accuracy for approximating $I_{m,K}^{(\ell+1)}(x, y)$, i.e.,

$$\left| \breve{I}_{m,K}^{(\ell+1)}(x, y) - I_{m,K}^{(\ell+1)}(x, y) \right| = O(h^{k+1}), \quad \forall (x, y) \in K, \tag{4.19}$$

and is positive at the Gauss-Lobatto points along the edge $\tilde{e}_K$

$$\breve{I}_{m,K}^{(\ell+1)}(x_e^{\vartheta}, y_e^{\vartheta}) \geq 0, \quad \vartheta = 1, \cdots, N. \tag{4.20}$$

Further, to guarantee the positivity of the radiative intensity at all the quadrature points $(x_K^{\alpha}, y_K^{\alpha}) \in G_K^k$, we need to apply the one-dimensional rotational positivity-preserving limiter to $\breve{I}_{m,K}^{(\ell+1)}(x, y)$ around the cell outflow boundary $\tilde{e}_K$. We assume $\tilde{e}_K$ to be the edge $\overline{V_2 V_3}$. For each point $(x_e^{\vartheta}, y_e^{\vartheta})$, $\vartheta = 2, \cdots, N-1$ on the edge $\overline{V_2 V_3}$, we need to perform three times the one-dimensional rotational transformation algorithm along line segments $\mathcal{T}_{g_1}^{\vartheta}$, $\mathcal{T}_{g_2}^{\vartheta}$, and $\mathcal{T}_{g_3}^{N-\vartheta+1}$, respectively. Fig. 7 shows the sketch of the line segments for $k = 4$, where $(x_e^{\vartheta}, y_e^{\vartheta})$ is the rotational center.

So we need to perform the one-dimensional rotational positivity-preserving limiter $3(N-2)$ times in all to obtain the modified values at all the quadrature points along these line segments. Let $\breve{I}_{\alpha}^{(rot)}$ be the value obtained by performing the rotational positivity-preserving limiter on $\breve{I}_{m,K}^{(\ell+1)}(x_K^{\alpha}, y_K^{\alpha})$. Using Lemma 4.2, we have

$$\breve{I}_{\alpha}^{(rot)} \geq 0, \quad \alpha = 1, \cdots, N_G, \tag{4.21}$$

and

$$\left| \breve{I}_{\alpha}^{(rot)} - \breve{I}_{m,K}^{(\ell+1)}(x_K^{\alpha}, y_K^{\alpha}) \right| = O(h^{k+1}), \quad \forall (x_K^{\alpha}, y_K^{\alpha}) \in G_K^k. \tag{4.22}$$

The modified polynomial $\overset{\smile}{\breve{I}}_{m,K}^{(\ell+1)}(x, y)$ of degree k is determined by the unique interpolation in the L_2-norm Least Square satisfying

$$\breve{I}_{m,K}^{(\ell+1)}(x,y) = \underset{\mathcal{P}(x,y)\in V_h^k}{\arg\min} \Big\{ \sum_{(x_K^\alpha, y_K^\alpha)\in G_K^k} \big(\mathcal{P}(x_K^\alpha, y_K^\alpha) - \breve{I}_\alpha^{(rot)}\big)^2 \Big\}, \tag{4.23}$$

subject to

$$\frac{1}{|K|} \int_K \mathcal{P}(x,y)dxdy = \sum_{\alpha=1}^{N_G} \hat{w}_\alpha \breve{I}_\alpha^{(rot)}. \tag{4.24}$$

The details on how to obtain the modified polynomial $\breve{I}_{m,K}^{(\ell+1)}(x,y)$ could be seen in the following proof of Theorem 4.3.

Theorem 4.3. *Assume $\breve{I}_{m,K}^{(\ell+1)}(x,y)$ to be a k-th degree polynomial defined on the triangular element K which approximates a smooth function, if the k-th degree polynomial $\breve{I}_{m,K}^{(\ell+1)}(x,y)$ defined by Equations (4.23), (4.24), and for all $(x_K^\alpha, y_K^\alpha) \in G_K^k$ satisfies (4.21), (4.22), then we have*

$$\left| \breve{I}_{m,K}^{(\ell+1)}(x,y) - \breve{I}_{m,K}^{(\ell+1)}(x,y) \right| = O(h^{k+1}), \tag{4.25}$$

and the cell average $\bar{\breve{I}}_{m,K}^{(\ell+1)} \geq 0$.

Proof. Obviously, the cell average

$$\bar{\breve{I}}_{m,K}^{(\ell+1)} = \sum_{\alpha=1}^{N_G} \hat{w}_\alpha \breve{I}_\alpha^{(rot)} \geq 0. \tag{4.26}$$

Because the optimal polynomial $\breve{I}_{m,K}^{(\ell+1)}(x,y)$ is in the space V_h^k defined in (2.20), then we can write it as

$$\breve{I}_{m,K}^{(\ell+1)}(x,y) = a_0 + \sum_{p=1}^{L-1} a_p \phi_p^{(K)}(x,y), \quad \forall (x,y)\in K, \tag{4.27}$$

where $a_0 = \sum_{\alpha=1}^{N_G} \hat{w}_\alpha \breve{I}_\alpha^{(rot)}$ and the coefficients a_p, $p = 1, \cdots, L-1$, need to be determined.

Using (2.19), we can also rewrite $\breve{I}_{m,K}^{(\ell+1)}(x,y)$ as

$$\breve{I}_{m,K}^{(\ell+1)}(x,y) = a_0 + \sum_{p=1}^{L-1} a_p b_p(\hat{x}(x,y), \hat{y}(x,y)), \quad \forall (x,y)\in K. \tag{4.28}$$

We would like to find $\boldsymbol{a} = (a_1, a_2, \cdots, a_{L-1})^{\mathrm{T}}$ by solving the least square problem

$$A\boldsymbol{a} = B, \tag{4.29}$$

where

$$A = \begin{pmatrix} b_1(\hat{x}^1, \hat{y}^1) & b_2(\hat{x}^1, \hat{y}^1) & \cdots & b_{L-1}(\hat{x}^1, \hat{y}^1) \\ b_1(\hat{x}^2, \hat{y}^2) & b_2(\hat{x}^2, \hat{y}^2) & \cdots & b_{L-1}(\hat{x}^2, \hat{y}^2) \\ \vdots & \vdots & \cdots & \vdots \\ b_1(\hat{x}^\alpha, \hat{y}^\alpha) & b_2(\hat{x}^\alpha, \hat{y}^\alpha) & \cdots & b_{L-1}(\hat{x}^\alpha, \hat{y}^\alpha) \\ \vdots & \vdots & \cdots & \vdots \\ b_1(\hat{x}^{N_G}, \hat{y}^{N_G}) & b_2(\hat{x}^{N_G}, \hat{y}^{N_G}) & \cdots & b_{L-1}(\hat{x}^{N_G}, \hat{y}^{N_G}) \end{pmatrix} \tag{4.30}$$

and

$$B = \Big(\breve{I}_1^{(rot)} - a_0, \quad \breve{I}_2^{(rot)} - a_0, \quad \cdots, \quad \breve{I}_{N_G}^{(rot)} - a_0 \Big)^{\mathrm{T}}. \tag{4.31}$$

Then we can obtain $\boldsymbol{a} = (A^{\mathrm{T}}A)^{-1}A^{\mathrm{T}}B$. By calculation, we can rewrite $\breve{I}_{m,K}^{(\ell+1)}(x,y)$ as follows

$$\breve{I}_{m,K}^{(\ell+1)}(x,y) = \sum_{\alpha=1}^{N_G} \breve{I}_\alpha^{(rot)} f_\alpha(\hat{x}, \hat{y}) = \sum_{\alpha=1}^{N_G} \breve{I}_\alpha^{(rot)} f_\alpha^{(K)}(x,y), \tag{4.32}$$

where the polynomial $f_\alpha(\hat{x}, \hat{y})$ is the linear combination of the basis functions $b_p(\hat{x}, \hat{y})$, $p = 0, 1, \cdots, L-1$, that is to say, $f_\alpha^{(K)}(x, y)$ is the linear combination of the basis functions $\phi_p^{(K)}(x, y)$, $p = 0, 1, \cdots, L-1$, and satisfies

$$\sum_{\alpha=1}^{N_G} f_\alpha^{(K)}(x, y) = \sum_{\alpha=1}^{N_G} f_\alpha(\hat{x}, \hat{y}) = 1.$$

Because the basis functions $b_p(\hat{x}, \hat{y})$, $p = 0, 1, \cdots, L-1$, over $\hat{K}$ are bounded continuous functions and using (2.19), then $f_\alpha^{(K)}(x, y)$ is also a bounded continuous function on K, i.e., there exists a constant C, independent of mesh size parameter h, such that

$$\left| f_\alpha^{(K)}(x, y) \right| \le C, \quad \alpha = 1, \cdots, N_G. \tag{4.33}$$

The specific form of $f_\alpha^{(K)}(x, y)$ is shown in Appendix C. Using (4.22) and (4.33), thus we have

$$
\begin{aligned}
&\left| \check{I}_{m,K}^{(\ell+1)}(x, y) - \breve{I}_{m,K}^{(\ell+1)}(x, y) \right| \\
&= \left| \sum_{\alpha=1}^{N_G} \check{I}_\alpha^{(rot)} f_\alpha^{(K)}(x, y) - \sum_{\alpha=1}^{N_G} \breve{I}_{m,K}^{(\ell+1)}(x_K^\alpha, y_K^\alpha) f_\alpha^{(K)}(x, y) \right| \\
&= \left| \sum_{\alpha=1}^{N_G} \left(\check{I}_\alpha^{(rot)} - \breve{I}_{m,K}^{(\ell+1)}(x_K^\alpha, y_K^\alpha) \right) f_\alpha^{(K)}(x, y) \right| \\
&\le \sum_{\alpha=1}^{N_G} \left| \check{I}_\alpha^{(rot)} - \breve{I}_{m,K}^{(\ell+1)}(x_K^\alpha, y_K^\alpha) \right| \left| f_\alpha^{(K)}(x, y) \right| \\
&\le C h^{k+1}. \quad \square
\end{aligned}
\tag{4.34}
$$

Finally, we will again perform the two-dimensional scaling positivity-preserving limiter defined in subsection 4.1 to modify $\breve{I}_{m,K}^{(\ell+1)}(x, y)$ over the triangular element K,

$$\hat{I}_{m,K}^{(\ell+1)}(x, y) = \lambda_K \left(\breve{I}_{m,K}^{(\ell+1)}(x, y) - \bar{\breve{I}}_{m,K}^{(\ell+1)} \right) + \bar{\breve{I}}_{m,K}^{(\ell+1)}, \tag{4.35}$$

where the parameter λ_K is determined as

$$\lambda_K = \min \left\{ \left| \frac{\bar{\breve{I}}_{m,K}^{(\ell+1)}}{\bar{\breve{I}}_{m,K}^{(\ell+1)} - z_K} \right|, 1 \right\}, \quad z_K = \min_{(x_K^\alpha, y_K^\alpha) \in G_K^k} \left(\breve{I}_{m,K}^{(\ell+1)}(x_K^\alpha, y_K^\alpha), 0 \right). \tag{4.36}$$

Thus, we can get the final modified DG polynomial $\hat{I}_{m,K}^{(\ell+1)}(x, y)$ satisfying

$$\hat{I}_{m,K}^{(\ell+1)}(x_K^\alpha, y_K^\alpha) \ge 0, \quad \forall (x_K^\alpha, y_K^\alpha) \in G_K^k, \tag{4.37}$$

and

$$\left| \hat{I}_{m,K}^{(\ell+1)}(x, y) - \breve{I}_{m,K}^{(\ell+1)}(x, y) \right| = O\left(h^{k+1} \right). \tag{4.38}$$

From the definition of the rotational positivity-preserving limiter on triangular meshes, we have the following conclusion.

Theorem 4.4. *Assume $I_{m,K}^{(\ell+1)}(x, y)$ is a k-th degree polynomial defined on the triangular element K which approximates a smooth function $I(x, y) \ge 0$ to $(k+1)$-th order accuracy, then the limited polynomial $\hat{I}_{m,K}^{(\ell+1)}(x, y)$ obtained by the above procedures achieves positivity-preserving property $\hat{I}_{m,K}^{(\ell+1)}(x_K^\alpha, y_K^\alpha) \ge 0$ for all $(x_K^\alpha, y_K^\alpha) \in G_K^k$ and maintains the same $(k+1)$-th order accuracy for approximating $I(x, y)$.*

Similarly, the two-dimensional high order positivity-preserving DG schemes proposed for the steady radiative transfer equation can naturally be extended to the unsteady radiative transfer equation.

Remark 4.5. We emphasize that neither the DG method itself nor the rotational positivity-preserving limiter depends on the particular choice of basis functions for the implementation. If other basis functions are used, a change of coefficients under different basis sets is needed.

Remark 4.6. It is proved in [26] that the usage of the rotational positivity-preserving limiter does not affect the original high order accuracy of the DG scheme for solving radiative transfer equation on rectangular meshes, nor does it affect convergence to weak solutions even if the scheme is not conservative. In this paper, we also have the same results on triangular meshes.

5. Numerical results

In this section, we carry out some numerical experiments in two dimensions to validate the high order accuracy and positivity-preserving properties of our DG schemes on triangular meshes. For the DG schemes with the positivity-preserving limiter, we test the following two types: "scaling limiter preferred" and "rotational limiter preferred". For the scaling-limiter-preferred procedure, we judge if the cell average $\bar{I}_{m,K}^{(\ell+1)} \geq 0$ first. If yes, then the scaling positivity-preserving limiter is employed; if not, then the rotational positivity-preserving limiter is applied. And for the rotational-limiter-preferred procedure, we judge if the outflow edge average $\tilde{I}_{m,\tilde{e}_K}^{(\ell+1)} \geq 0$ first. If yes, then the rotational positivity-preserving limiter is applied; if not, then the scaling positivity-preserving limiter is used. Regarding the discrete-ordinate quadrature rule, we adopt the Legendre-Chebyshev P_N-T_N quadrature [16] in which the μ-levels are equal to the roots of the Gauss-Legendre quadrature, and the azimuthal angles φ are determined from the roots of the orthogonal Chebyshev polynomials. To be more specific, P_8-T_8 are used for all the following tests with nonzero scattering terms, unless otherwise stated.

For the accuracy test of the DG schemes, the error in the computed solution is measured in the L^1, and L^∞ norms. We used 21 quadrature points $\{(x_s^K, y_s^K)\}$ on each triangle K to compute the L^1 and L^∞ norms i.e.,

$$\|e_h\|_{L^1} = \max_m \left\{ \sum_{K \in \mathcal{T}_h} \left(\frac{|K|}{21} \sum_{s=1}^{21} \left| I_{m,K}^h(x_s^K, y_s^K) - I_{m,K}(x_s^K, y_s^K) \right| \right) \right\},$$

$$\|e_h\|_{L^\infty} = \max_m \left\{ \max_{K \in \mathcal{T}_h} \left(\max_s \left| I_{m,K}^h(x_s^K, y_s^K) - I_{m,K}(x_s^K, y_s^K) \right| \right) \right\},$$

where these quadrature points $\{(x_s^K, y_s^K)\}$ on the triangle K are obtained by the affine transformation (2.17) from the reference triangle $\widehat{K}$ to K, and the corresponding points on $\widehat{K}$ are

$$\left\{ \left(\frac{i}{5}, \frac{j}{5}\right), \ j = 0, \cdots, 5; \ i = 0, \cdots, 5 - j \right\}.$$

Example 5.1 (*The accuracy test of the DG schemes for the two-dimensional steady radiative transfer equation simulating the purely absorbing model [26]*).

In this test, we solve the two-dimensional steady radiative transfer equation (2.12) with $\sigma_t = 1$, $\sigma_s = 0$, and the source function $q = 0$. The computational domain is $\mathbb{D} = [0, 1] \times [0, 1]$. $\zeta = 0.5$, $\eta = 0.1$. The boundary conditions are

$$I(x, 0, \zeta, \eta) = 0, \quad I(0, y, \zeta, \eta) = \sin^6(\pi y).$$

In this case, the problem has the exact solution given as follows:

$$I(x, y, \zeta, \eta) = \begin{cases} 0, & y < \frac{\eta}{\zeta} x, \\ \sin^6(\pi (y - \frac{\eta}{\zeta} x)) e^{-\frac{\sigma_t}{\zeta} x}, & \text{otherwise.} \end{cases} \tag{5.1}$$

For this problem, numerically negative radiative intensity appears if the positivity-preserving limiter is not used in the high order DG schemes. The errors and orders of accuracy for the $\{P^1, P^2, P^3, P^4\}$ DG schemes without the positivity-preserving limiters and with the positivity-preserving limiters (both the scaling limiter preferred and the rotational limiter preferred procedures) are shown in Tables 1–4, respectively. In these tables, we also list the percentages of the cells where either the scaling positivity-preserving limiter or the rotational positivity-preserving limiter (denoted as "*limiter*" in the tables) is performed in the computation, respectively. The conservation errors (denoted as "*c_err*" in the tables) produced by the positivity-preserving limiters are also shown in the tables. We also notice that the conservation error converges to 0 asymptotically with the refinement of the mesh, and higher order DG schemes produce smaller conservation errors. We can clearly see from these tables that, on our triangular meshes, the DG schemes with the above mentioned two types of the positivity-preserving limiting procedures can achieve the same designed order of accuracy as the DG schemes without the positivity-preserving limiters in both the L^1 and L^∞ norms. Moreover the DG schemes with the positivity-preserving limiter can also keep the positivity of the radiative intensity.

Example 5.2 (*The positivity-preserving test of the DG schemes for the two-dimensional steady radiative transfer equation simulating the transparent model [26]*).

Table 1
Errors of the P^1 DG scheme for the two-dimensional steady radiative transfer equation simulating the purely absorbing model on triangular meshes.

h	L^1-error	Order	L^∞-error	Order	*limiter(%)*	*c_err*
Without positivity-preserving limiter						
1/10	2.893E-03		5.191E-02			
1/20	7.254E-04	1.996	1.606E-02	1.692		
1/40	1.800E-04	2.011	4.586E-03	1.808		
1/80	4.468E-05	2.010	1.190E-03	1.946		
With positivity-preserving limiter (scaling limiter preferred)						
1/10	3.024E-03		5.191E-02		17.63	0.0
1/20	7.409E-04	2.029	1.606E-02	1.692	10.74	0.0
1/40	1.808E-04	2.035	4.586E-03	1.808	7.51	0.0
1/80	4.473E-05	2.016	1.190E-03	1.946	5.72	0.0
With positivity-preserving limiter (rotational limiter preferred)						
1/10	3.742E-03		5.191E-02		10.90	1.311E-04
1/20	7.511E-04	2.317	1.606E-02	1.692	4.57	2.916E-06
1/40	1.800E-04	2.061	4.586E-03	1.808	2.02	1.437E-08
1/80	4.468E-05	2.011	1.190E-03	1.946	1.00	1.339E-10

Table 2
Errors of the P^2 DG scheme for the two-dimensional steady radiative transfer equation simulating the purely absorbing model on triangular meshes.

h	L^1-error	Order	L^∞-error	Order	limiter(%)	*c_err*
Without positivity-preserving limiter						
1/10	3.191E-04		4.187E-03			
1/20	3.819E-05	3.063	7.925E-04	2.402		
1/40	4.491E-06	3.088	1.237E-04	2.679		
1/80	5.303E-07	3.082	1.641E-05	2.915		
With positivity-preserving limiter (scaling limiter preferred)						
1/10	3.211E-04		4.187E-03		8.97	0.0
1/20	3.825E-05	3.069	7.925E-04	2.402	5.29	0.0
1/40	4.491E-06	3.090	1.237E-04	2.679	4.59	0.0
1/80	5.303E-07	3.082	1.641E-05	2.915	2.93	0.0
With positivity-preserving limiter (rotational limiter preferred)						
1/10	3.221E-04		4.187E-03		10.26	1.142E-06
1/20	3.829E-05	3.073	7.925E-04	2.402	4.65	1.037E-08
1/40	4.492E-06	3.091	1.237E-04	2.679	3.49	1.277E-10
1/80	5.303E-07	3.083	1.641E-05	2.915	3.09	3.898E-13

Table 3
Errors of the P^3 DG scheme for the two-dimensional steady radiative transfer equation simulating the purely absorbing model on triangular meshes.

h	L^1-error	Order	L^∞-error	Order	limiter(%)	*c_err*
Without positivity-preserving limiter						
1/10	3.046E-05		4.637E-04			
1/20	1.806E-06	4.076	3.691E-05	3.651		
1/40	1.101E-07	4.035	2.910E-06	3.665		
1/80	6.549E-09	4.072	1.908E-07	3.930		
With positivity-preserving limiter (scaling limiter preferred)						
1/10	4.083E-05		6.299E-04		8.97	0.0
1/20	2.022E-06	4.336	3.691E-05	4.093	6.65	0.0
1/40	1.131E-07	4.161	2.910E-06	3.665	5.03	0.0
1/80	6.567E-09	4.106	1.908E-07	3.930	3.84	0.0
With positivity-preserving limiter (rotational limiter preferred)						
1/10	3.570E-05		4.637E-04		8.01	8.430E-07
1/20	1.886E-06	4.243	3.691E-05	3.651	4.01	6.726E-09
1/40	1.111E-07	4.085	2.910E-06	3.665	3.15	4.376E-11
1/80	6.556E-09	4.083	1.908E-07	3.930	2.21	1.509E-13

Table 4
Errors of the P^4 DG scheme for the two-dimensional steady radiative transfer equation simulating the purely absorbing model on triangular meshes.

h	L^1-error	Order	L^∞-error	Order	limiter(%)	c_err
Without positivity-preserving limiter						
1/10	2.565E-06		4.907E-05			
1/20	7.397E-08	5.116	2.202E-06	4.478		
1/40	2.148E-09	5.106	7.962E-08	4.790		
1/80	6.327E-11	5.085	2.550E-09	4.964		
With positivity-preserving limiter (scaling limiter preferred)						
1/10	2.998E-06		5.661E-05		9.94	0.0
1/20	7.835E-08	5.258	2.202E-06	4.684	5.45	0.0
1/40	2.183E-09	5.166	7.962E-08	4.790	4.15	0.0
1/80	6.367E-11	5.100	2.550E-09	4.964	3.33	0.0
With positivity-preserving limiter (rotational limiter preferred)						
1/10	2.653E-06		4.907E-05		8.97	1.500E-08
1/20	7.516E-08	5.141	2.202E-06	4.478	5.37	9.043E-11
1/40	2.158E-09	5.122	7.962E-08	4.790	3.87	4.124E-13
1/80	6.337E-11	5.089	2.550E-09	4.964	2.82	1.748E-15

(a) P^1 (b) P^2 (c) P^3 (d) P^4
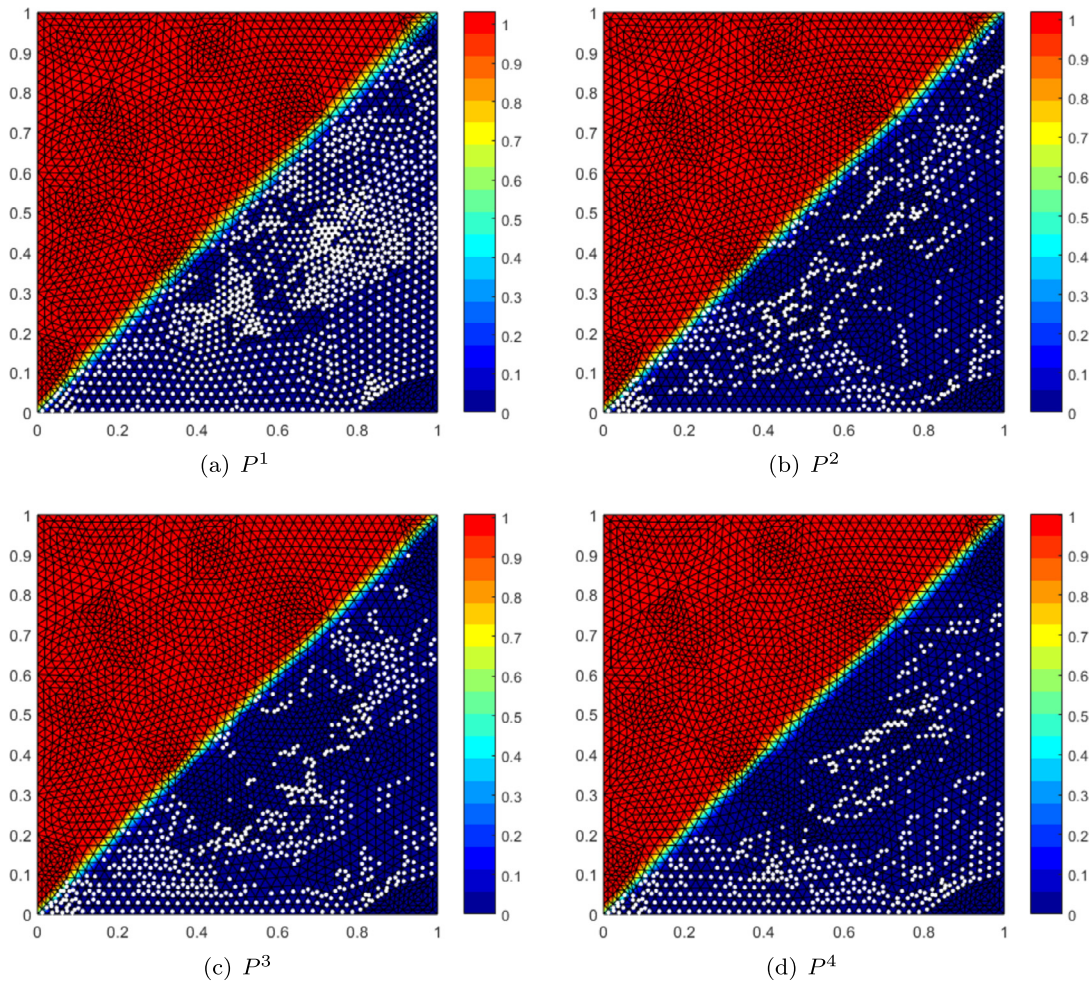
Fig. 8. The meshes and the contours of the radiative intensity for the transparent model simulated by the DG schemes with the scaling-limiter-preferred procedure on the mesh size $h = \frac{1}{40}$. The white points represent the cells where the positivity-preserving limiters have been performed in the computation.
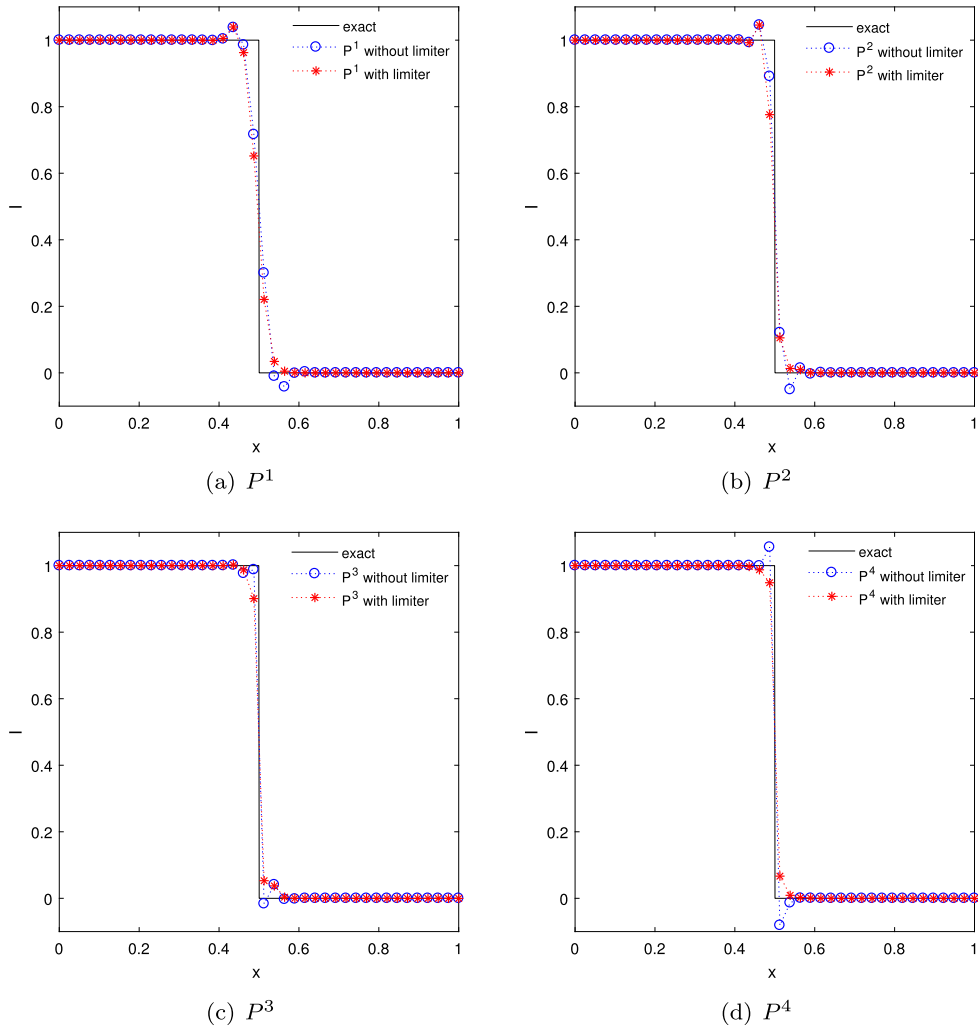
Fig. 9. The comparison of the radiative intensity cut along $y = 0.5$ for the transparent model simulated by the DG schemes without the positivity-preserving limiters and with the scaling-limiter-preferred procedure on the mesh size $h = \frac{1}{40}$. The dots represent the radiative intensity at the points $(\frac{i}{39}, 0.5)$, $i = 0, 1, \cdots, 39$.

This problem is a two-dimensional transparent medium which is described by equation (2.12) with $\sigma_t = 0$, $\sigma_s = 0$ and the source term $q = 0$. The computational domain is $[0, 1] \times [0, 1]$. $\zeta = 0.7$, $\eta = 0.7$. The boundary conditions are

$$I(x, 0, \zeta, \eta) = 0, \quad I(0, y, \zeta, \eta) = 1. \tag{5.2}$$

The problem has the exact solution given as follows

$$I(x, y, \zeta, \eta) = \begin{cases} 0, & y < \frac{\eta}{\zeta} x, \\ 1, & \text{otherwise}, \end{cases} \tag{5.3}$$

which exhibits a discontinuity along with $y = \frac{\eta}{\zeta} x$. Notice that we generate the triangular meshes on the computational domain by MATLAB pdetool for all examples. The triangular meshes which are shown in Figs. 8 and 11 don't align with the discontinuity in the solution.

In this test, a negative solution will appear if we do not adopt the positivity-preserving limiter in the DG schemes, while the DG schemes with the positivity-preserving limiter can always get a nonnegative solution. Figs. 8(a)(b)(c)(d) show the contours of the radiative intensity obtained by the $\{P^1, P^2, P^3, P^4\}$ DG schemes with the mesh size $h = \frac{1}{40}$ and the cells where the scaling-limiter-preferred procedure has been enacted in the simulation, respectively. Figs. 11(a)(b)(c)(d) show the case with the rotational-limiter-preferred procedure. In these pictures, we mark the cells where the positivity-preserving limiter has been performed by discrete white points as well. It can be seen that, by using two types of limiters a positive solution can be obtained in our numerical experiments. Figs. 9–10 show the comparison of the radiative intensity cut along the lines $y = 0.5$ and $x = 0.5$ obtained by $P^k (k = 1, 2, 3, 4)$ DG schemes without the positivity-preserving limiters and
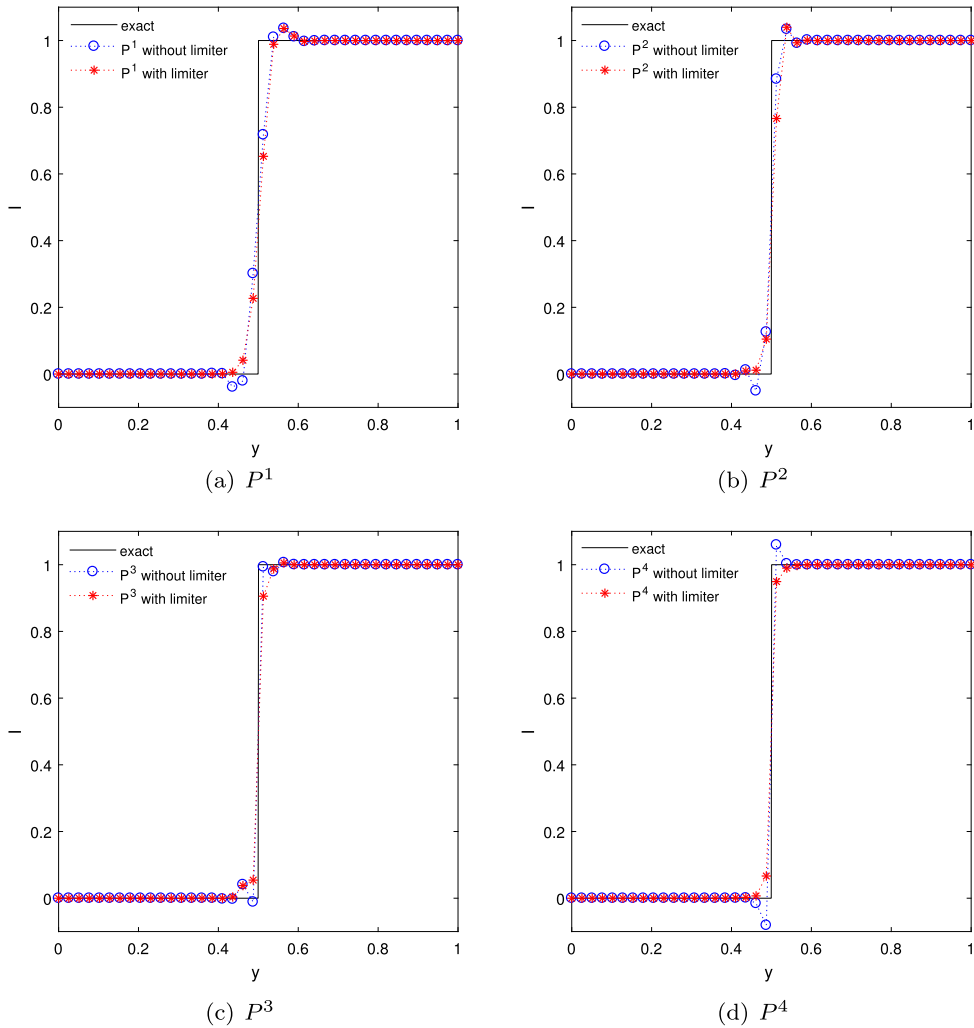
Fig. 10. The comparison of the radiative intensity cut along $x = 0.5$ for the transparent model simulated by the DG schemes without the positivity-preserving limiters and with the scaling-limiter-preferred procedure on the mesh size $h = \frac{1}{40}$. The dots represent the radiative intensity at the points $(0.5, \frac{i}{39})$, $i = 0, 1, \cdots, 39$.

with the scaling-limiter-preferred procedure on the mesh size $h = \frac{1}{40}$, respectively. And Figs. 12–13 show the comparison of the radiative intensity cut along the lines $y = 0.5$ and $x = 0.5$ obtained by $P^k (k = 1, 2, 3, 4)$ DG schemes without the positivity-preserving limiters and with the rotational-limiter-preferred procedure on the mesh size $h = \frac{1}{40}$, respectively. From these pictures, we can observe that the positivity-preserving limiter is necessary for the DG schemes to produce nonnegative solutions and the limiter can also maintain good resolution.

Notice that in this paper, we have not used any nonoscillatory limiters such as the TVB limiter [3], the WENO limiter [31], or the HWENO limiter [32]. So in Figs. 9–10 and Figs. 12–13, there are some localized spurious oscillations near the discontinuities in the numerical solutions, which are not eliminated by the positivity-preserving limiters if they are not near zero.

Example 5.3 (*The positivity-preserving test of the DG schemes for the two-dimensional steady radiative transfer equation simulating the purely absorbing model [26]*).

We test the schemes on the purely absorbing model expressed by (2.12) with $\sigma_t = 1$, $\sigma_s = 0$, and $q = 0$. The computational domain is $[0, 1] \times [0, 1]$. $\zeta = 0.7$, $\eta = 0.7$. The boundary conditions are

$$I(x, 0, \zeta, \eta) = 0, \quad I(0, y, \zeta, \eta) = 1. \tag{5.4}$$

In this case, the problem has the exact solution given as follows:

(a) P^1

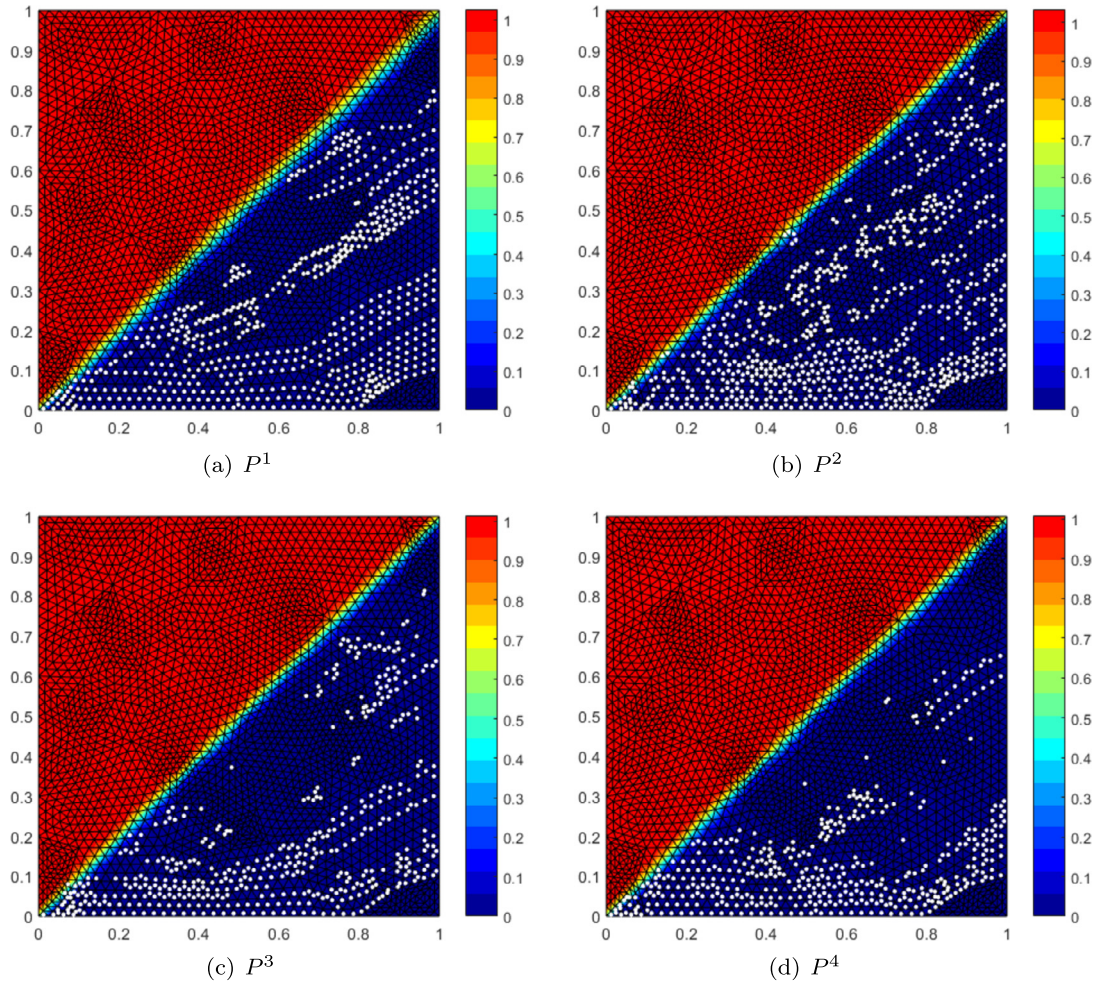(b) P^2

(c) P^3

(d) P^4

Fig. 11. The meshes and the contours of the radiative intensity for the transparent model simulated by the DG schemes with the rotational-limiter-preferred procedure on the mesh size $h = \frac{1}{40}$. The white points represent the cells where the positivity-preserving limiters have been performed in the computation.

$$I(x, y, \zeta, \eta) = \begin{cases} 0, & y < \frac{\eta}{\zeta}x, \\ e^{-\frac{\sigma_t}{\zeta}x}, & \text{otherwise,} \end{cases} \tag{5.5}$$

which exhibits a discontinuity along with $y = \frac{\eta}{\zeta}x$. Notice that the triangular meshes used in this example don't align with the discontinuity in the solution.

Similarly as the last example, a negative solution will appear if we do not adopt the positivity-preserving limiter. Figs. 14(a)(b)(c)(d) plot the contours of the radiative intensity simulated by the $\{P^1, P^2, P^3, P^4\}$ DG schemes with the scaling-limiter-preferred procedure, respectively. Fig. 17 shows the case with the rotational-limiter-preferred procedure. In Figs. 15–16, the comparison of the radiative intensity cut along the lines $y = 0.5$ and $x = 0.5$ obtained by P^k $(k = 1, 2, 3, 4)$ DG schemes without the positivity-preserving limiters and with the scaling-limiter-preferred procedure on the mesh size $h = \frac{1}{40}$ are shown, respectively. And in Figs. 18–19, the comparison of the radiative intensity cut along the lines $y = 0.5$ and $x = 0.5$ obtained by $P^k(k = 1, 2, 3, 4)$ DG schemes without the positivity-preserving limiters and with the rotational-limiter-preferred procedure are presented, respectively. We can clearly see that our positivity-preserving DG schemes can keep the radiative intensity positive during the simulation on triangular meshes.

We plot the comparison of the radiative intensity cut along the line $y = 0.5$ obtained by P^4 DG scheme with the mesh sizes $h = \frac{1}{10}, \frac{1}{20}, \frac{1}{40}, \frac{1}{80}$ in Fig. 20, and the comparison of the radiative intensity cut along the line $x = 0.5$ in Fig. 21. We can easily see that the resolution near the discontinuities of the solution is better with the mesh size $h = \frac{1}{80}$ compared to the solutions obtained with the mesh sizes $h = \frac{1}{10}, \frac{1}{20}$ and $\frac{1}{40}$. We find that the overshoots become weakened as the mesh is refined.
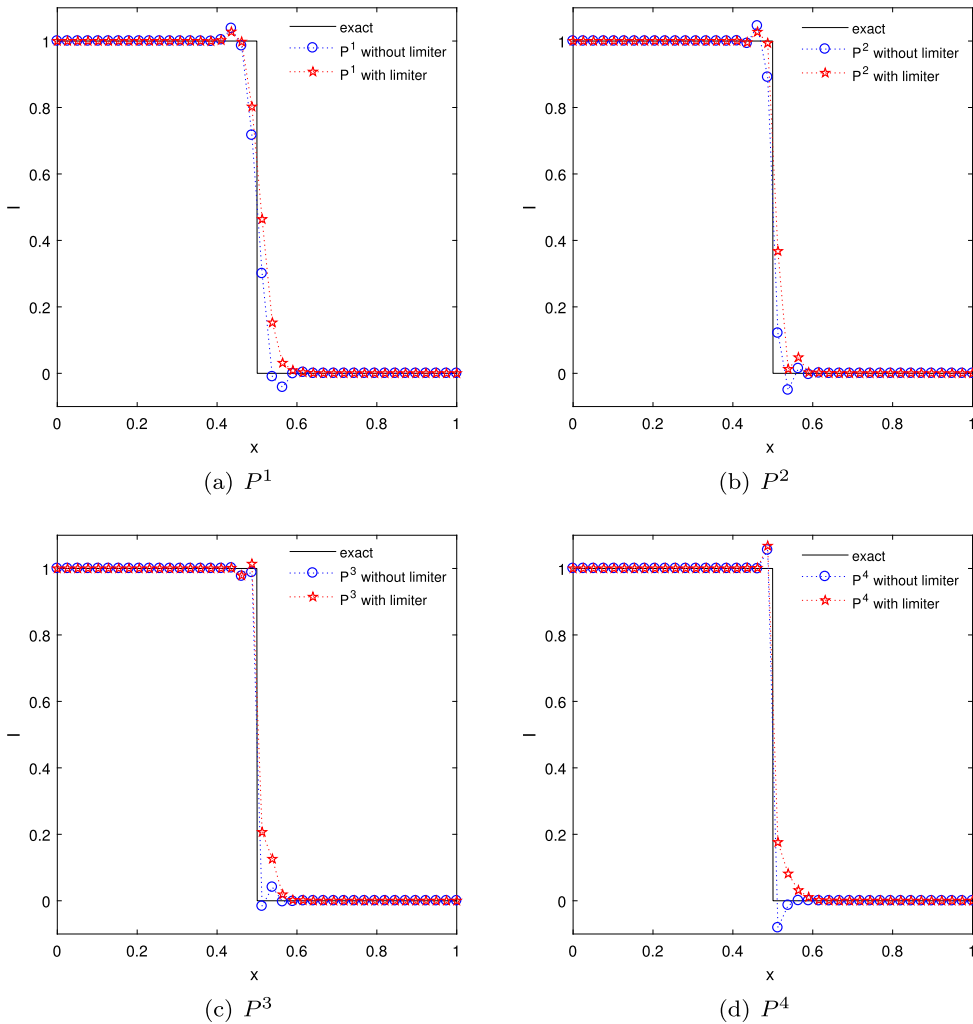
Fig. 12. The comparison of the radiative intensity cut along the line $y = 0.5$ for the transparent model simulated by the DG schemes without the positivity-preserving limiters and with the rotational-limiter-preferred procedure on the mesh size $h = \frac{1}{40}$. The dots represent the radiative intensity at the points $(\frac{i}{39}, 0.5)$, $i = 0, 1, \cdots, 39$.

Like the previous example, in Figs. 15–16 and Figs. 18–19, there are some localized spurious oscillations near the discontinuities in the numerical solution, which are not eliminated by the positivity-preserving limiters if they are not near zero.

Example 5.4 *(The positivity-preserving test of the DG schemes for the two-dimensional steady radiative transfer equation simulating the purely absorbing model on circular domain).*

In order to show the advantage of the triangular meshes to handle complicated geometries, we test the schemes for the two-dimensional steady radiative transfer equation (2.12) on a circular domain. In this example, we take $\sigma_t = 1$, $\sigma_s = 0$, and $q = 0$. The computational domain is a unit disk $(x^2 + y^2) \leq 1$, and $\zeta = 0.4$, $\eta = -0.7$. We define $\partial \mathbb{D}_{in} = \{(x, y)|x^2 + y^2 = 1, \boldsymbol{n}(x, y) \cdot \Omega < 0\}$ and the boundary condition is

$$I(x, y, \zeta, \eta) = \sin^8(\pi(x + y)), \quad (x, y) \in \partial \mathbb{D}_{in}, \tag{5.6}$$

where $\boldsymbol{n}(x, y)$ is the unit outward normal vector at the point (x, y) on the boundary $x^2 + y^2 = 1$ and the vector $\Omega = (\zeta, \eta)$. In this problem, we have the exact solution as follows:

$$I(x, y, \zeta, \eta) = \sin^8(\pi(x + y - (\zeta + \eta)\xi))e^{-\sigma_t \xi}, \tag{5.7}$$

with $\xi = (\zeta x + \eta y + \sqrt{\zeta^2 + \eta^2 - (\eta x - \zeta y)^2})/(\zeta^2 + \eta^2)$.

Fig. 22 shows the contours of the radiative intensity simulated by the $\{P^1, P^2, P^3, P^4\}$ DG schemes with the scaling-limiter-preferred procedure, respectively, while Fig. 23 shows the case with the rotational-limiter-preferred procedure. Our
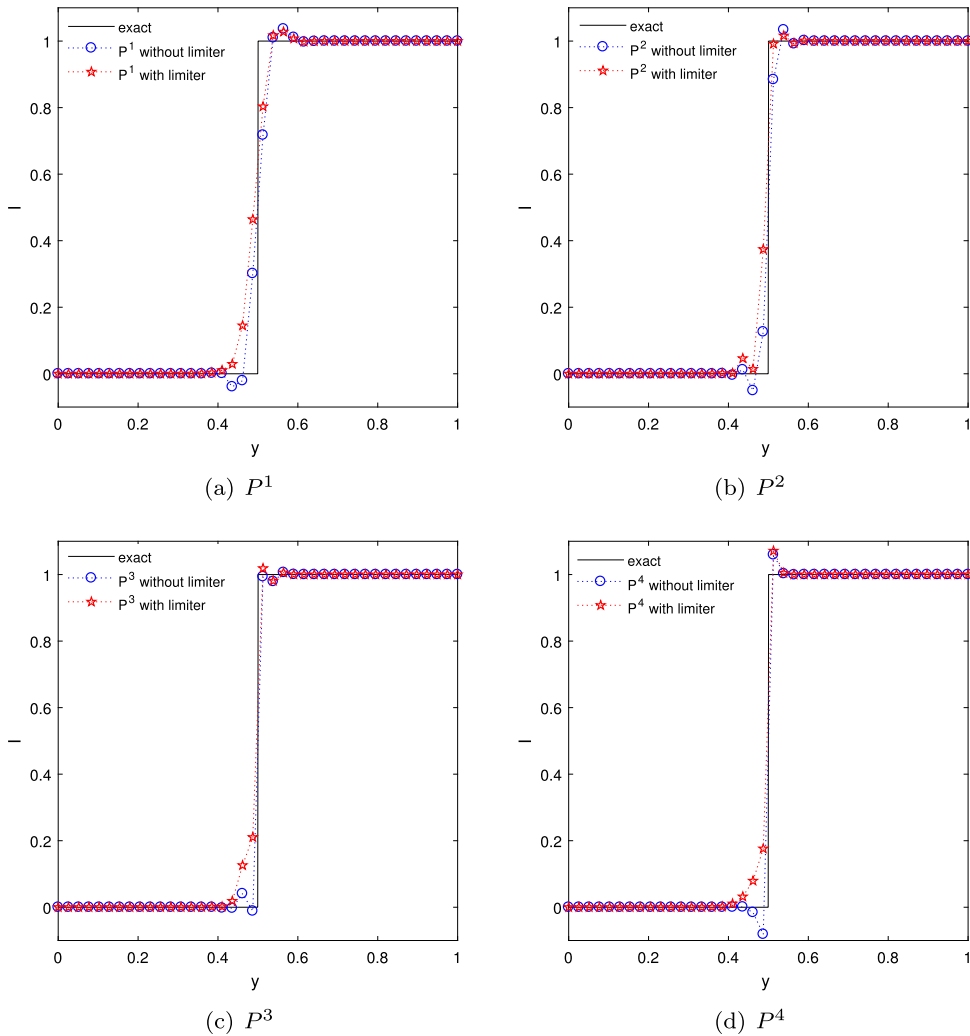
Fig. 13. The comparison of the radiative intensity cut along the line $x = 0.5$ for the transparent model simulated by the DG schemes without the positivity-preserving limiters and with the rotational-limiter-preferred procedure on the mesh size $h = \frac{1}{40}$. The dots represent the radiative intensity at the points $(0.5, \frac{i}{39})$, $i = 0, 1, \cdots, 39$.

schemes with the positivity-preserving limiters obtain a positive solution while the negative solution appears when we do not use the positivity-preserving limiters. From the figures we can see that, our limiters perform very well similarly as in the previous examples on the triangular meshes. The positivity of the radiative intensity is preserved by both positivity-preserving limiters.

Example 5.5 *(The positivity-preserving test of the DG schemes for the two-dimensional steady radiative transfer equation simulating the purely scattering models).*

In this problem, we test the schemes on the purely scattering model (2.12) with $\sigma_t = 1$, $\sigma_s = 1$, and $q = 0$. The computational domain is $[0, 1] \times [0, 1]$. The boundary condition is set as follows:

$$
\begin{aligned}
I(x, 0, \zeta, \eta) = 0, && \eta > 0; && I(x, 1, \zeta, \eta) = 0, && \eta < 0; \\
I(0, y, \zeta, \eta) = 1 - \cos(4\pi y), && \zeta > 0; && I(1, y, \zeta, \eta) = 0, && \zeta < 0.
\end{aligned}
\tag{5.8}
$$

Figs. 24(a)(b)(c)(d) show the contours of the radiative intensity in the direction $\Omega = (0.2578, 0.1068)$ simulated by the $\{P^1, P^2, P^3, P^4\}$ DG schemes with the scaling-limiter-preferred procedure and the cells where the positivity-preserving limiters have been enacted in the simulation, respectively. Fig. 25 shows the case with the rotational-limiter-preferred procedure. The white points mean the cells enacted by the positivity-preserving limiters in our simulation. We can see that the numerical results verify the positivity-preserving property of our schemes again. The results also indicate the effectiveness of our schemes on triangular meshes.
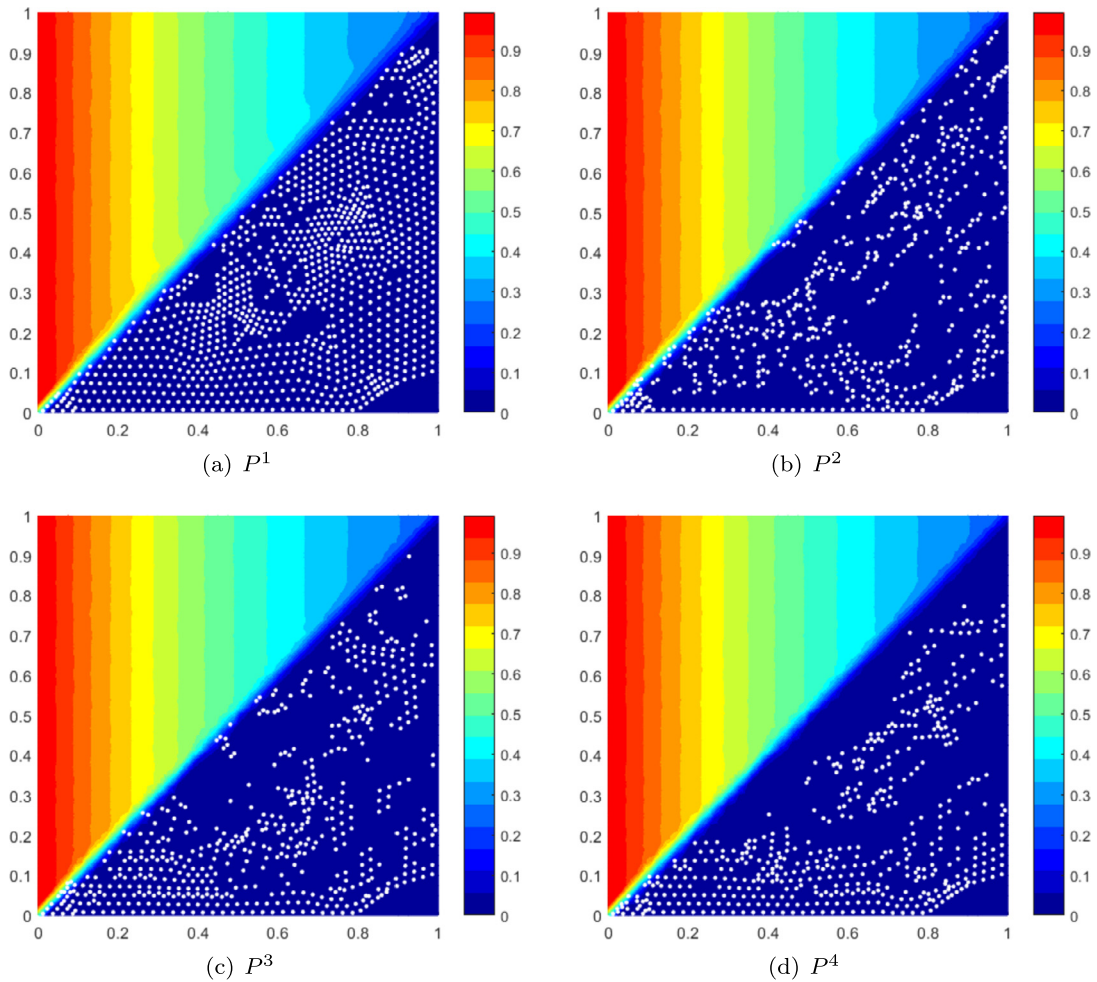
Fig. 14. The contours of the radiative intensity for the purely absorbing model simulated by the DG schemes with the scaling-limiter-preferred procedure on the mesh size $h = \frac{1}{40}$. The white points represent the cells where the positivity-preserving limiters have been enacted in the computation.

In order to see how the method behaves in the diffusive regime, where the problem is purely scattering and the problem is optically thick, we repeat the example with $\sigma_t = \sigma_s = 100$. We plot the numerical radiative intensity contours obtained with the scaling-limiter-preferred procedure and with the rotational-limiter-preferred procedure in Figs. 26 and 27, respectively. The figures show that our positivity-preserving limiters can also work well in diffusive regime.

Additionally, we list the number of the source iterations simulated by the $\{P^1, P^2, P^3, P^4\}$ DG schemes (with the mesh size $h = \frac{1}{40}$) with the positivity-preserving limiters and without the limiters in Table 5. We can see that our positivity-preserving limiters do not degrade the iterative performance for the diffusive problem.

Example 5.6 (*The accuracy test of the DG schemes for the two-dimensional unsteady radiative transfer equation simulating the absorbing-scattering model*).

To verify our schemes can keep both properties of high order accuracy and positivity-preserving for the two-dimensional unsteady radiative transfer equation (2.11), we take $\sigma_t = 22000$, $\sigma_s = 1$ and the source term $q(x, y, \zeta, \eta, t) = e^t \big(- 2\pi (\zeta + \eta)(\zeta^2 + \eta^2) \cos^3(\frac{\pi}{2}(x + y)) \sin(\frac{\pi}{2}(x + y)) + (\frac{1}{c} + \sigma_t)((\zeta^2 + \eta^2) \cos^4(\frac{\pi}{2}(x + y)) + a) - \sigma_s(\frac{2}{3} \cos^4(\frac{\pi}{2}(x + y)) + a) \big)$. Here the photon speed $c = 3.0 \times 10^8$, and the small parameter $a = 10^{-14}$ is used to ensure the source term to be nonnegative. The computational domain is $[0, 1] \times [0, 1]$. The initial condition is

$$I(x, y, \zeta, \eta, 0) = (\zeta^2 + \eta^2) \cos^4(\frac{\pi}{2}(x + y)) + a, \tag{5.9}$$
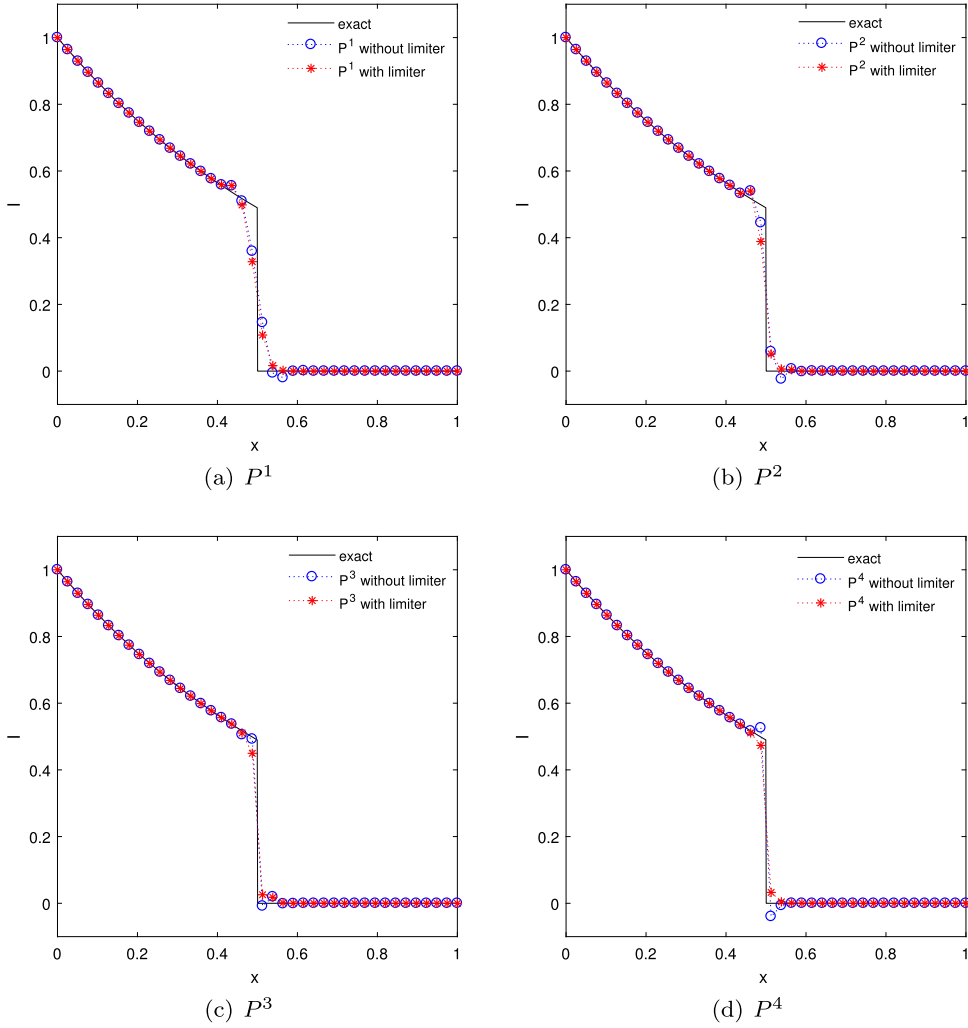
and the boundary conditions are

Fig. 15. The comparison of the radiative intensity cut along the line $y = 0.5$ for the purely absorbing model simulated by the DG schemes without the positivity-preserving limiters and with the scaling-limiter-preferred procedure on the mesh size $h = \frac{1}{40}$. The dots represent the radiative intensity at the points $(\frac{i}{39}, 0.5)$, $i = 0, 1, \cdots, 39$.

$$I(x, 0, \zeta, \eta, t) = e^t \left((\zeta^2 + \eta^2) \cos^4(\frac{\pi}{2} x) + a \right), \qquad \eta > 0,$$

$$I(x, 1, \zeta, \eta, t) = e^t \left((\zeta^2 + \eta^2) \cos^4\left(\frac{\pi}{2}(x+1)\right) + a \right), \quad \eta < 0,$$

$$I(0, y, \zeta, \eta, t) = e^t \left((\zeta^2 + \eta^2) \cos^4(\frac{\pi}{2} y) + a \right), \qquad \zeta > 0,$$

$$I(1, y, \zeta, \eta, t) = e^t \left((\zeta^2 + \eta^2) \cos^4\left(\frac{\pi}{2}(y+1)\right) + a \right), \quad \zeta < 0.$$

(5.10)

Obviously, the exact solution can be expressed as:

$$I(x, y, \zeta, \eta, t) = e^t \left((\zeta^2 + \eta^2) \cos^4(\frac{\pi}{2}(x+y)) + a \right).$$

(5.11)

It is a unsteady problem on a rectangle domain. The final computational time is $t = 0.1$, and in order to make the spatial accuracy dominated, we choose the small time step $\Delta t = 10^{-3}$. Similarly, a negative solution will appear if we do not adopt the positivity-preserving limiter in the DG schemes, while the DG schemes with the positivity-preserving limiter can always maintain the nonnegative solution. We show the contours of the radiative intensity in the direction $\Omega = (-0.7860, 0.3255)$ simulated by the DG schemes with the mesh size $h = \frac{1}{40}$ with the scaling-limiter-preferred procedure in Fig. 28 and with the rotational-limiter-preferred procedure in Fig. 29, respectively. The white points represent the cells where the positivity-preserving limiters have been enacted in the simulation. The errors and orders of accuracy for the $\{P^1, P^2, P^3, P^4\}$ DG schemes without the positivity-preserving limiters and with the positivity-preserving limiters
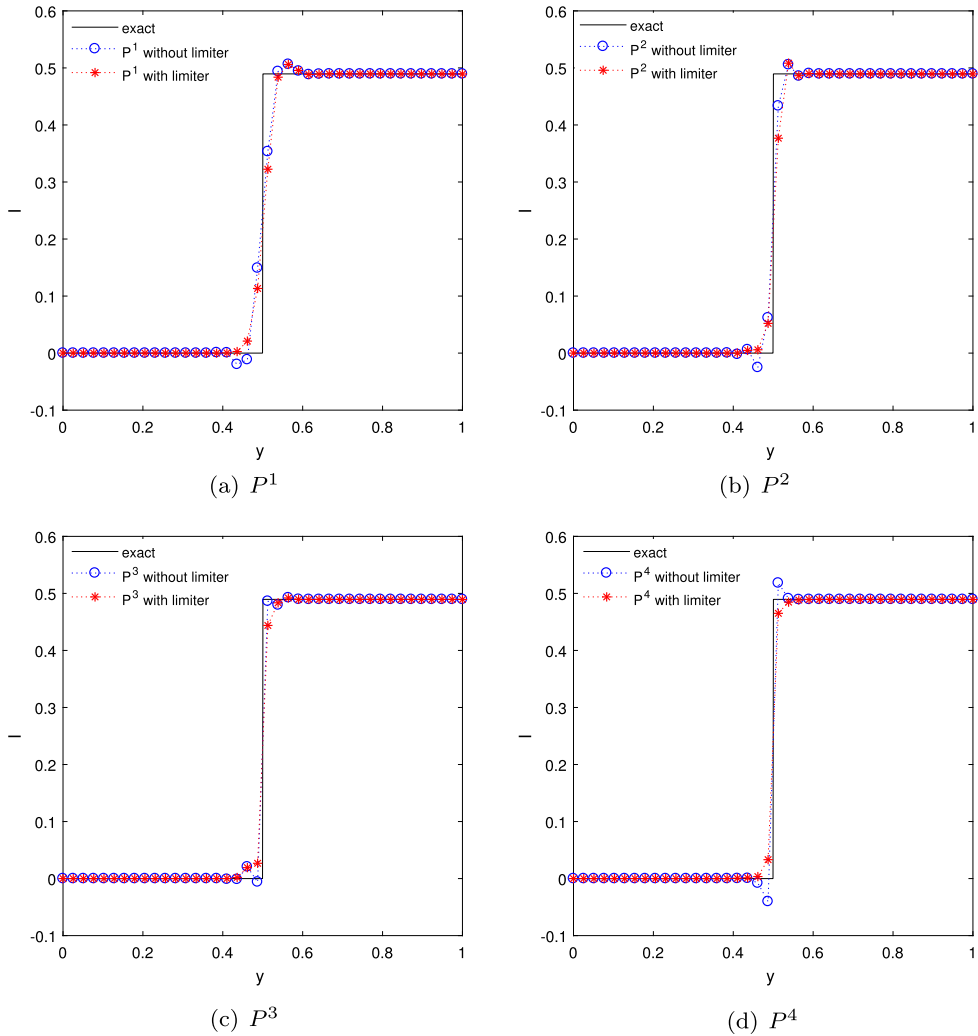
Fig. 16. The comparison of the radiative intensity cut along the line $x = 0.5$ for the purely absorbing model simulated by the DG schemes without the positivity-preserving limiters and with the scaling-limiter-preferred procedure on the mesh size $h = \frac{1}{40}$. The dots represent the radiative intensity at the points $(0.5, \frac{i}{39})$, $i = 0, 1, \cdots, 39$.

Table 5
The iterative numbers of the source iteration combined with positivity-preserving limiters and without limiters.

	P^k	Without limiters	Scaling limiter preferred	Rotational limiter preferred
	P^1	21	21	21
$\sigma_t = 1$	P^2	21	21	21
$\sigma_s = 1$	P^3	21	21	21
	P^4	21	21	21
	P^1	16282	16239	16312
$\sigma_t = 100$	P^2	16284	16262	16304
$\sigma_s = 100$	P^3	16284	16274	16291
	P^4	16284	16280	16286

(both the scaling-limiter-preferred and the rotational-limiter-preferred procedures) are shown in the Tables 6–9, respectively. In these tables, we also list the percentage of the cells where either the scaling positivity-preserving limiter or the rotational positivity-preserving limiter has been enacted in the computation, respectively. We also show the conservation errors in the tables. We notice that the conservation error goes to 0 with the refinement of the mesh, and higher order DG schemes generate smaller conservation errors. The numerical results verify the properties of high order accuracy and positivity-preserving of our schemes.
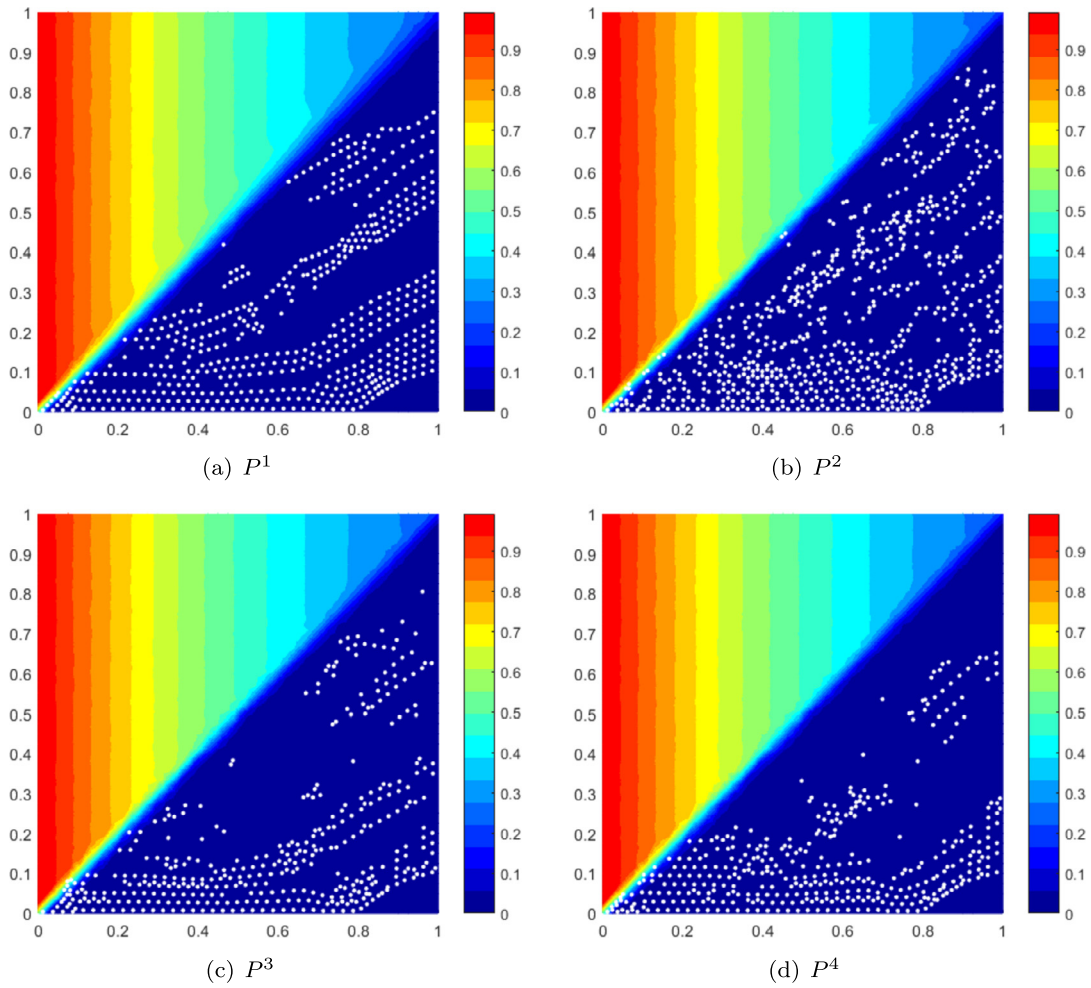
(a) P^1

(b) P^2

(c) P^3

(d) P^4

Fig. 17. The contours of the radiative intensity for the purely absorbing model simulated by the DG schemes with the rotational-limiter-preferred procedure on the mesh size $h = \frac{1}{40}$. The white points represent the cells where the positivity-preserving limiters have been performed in the computation.

Example 5.7 (*The positivity-preserving test of the DG schemes for the two-dimensional unsteady radiative transfer equation simulating the purely absorbing model on circular domain*).

In this final example, we test the schemes for the two-dimensional unsteady radiative transfer equation (2.11) on a circular domain where the triangular meshes are used to handle such irregular geometry. Take $\sigma_t = 22000$, $\sigma_s = 0$, and the source term $q(x, y, \zeta, \eta, t) = e^t \big((\sigma_t + \frac{1}{c})((\zeta^2 + \eta^2) \cos^4(\pi(x^2 + y^2)) + a) - 8\pi(\zeta x + \eta y)(\zeta^2 + \eta^2) \cos^3(\pi(x^2 + y^2)) \sin(\pi(x^2 + y^2)) \big)$. $\zeta = -0.8$, $\eta = -0.8$. $c = 3.0 \times 10^8$, and $a = 10^{-14}$ is used to ensure the source term to be nonnegative. The computational domain is a unit disk $(x^2 + y^2) \leq 1$. The initial condition is

$$I(x, y, \zeta, \eta, 0) = (\zeta^2 + \eta^2) \cos^4(\pi(x^2 + y^2)) + a, \tag{5.12}$$

We define $\partial \mathbb{D}_{in} = \{(x, y) | x^2 + y^2 = 1, \boldsymbol{n}(x, y) \cdot \Omega < 0\}$ and the boundary condition is

$$I(x, y, \zeta, \eta, t) = e^t \big((\zeta^2 + \eta^2) + a \big), \quad (x, y) \in \partial \mathbb{D}_{in}, \tag{5.13}$$

where $\boldsymbol{n}(x, y)$ is the unit outward normal vector at the point (x, y) on the boundary $x^2 + y^2 = 1$ and vector $\Omega = (\zeta, \eta)$. The exact solution can be expressed as:

$$I(x, y, \zeta, \eta, t) = e^t \big((\zeta^2 + \eta^2) \cos^4(\pi(x^2 + y^2)) + a \big). \tag{5.14}$$

It is a unsteady problem on a circular domain. The final computational time is $t = 0.1$. We choose the small time step $\Delta t = 10^{-3}$ similar as the last example. Similarly, a negative solution will appear if we do not adopt the positivity-preserving limiter in the DG schemes, while the DG schemes with the positivity-preserving limiter can always maintain the nonnegative solution. Figs. 30(a)(c)(e)(g) plot the contours of the radiative intensity simulated by the $\{P^1, P^2, P^3, P^4\}$ DG schemes without the positivity-preserving limiters, and the corresponding negative values are shown in Figs. 30(b)(d)(f)(h), respectively.
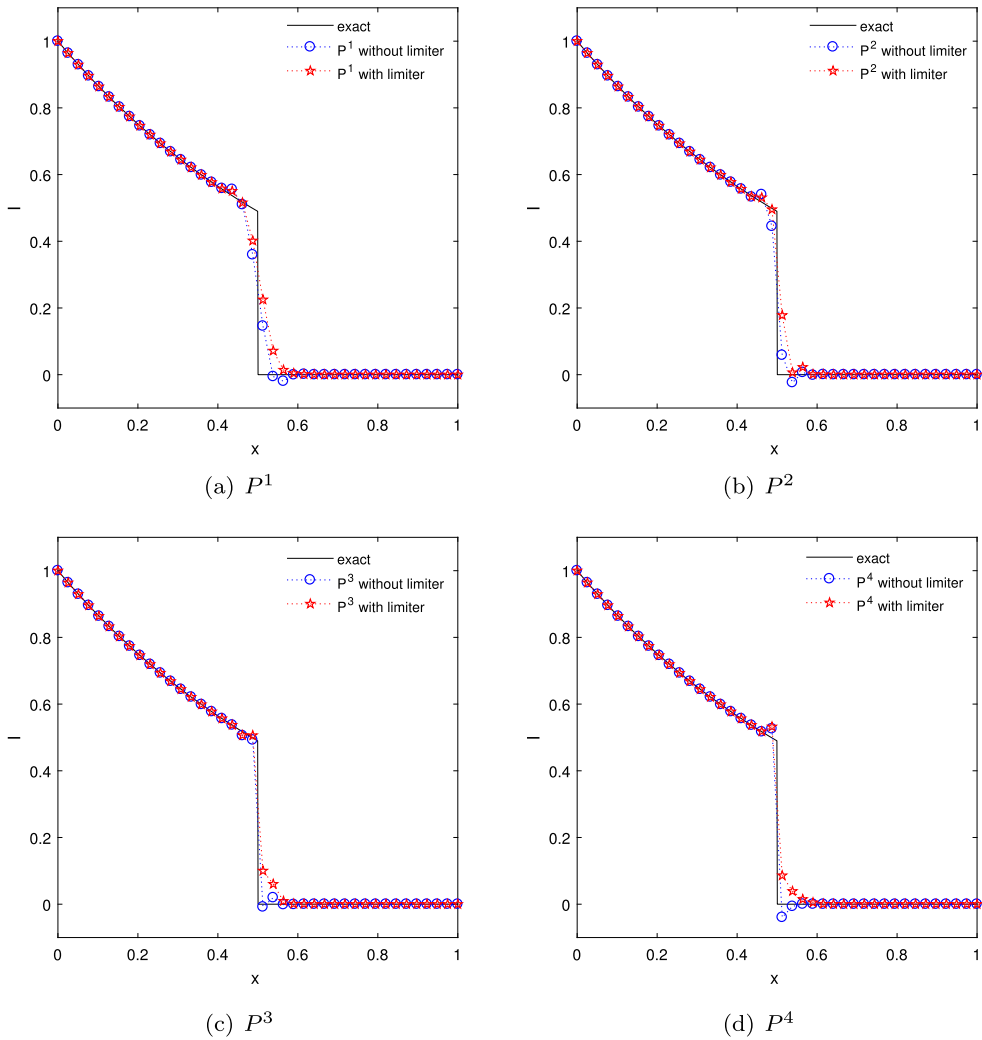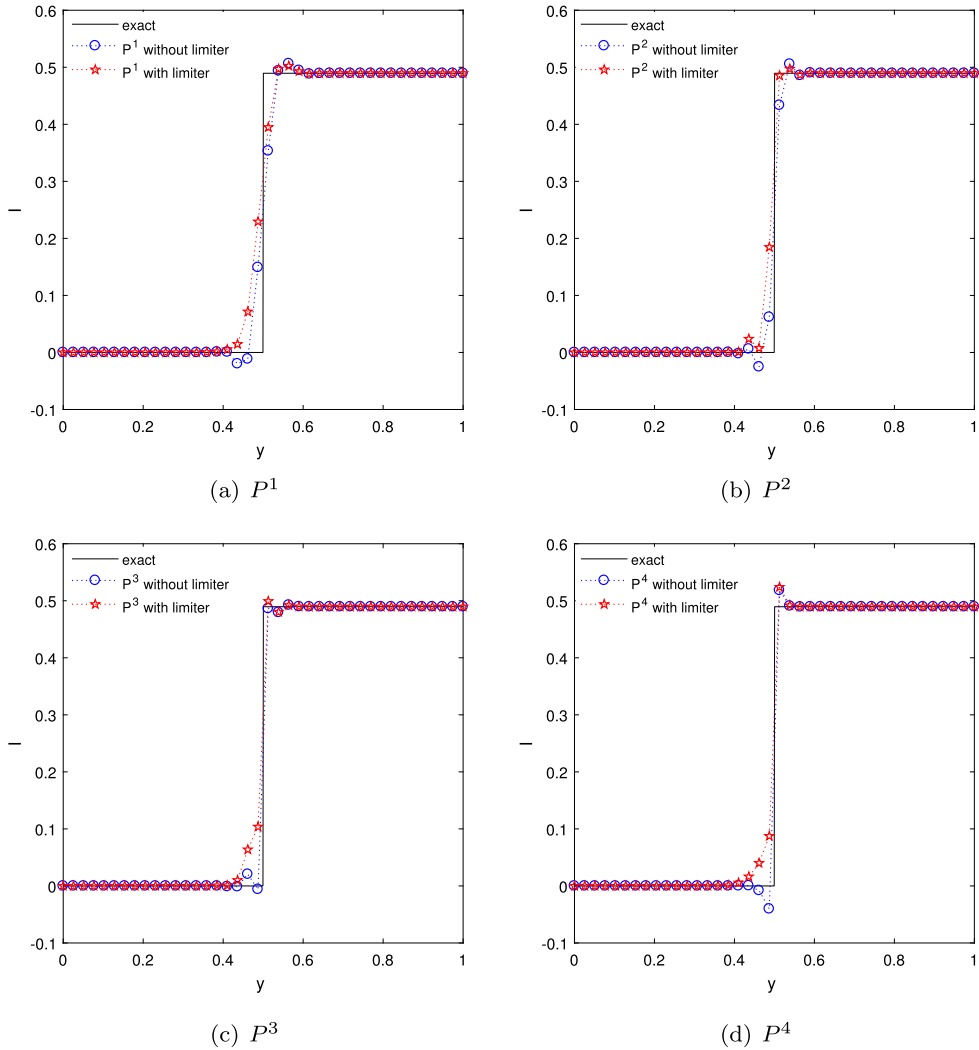
Fig. 18. The comparison of the radiative intensity cut along the line $y = 0.5$ for the purely absorbing model simulated by the DG schemes without the positivity-preserving limiters and with the rotational-limiter-preferred procedure on the mesh size $h = \frac{1}{40}$. The dots represent the radiative intensity at the points $(\frac{i}{39}, 0.5)$, $i = 0, 1, \cdots, 39$.

Table 6
Errors of the P^1 DG scheme for the two-dimensional unsteady radiative transfer equation simulating the absorbing-scattering model on triangular meshes.

h	L^1-error	Order	L^∞-error	Order	limiter(%)	c_err
Without positivity-preserving limiter						
1/10	1.339E-03		1.751E-02			
1/20	3.353E-04	1.998	4.813E-03	1.863		
1/40	8.390E-05	1.999	1.253E-03	1.941		
1/80	2.099E-05	1.999	3.202E-04	1.969		
With positivity-preserving limiter (scaling limiter preferred)						
1/10	1.367E-03		1.751E-02		36.22	0.0
1/20	3.366E-04	2.022	4.813E-03	1.863	19.63	0.0
1/40	8.394E-05	2.004	1.253E-03	1.941	9.93	0.0
1/80	2.100E-05	1.999	3.202E-04	1.969	5.04	0.0
With positivity-preserving limiter (rotational limiter preferred)						
1/10	1.410E-03		1.751E-02		36.22	9.795E-05
1/20	3.383E-04	2.060	4.813E-03	1.863	19.63	4.338E-06
1/40	8.399E-05	2.010	1.253E-03	1.941	9.92	1.412E-07
1/80	2.100E-05	2.000	3.202E-04	1.969	5.04	4.131E-09

(a) P^1

(b) P^2

(c) P^3

(d) P^4

Fig. 19. The comparison of the radiative intensity cut along the line $x = 0.5$ for the purely absorbing model simulated by the DG schemes without the positivity-preserving limiters and with the rotational-limiter-preferred procedure on the mesh size $h = \frac{1}{40}$. The dots represent the radiative intensity at the points $(0.5, \frac{i}{39})$, $i = 0, 1, \cdots, 39$.

Fig. 31 plots the contours of the radiative intensity simulated by the $\{P^1, P^2, P^3, P^4\}$ DG schemes with the scaling-limiter-preferred procedure, respectively. Fig. 32 shows the cases with the rotational-limiter-preferred procedure. In the Figs. 31 and 32, we mark the cells where the positivity-preserving limiters have been enacted by discrete white points as well. The numerical results verify the positivity-preserving property of our schemes.

6. Conclusion

In this paper, we develop a positivity-preserving limiter which is combined of the scaling positivity-preserving limiter [29] and our two-dimensional rotational positivity-preserving limiter to solve the radiative transfer equations on triangular meshes by the implicit or iterative DG method with P^k polynomials. Our two-dimensional rotational positivity-preserving limiter is constructed based on the one-dimensional rotational positivity-preserving limiter for DG schemes in [26]. The one difficulty for the extension is how to find a special quadrature rule on the triangular element, which is one of the keypoints of this paper, such that the quadrature points can be arranged on certain line segments and on these certain line segments we could use the one-dimensional rotational positivity-preserving limiter. Since the number of the quadrature points is larger than the number of basis functions of P^k polynomial space, the modified polynomial cannot be interpolated directly. To solve this problem, we determine a k-th polynomial by a L_2-norm Least Square subject to its cell average being equal to the weighted average of the values on the quadrature points after using the rotational positivity-preserving limiter, whose weights are the quadrature weights, thus the cell average of the modified polynomial is nonnegative. This
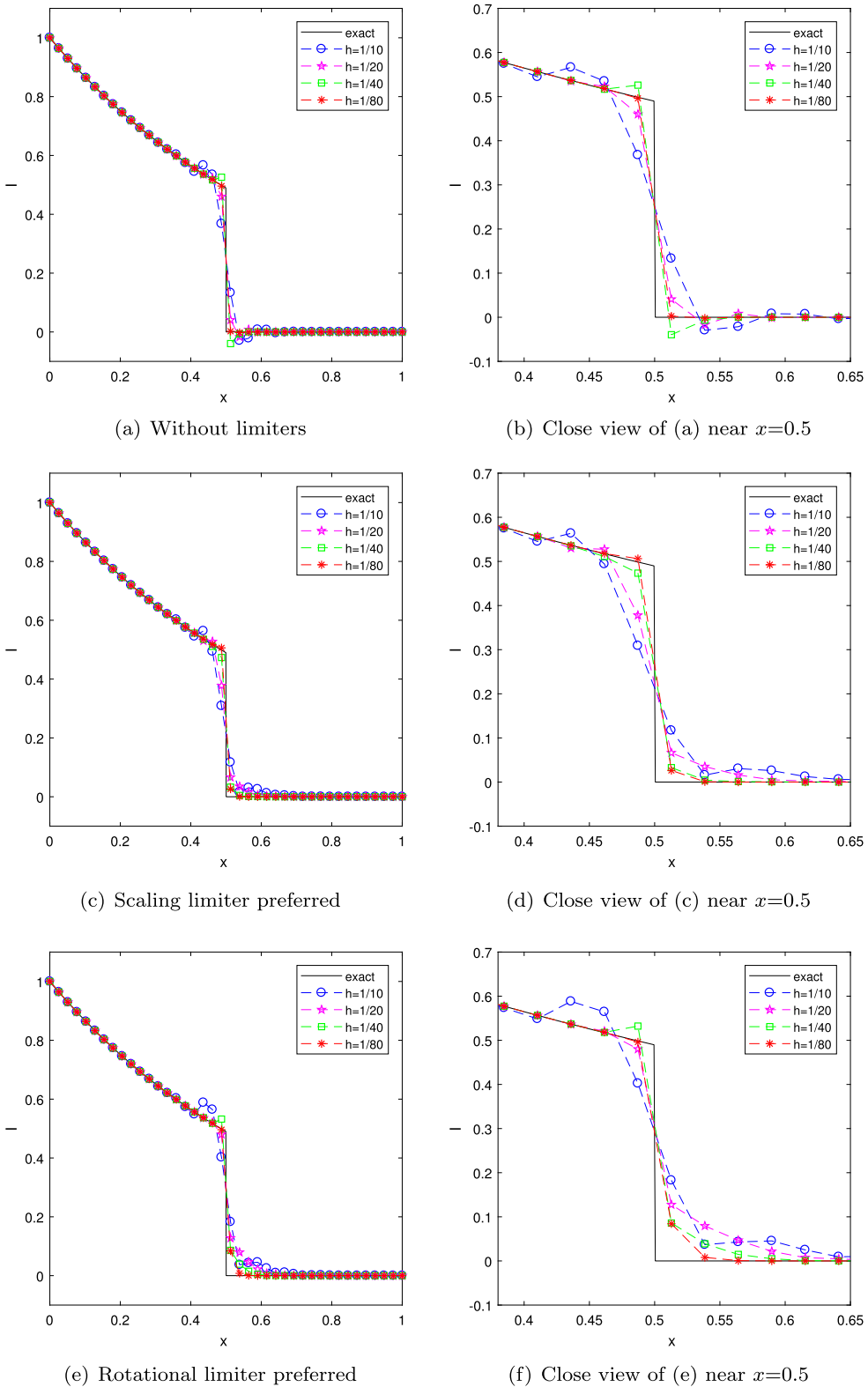
(a) Without limiters

(b) Close view of (a) near x=0.5

(c) Scaling limiter preferred

(d) Close view of (c) near x=0.5

(e) Rotational limiter preferred
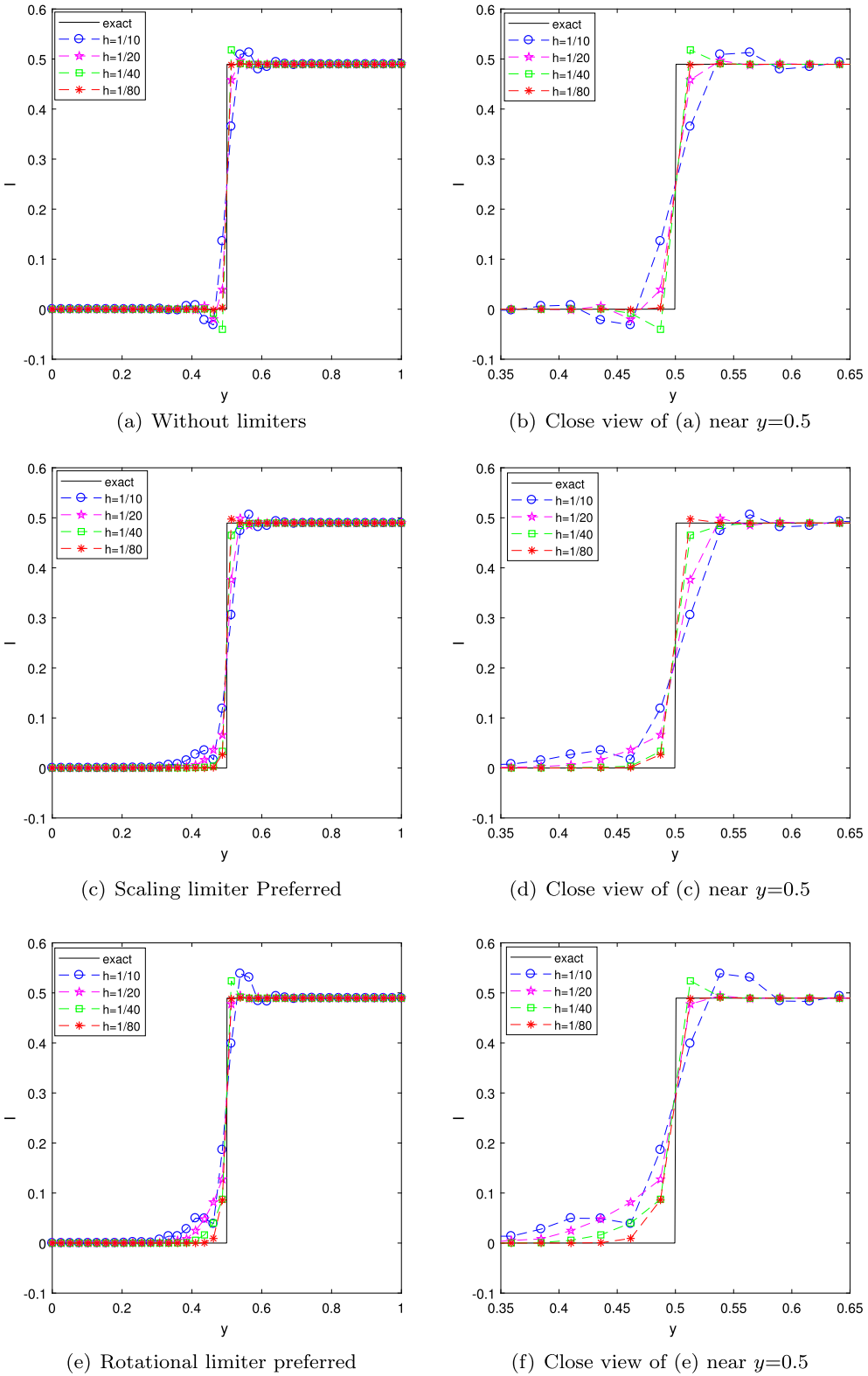
(f) Close view of (e) near x=0.5

Fig. 20. The comparison of the radiative intensity cut along the line $y = 0.5$ for the purely absorbing model obtained by P^4 DG scheme with the mesh sizes $h = \frac{1}{10}, \frac{1}{20}, \frac{1}{40}, \frac{1}{80}$. The dots represent the radiative intensity at the points $(\frac{i}{39}, 0.5)$, $i = 0, 1, \cdots, 39$.

Fig. 21. The comparison of the radiative intensity cut along the line $x = 0.5$ for the purely absorbing model obtained by P^4 DG scheme with the mesh sizes $h = \frac{1}{10}, \frac{1}{20}, \frac{1}{40}, \frac{1}{80}$. The dots represent the radiative intensity at the points $(0.5, \frac{i}{39})$, $i = 0, 1, \cdots, 39$.
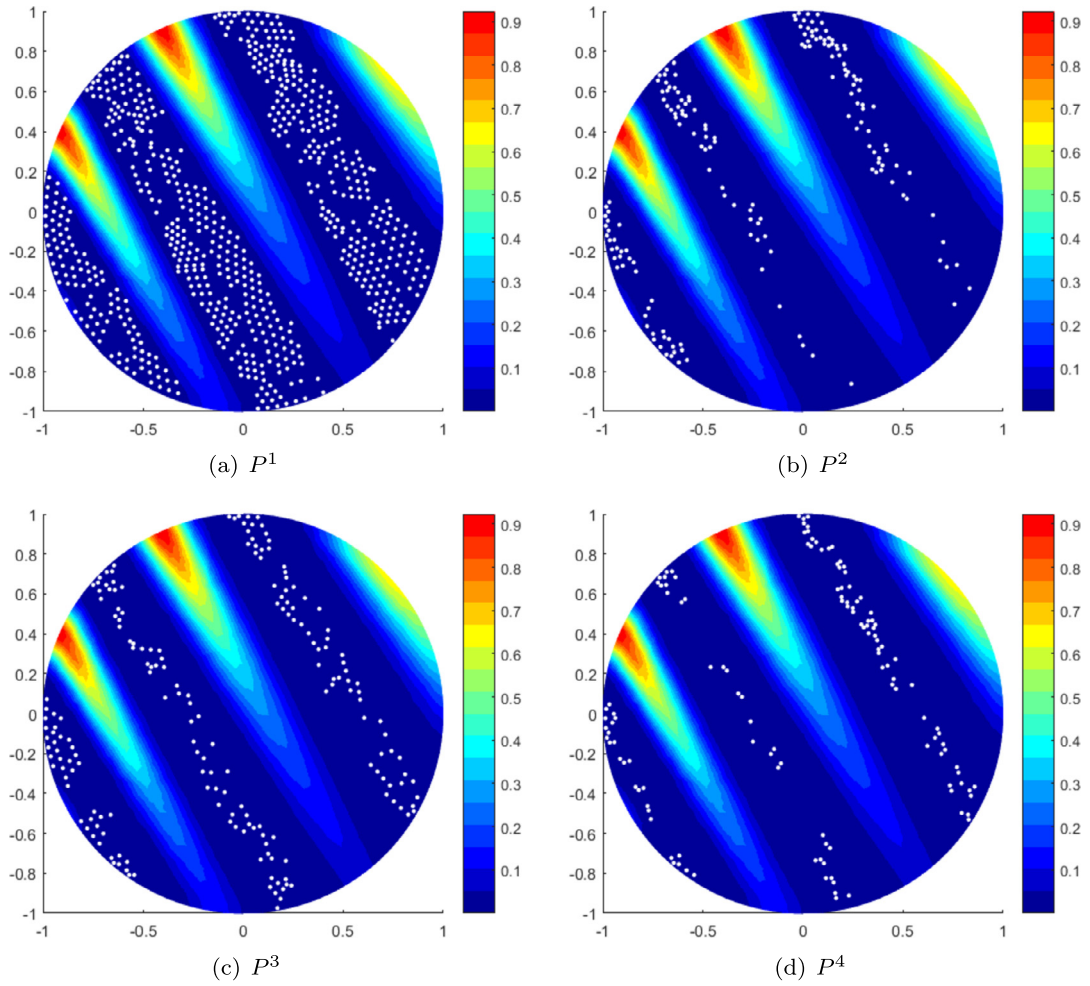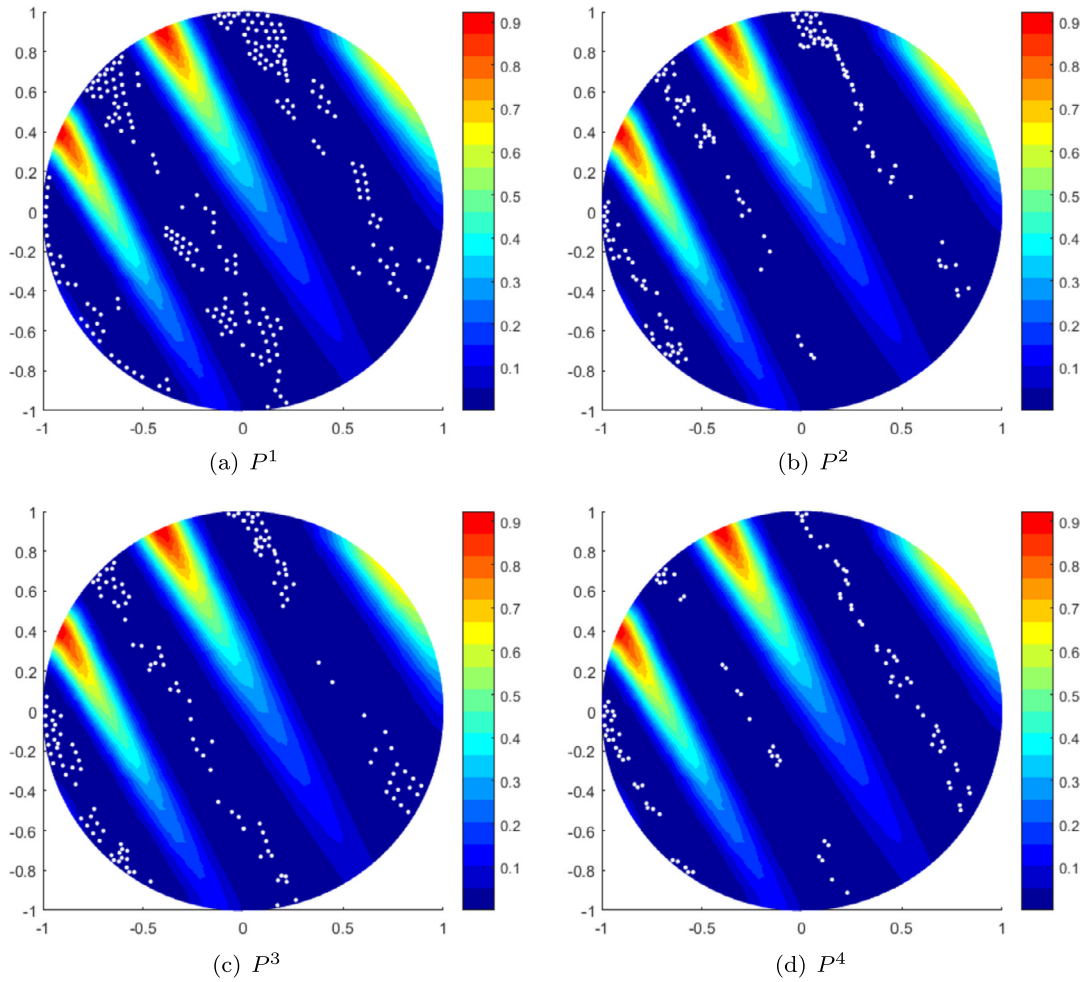
Fig. 22. The contours of the radiative intensity for the purely absorbing model simulating by the DG schemes with the scaling-limiter-preferred procedure on the mesh size $h = \frac{1}{40}$. The white points represent the cells where the positivity-preserving limiters have been enacted in the computation.

Table 7
Errors of the P^2 DG scheme for the two-dimensional unsteady radiative transfer equation simulating the absorbing-scattering model on triangular meshes.

h	L^1-error	Order	L^∞-error	Order	limiter(%)	c_err
Without positivity-preserving limiter						
1/10	9.327E-05		1.683E-03			
1/20	1.174E-05	2.990	2.377E-04	2.824		
1/40	1.468E-06	2.999	3.095E-05	2.942		
1/80	1.836E-07	2.999	3.940E-06	2.973		
With positivity-preserving limiter (scaling limiter preferred)						
1/10	9.404E-05		1.683E-03		12.18	0.0
1/20	1.176E-05	3.000	2.377E-04	2.824	5.85	0.0
1/40	1.469E-06	3.001	3.095E-05	2.942	2.88	0.0
1/80	1.836E-07	3.000	3.940E-06	2.973	1.41	0.0
With positivity-preserving limiter (rotational limiter preferred)						
1/10	9.386E-05		1.683E-03		12.18	4.619E-07
1/20	1.175E-05	2.998	2.377E-04	2.824	5.85	1.385E-08
1/40	1.469E-06	3.001	3.095E-05	2.942	2.88	3.591E-10
1/80	1.836E-07	2.999	3.940E-06	2.973	1.41	1.237E-11

Fig. 23. The contours of the radiative intensity for the purely absorbing model simulating by the DG schemes with the rotational-limiter-preferred procedure on the mesh size $h = \frac{1}{40}$. The white points represent the cells where the positivity-preserving limiters have been enacted in the computation.

Table 8
Errors of the P^3 DG scheme for the two-dimensional unsteady radiative transfer equation simulating the absorbing-scattering model on triangular meshes.

h	L^1-error	Order	L^∞-error	Order	limiter(%)	c_err
Without positivity-preserving limiter						
1/10	5.074E-06		1.201E-04			
1/20	3.193E-07	3.990	7.930E-06	3.920		
1/40	2.000E-08	3.997	5.022E-07	3.981		
1/80	1.254E-09	3.996	3.164E-08	3.989		
With positivity-preserving limiter (scaling limiter preferred)						
1/10	9.199E-06		5.309E-04		19.55	0.0
1/20	4.373E-07	4.395	3.652E-05	3.862	9.94	0.0
1/40	2.310E-08	4.242	2.148E-06	4.087	4.91	0.0
1/80	1.353E-09	4.094	1.502E-07	3.839	2.49	0.0
With positivity-preserving limiter (rotational limiter preferred)						
1/10	7.312E-06		5.255E-04		19.55	1.668E-06
1/20	3.895E-07	4.231	3.584E-05	3.874	9.94	5.266E-08
1/40	2.188E-08	4.154	2.037E-06	4.137	4.91	1.465E-09
1/80	1.310E-09	4.062	1.298E-07	3.971	2.49	4.561E-11

(a) P^1

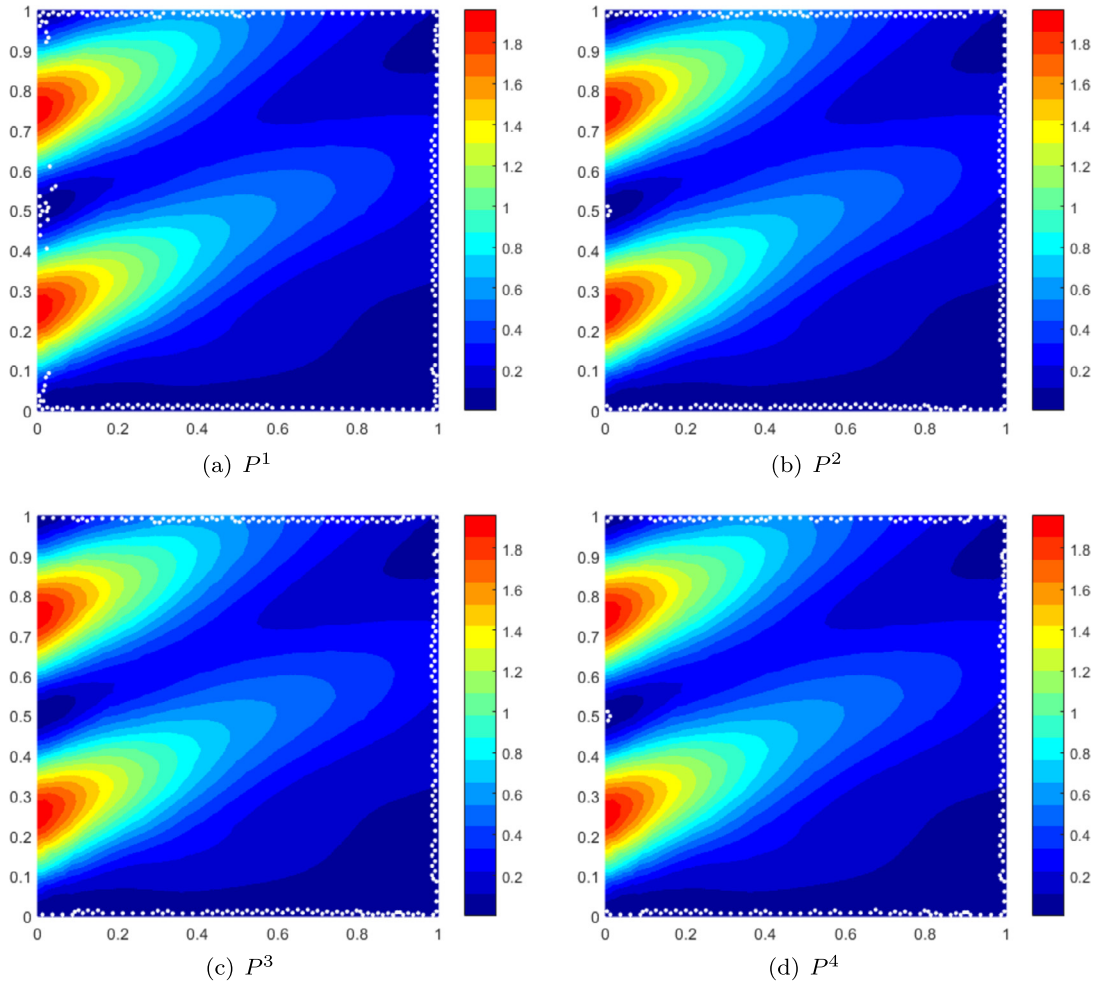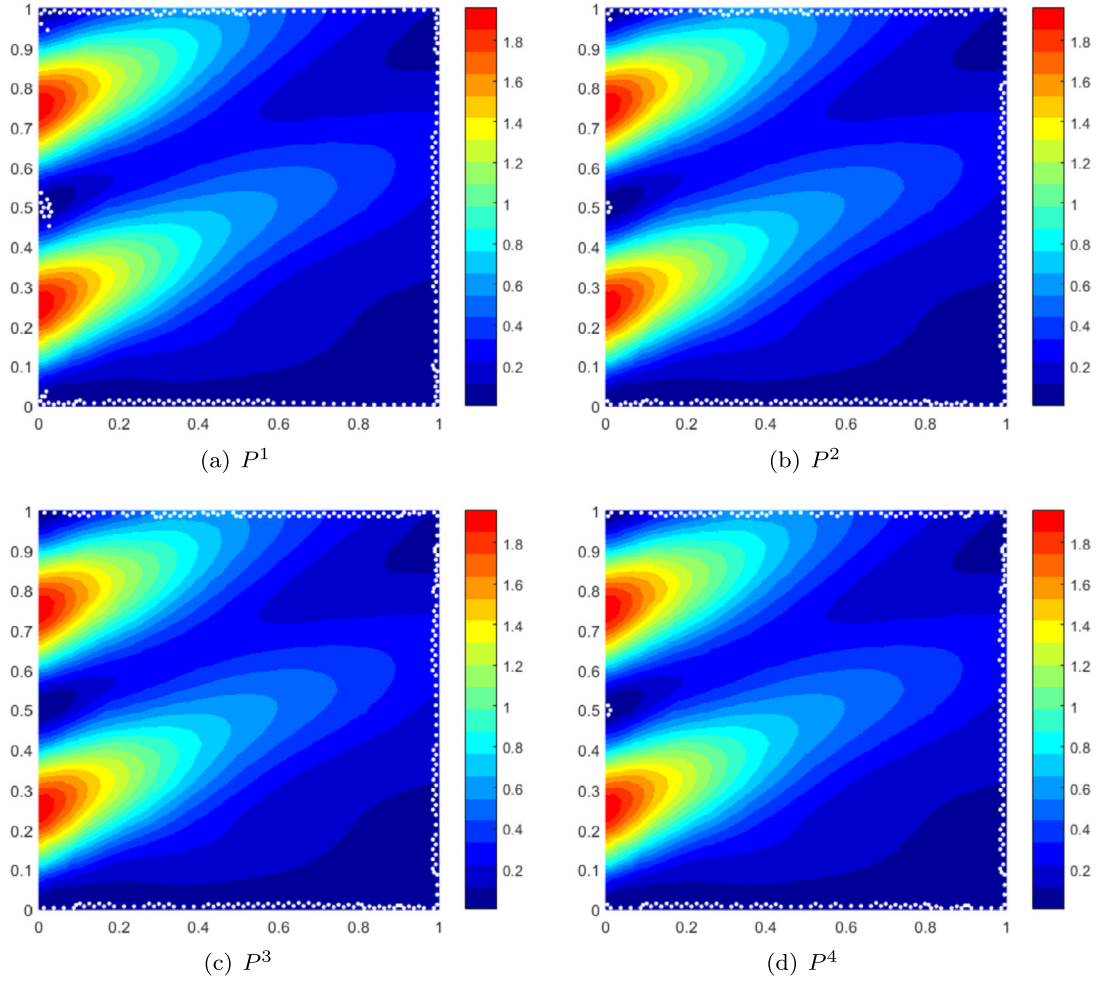(b) P^2

(c) P^3

(d) P^4

Fig. 24. The contours of the radiative intensity in the direction $\Omega = (0.2578, 0.1068)$ for the purely scattering model simulated by the DG schemes with the scaling-limiter-preferred procedure on the mesh size $h = \frac{1}{40}$. The white points represent the cells where the positivity-preserving limiters have been enacted in the computation.

Table 9
Errors of the P^4 DG scheme for the two-dimensional unsteady radiative transfer equation simulating the absorbing-scattering model on triangular meshes.

h	L^1-error	Order	L^∞-error	Order	limiter(%)	c_err
Without positivity-preserving limiter						
1/10	2.085E-07		6.644E-06			
1/20	6.506E-09	5.002	2.070E-07	5.004		
1/40	2.031E-10	5.002	7.217E-09	4.842		
1/80	6.332E-12	5.003	2.379E-10	4.923		
With positivity-preserving limiter (scaling limiter preferred)						
1/10	2.534E-07		9.063E-06		15.38	0.0
1/20	6.692E-09	5.243	2.070E-07	5.452	5.21	0.0
1/40	2.034E-10	5.040	7.217E-09	4.842	2.03	0.0
1/80	6.337E-12	5.004	2.379E-10	4.923	0.57	0.0
With positivity-preserving limiter (rotational limiter preferred)						
1/10	2.452E-07		6.644E-06		15.39	2.401E-08
1/20	6.672E-09	5.200	2.070E-07	5.004	5.21	9.710E-11
1/40	2.033E-10	5.037	7.217E-09	4.842	2.03	1.723E-13
1/80	6.335E-12	5.004	2.379E-10	4.923	0.57	2.567E-15

(a) P^1

(b) P^2

(c) P^3

(d) P^4

Fig. 25. The contours of the radiative intensity in the direction $\Omega = (0.2578, 0.1068)$ for the purely scattering model simulated by the DG schemes with the rotational-limiter-preferred procedure on the mesh size $h = \frac{1}{40}$. The white points represent the cells where the positivity-preserving limiters have been enacted in the computation.

is the other keypoints of this paper. After that, using the two-dimensional scaling positivity-preserving limiter [29] on the triangular element, we obtain the final modified polynomial. Our two-dimensional rotational positivity-preserving limiter is theoretically proved to keep both high order accuracy and positivity on triangular meshes. The numerical experiments for the two-dimensional radiative transfer equations on triangular meshes demonstrate the properties of high order accuracy and positivity-preserving of our schemes. The advantage of the triangular meshes on handling the complex domain is also presented in our numerical examples.

It is worth pointing out that we prefer to use the "scaling limiter preferred" strategy in the practical computations, since the scaling positivity-preserving limiter does not change the cell averages and is relatively simpler to implement, thus the scaling-limiter-preferred procedure produces smaller conservation error and is more efficient.

Appendix A. The Orthogonal basis function over the reference element $\hat{K}$

Assume the reference element $\hat{K}$, the vertices $(\hat{x}, \hat{y})$ in clockwise order to be $\{(0, 1), (1, 0), (0, 0)\}$, then we can define the orthogonal basis functions over $\hat{K}$, let $\hat{u} = \sqrt{2}(\hat{x} - \frac{1}{3})$, $\hat{v} = \sqrt{2}(\hat{y} - \frac{1}{3})$, then

$$b_0(\hat{x}, \hat{y}) = 1,$$
$$b_1(\hat{x}, \hat{y}) = \hat{u},$$
$$b_2(\hat{x}, \hat{y}) = \frac{1}{2}\hat{u} + \hat{v},$$
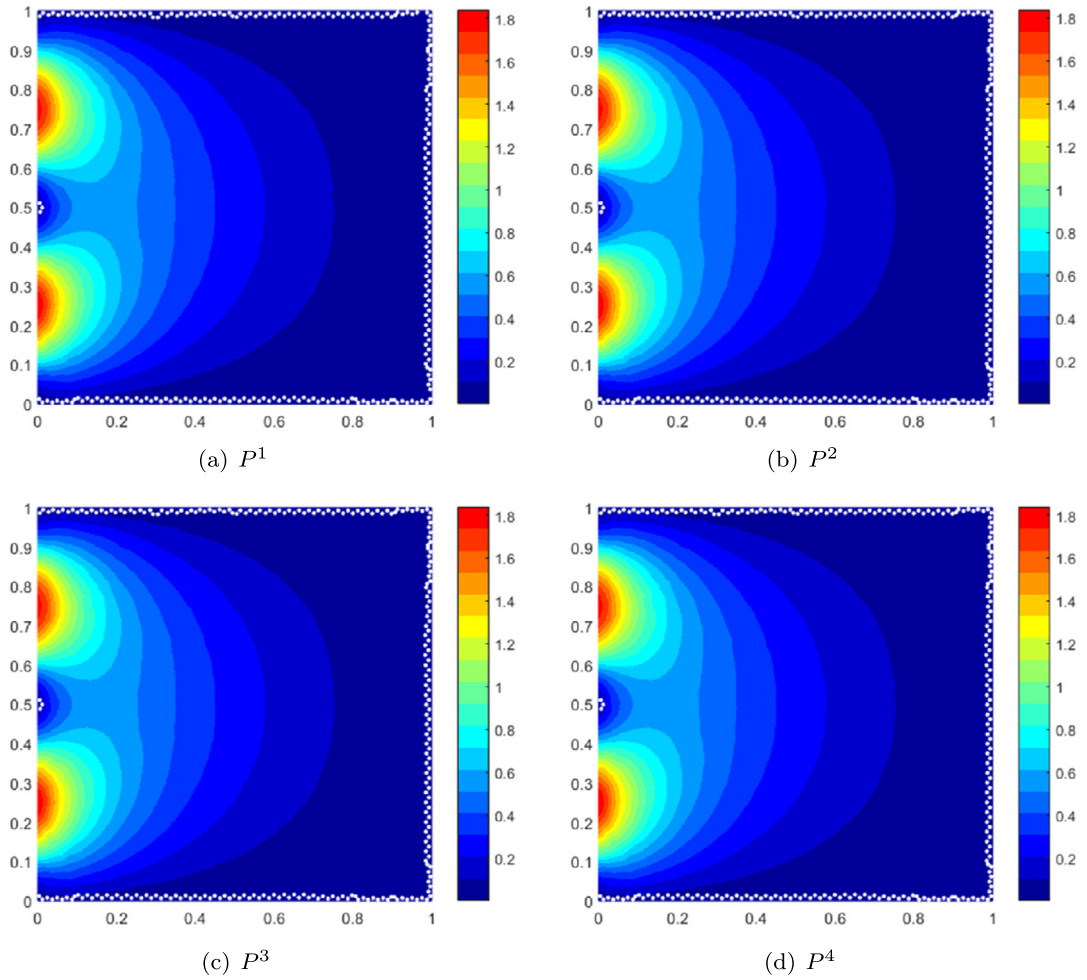$$b_3(\hat{x}, \hat{y}) = \hat{u}^2 - \frac{2\sqrt{2}}{15}\hat{u} - \frac{1}{9},$$

Fig. 26. The contours of the radiative intensity in the direction $\Omega = (0.2578, 0.1068)$ for the optical thick model ($\sigma_t = \sigma_s = 100$) in simulated by the DG schemes with the scaling-limiter-preferred procedure on the mesh size $h = \frac{1}{40}$. The white points represent the cells where the positivity-preserving limiters have been enacted in the computation.

$$b_4(\hat{x}, \hat{y}) = \frac{1}{2}\hat{u}^2 + \hat{u}\hat{v} + \frac{\sqrt{2}}{15}\hat{u} + \frac{2\sqrt{2}}{15}\hat{v},$$

$$b_5(\hat{x}, \hat{y}) = \frac{1}{6}\hat{u}^2 + \hat{v}^2 + \hat{u}\hat{v} + \frac{\sqrt{2}}{9}\hat{u} - \frac{2}{27},$$

$$b_6(\hat{x}, \hat{y}) = \hat{u}^3 - \frac{2\sqrt{2}}{7}\hat{u}^2 - \frac{4}{21}\hat{u} + \frac{16\sqrt{2}}{945},$$

$$b_7(\hat{x}, \hat{y}) = \frac{1}{2}\hat{u}^3 + \hat{u}^2\hat{v} + \frac{\sqrt{2}}{21}\hat{u}^2 + \frac{2\sqrt{2}}{21}\hat{u}\hat{v} - \frac{2}{63}\hat{u} - \frac{4}{63}\hat{v},$$

$$b_8(\hat{x}, \hat{y}) = \frac{1}{6}\hat{u}^3 + \hat{u}^2\hat{v} + \hat{u}\hat{v}^2 + \frac{\sqrt{2}}{7}\hat{u}^2 + \frac{4\sqrt{2}}{21}\hat{v}^2 + \frac{4\sqrt{2}}{21}\hat{u}\hat{v} - \frac{2}{63}\hat{u} - \frac{8\sqrt{2}}{567},$$

$$b_9(\hat{x}, \hat{y}) = \frac{1}{20}\hat{u}^3 + \hat{v}^3 + \frac{3}{5}\hat{u}^2\hat{v} + \frac{3}{2}\hat{u}\hat{v}^2 + \frac{\sqrt{2}}{10}\hat{u}^2 + \frac{\sqrt{2}}{5}\hat{u}\hat{v} - \frac{1}{15}\hat{u} - \frac{2}{15}\hat{v},$$

$$b_{10}(\hat{x}, \hat{y}) = \hat{u}^4 - \frac{4\sqrt{2}}{9}\hat{u}^3 - \frac{2}{9}\hat{u}^2 + \frac{4\sqrt{2}}{63}\hat{u} + \frac{2}{243},$$

$$b_{11}(\hat{x}, \hat{y}) = \frac{1}{2}\hat{u}^4 + \hat{u}^3\hat{v} - \frac{1}{12}\hat{u}^2 - \frac{1}{6}\hat{u}\hat{v} - \frac{\sqrt{2}}{378}\hat{u} - \frac{\sqrt{2}}{189}\hat{v},$$

$$b_{12}(\hat{x}, \hat{y}) = \frac{1}{6}\hat{v}^4 + \hat{u}^3\hat{v} + \hat{u}^2\hat{v}^2 + \frac{4\sqrt{2}}{27}\hat{u}^3 + \frac{2\sqrt{2}}{9}\hat{u}^2\hat{v} + \frac{2\sqrt{2}}{9}\hat{u}\hat{v}^2 - \frac{1}{36}\hat{u}^2 - \frac{1}{54}\hat{v}^2$$
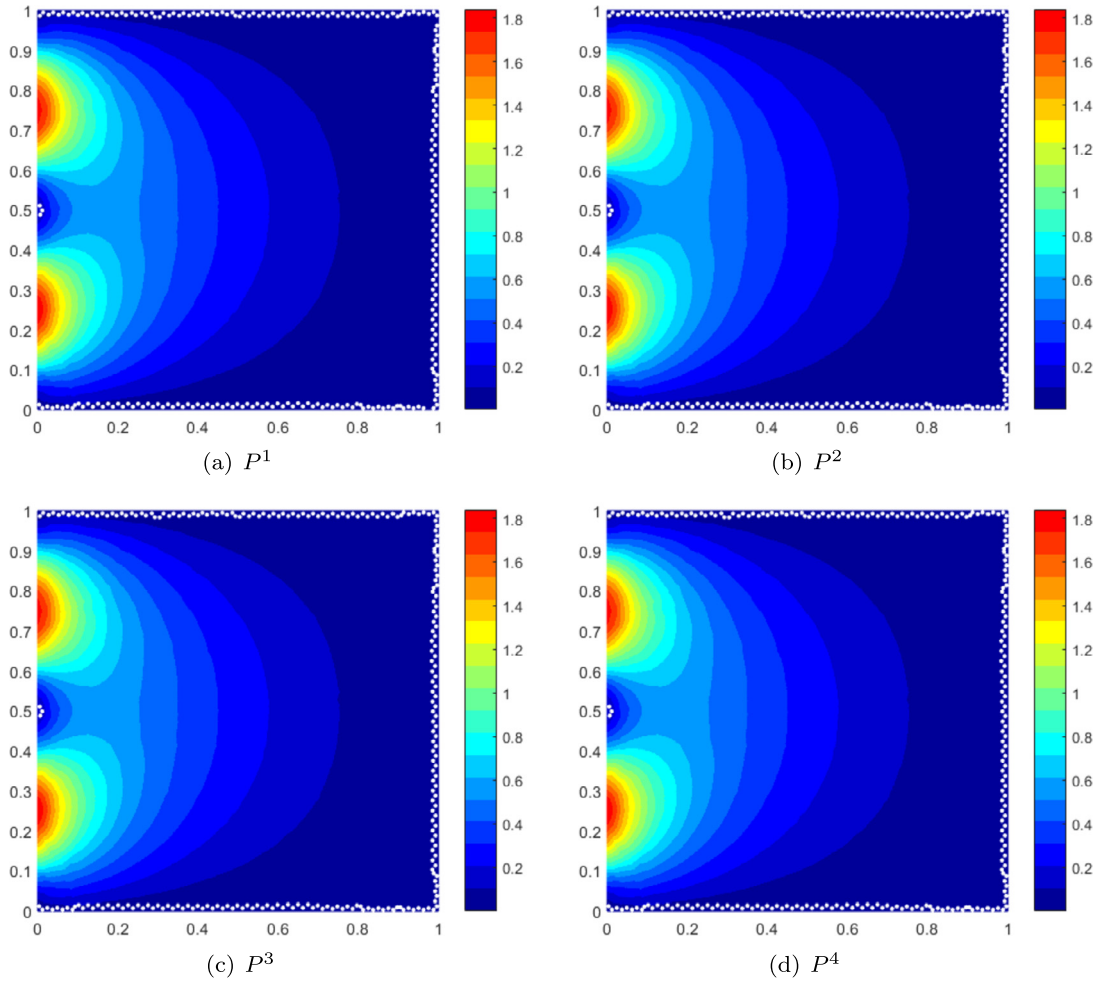
Fig. 27. The contours of the radiative intensity in the direction $\Omega = (0.2578, 0.1068)$ for the optical thick model ($\sigma_t = \sigma_s = 100$) simulated by the DG schemes with the rotational-limiter-preferred procedure on the mesh size $h = \frac{1}{40}$. The white points represent the cells where the positivity-preserving limiters have been enacted in the computation.

$$
-\frac{1}{54}\hat{u}\hat{v} - \frac{\sqrt{2}}{54}\hat{u} + \frac{1}{729},
$$

$$
b_{13}(\hat{x}, \hat{y}) = \frac{1}{20}\hat{u}^4 + \frac{3}{5}\hat{u}^3\hat{v} + \frac{3}{2}\hat{u}^2\hat{v}^2 + \hat{u}\hat{v}^3 + \frac{\sqrt{2}}{9}\hat{u}^3 + \frac{2\sqrt{2}}{9}\hat{v}^3 + \frac{\sqrt{2}}{3}\hat{u}^2\hat{v} + \frac{\sqrt{2}}{3}\hat{u}\hat{v}^2
$$

$$
- \frac{1}{45}\hat{u}^2 - \frac{2}{45}\hat{u}\hat{v} - \frac{2\sqrt{2}}{135}\hat{u} - \frac{4\sqrt{2}}{135}\hat{v},
$$

$$
b_{14}(\hat{x}, \hat{y}) = \frac{1}{70}\hat{u}^4 + \hat{v}^4 + \frac{2}{7}\hat{u}^3\hat{v} + \frac{9}{7}\hat{u}^2\hat{v}^2 + 2\hat{u}\hat{v}^3 + \frac{2\sqrt{2}}{35}\hat{u}^3 + \frac{2\sqrt{2}}{7}\hat{u}^2\hat{v} + \frac{2\sqrt{2}}{7}\hat{u}\hat{v}^2
$$

$$
- \frac{2}{105}\hat{u}^2 - \frac{4}{21}\hat{v}^2 - \frac{4}{21}\hat{u}\hat{v} - \frac{4\sqrt{2}}{315}\hat{u} + \frac{4}{945}.
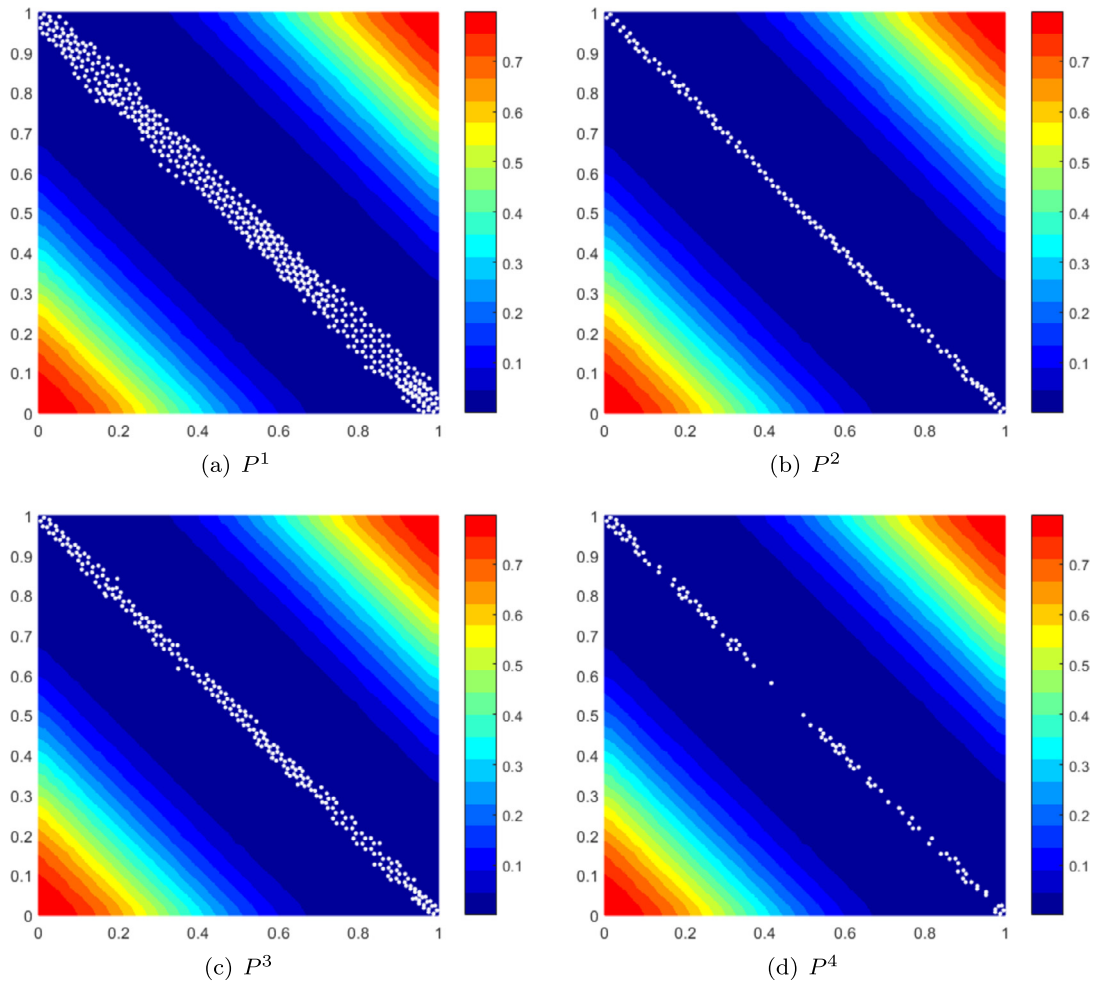$$

Fig. 28. The contours of the radiative intensity in the direction $\Omega = (-0.7860, 0.3255)$ for the absorbing-scattering model simulated by the DG schemes with the scaling-limiter-preferred procedure on the mesh size $h = \frac{1}{40}$. The white points represent the cells where the positivity-preserving limiters have been enacted in the computation.
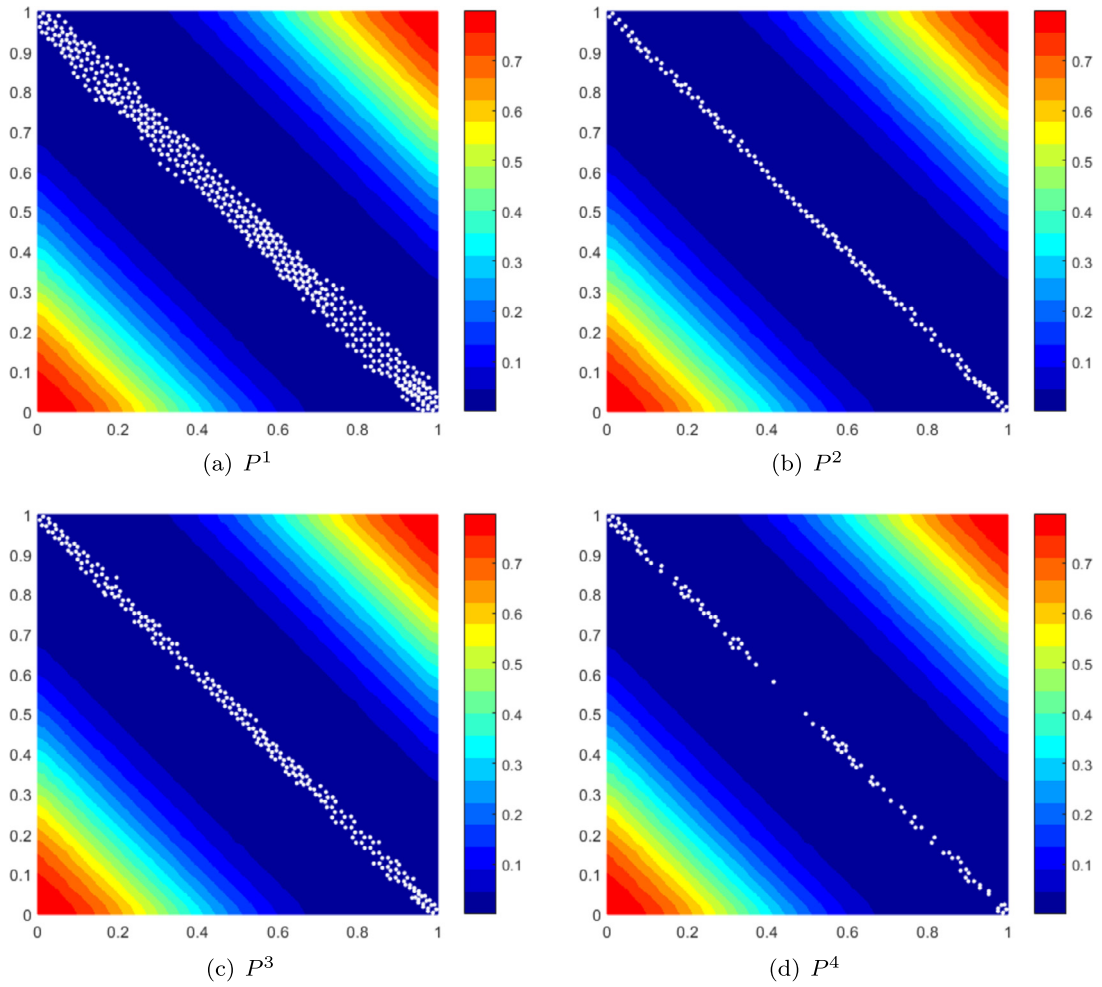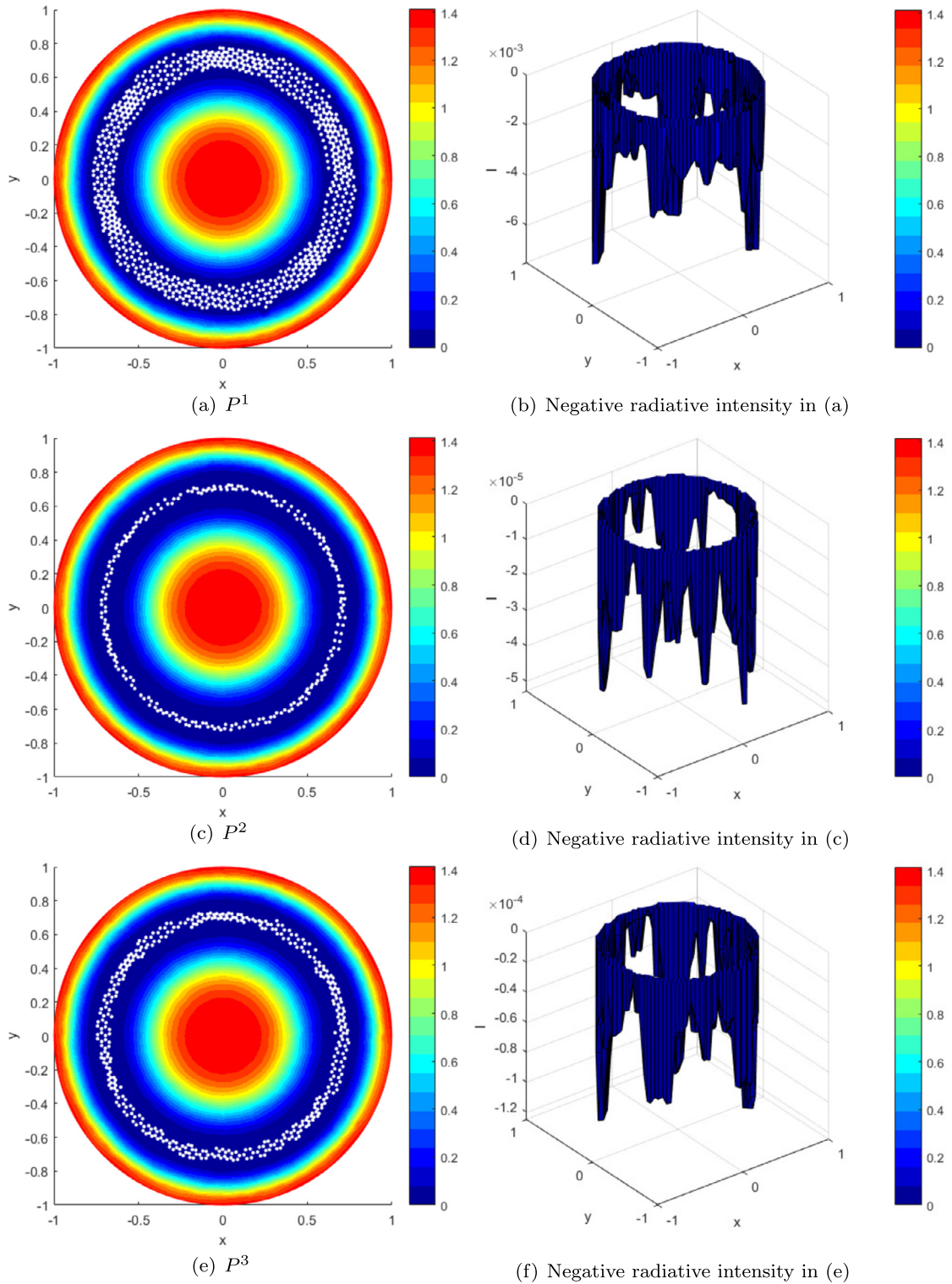
Fig. 29. The contours of the radiative intensity in the direction $\Omega = (-0.7860, 0.3255)$ for the absorbing-scattering model simulated by the DG schemes with the rotational-limiter-preferred procedure on the mesh size $h = \frac{1}{40}$. The white points represent the cells where the positivity-preserving limiters have been enacted in the computation.

(a) P^1

(b) Negative radiative intensity in (a)

(c) P^2

(d) Negative radiative intensity in (c)

(e) P^3

(f) Negative radiative intensity in (e)

Fig. 30. The contours of the radiative intensity for the purely absorbing model simulated by the DG schemes without the positivity-preserving limiters on the mesh size $h = \frac{1}{40}$. The white points represent where the radiative intensity is negative.
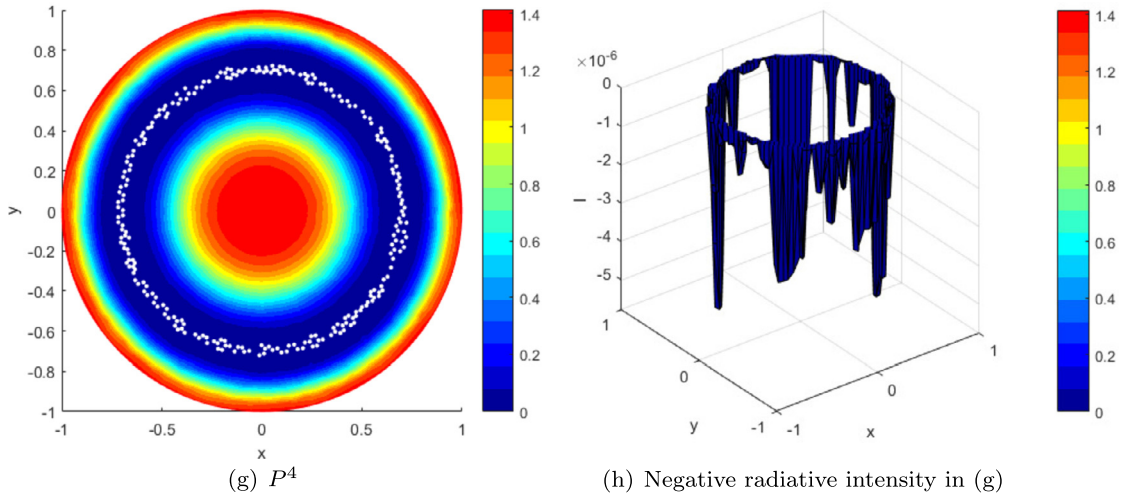
(g) P^4

(h) Negative radiative intensity in (g)

Fig. 30. (*continued*)

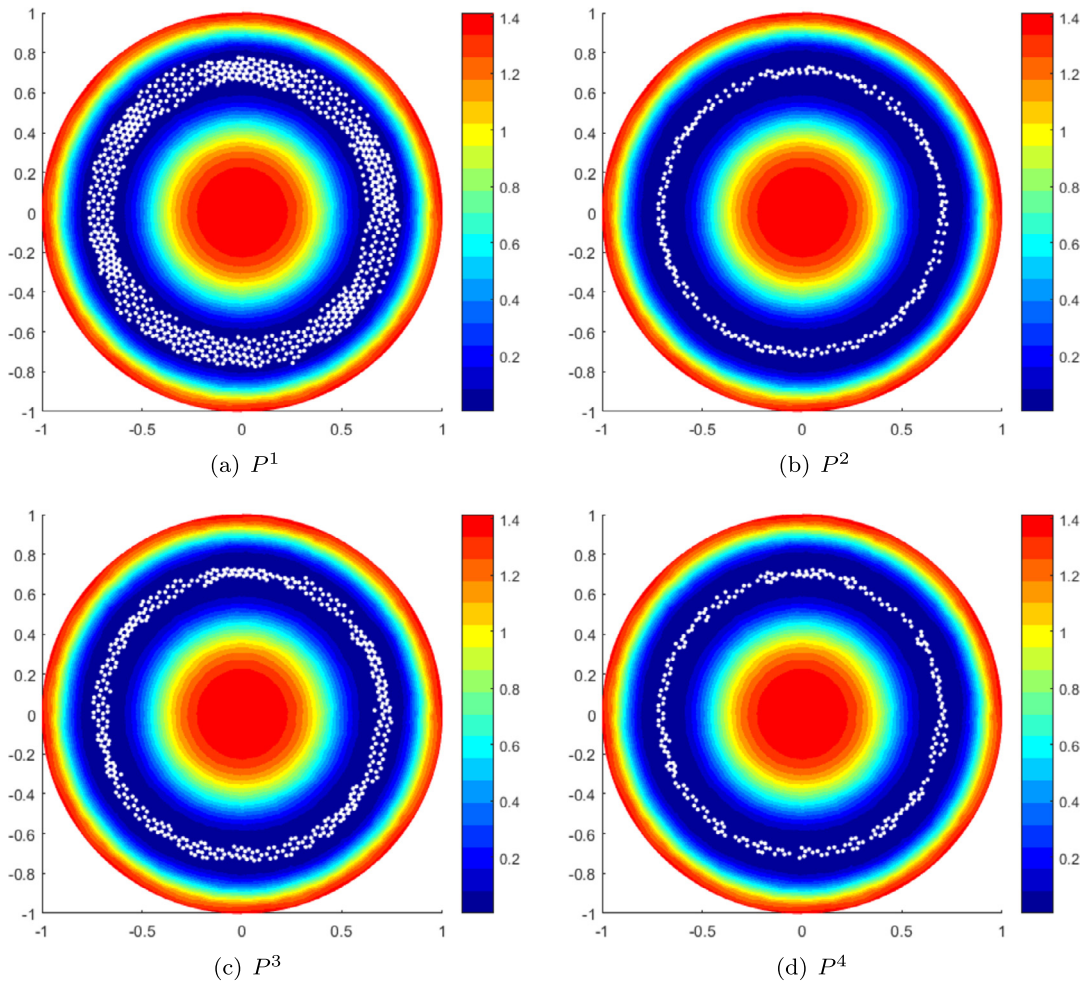(a) P^1

(b) P^2

(c) P^3

(d) P^4

Fig. 31. The contours of the radiative intensity for the purely absorbing model simulated by the DG schemes with the scaling-limiter-preferred procedure on the mesh size $h = \frac{1}{40}$. The white points represent the cells where the positivity-preserving limiters have been enacted.
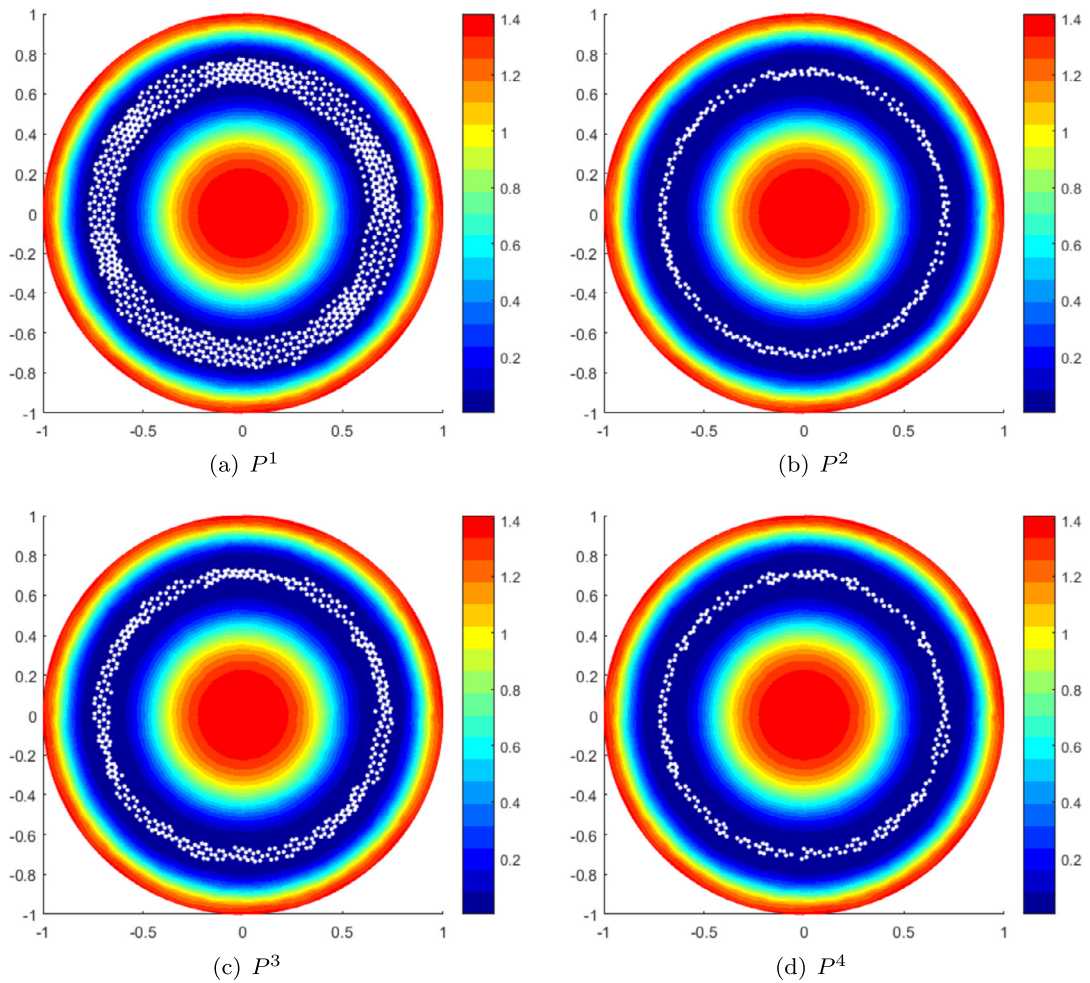
(a) P^1

(b) P^2

(c) P^3

(d) P^4

Fig. 32. The contours of the radiative intensity for the purely absorbing model simulated by the DG schemes with the rotational-limiter-preferred procedure on the mesh size $h = \frac{1}{40}$. The white points represent the cells where the positivity-preserving limiters have been enacted.

Appendix B. The specific quadrature points and the corresponding weights on the reference triangular element $\hat{K}$

Table 10
The quadrature points and corresponding weights for the case of $k = 1, 2$.

α	$(\hat{x}_\alpha, \hat{y}_\alpha)$	w_α	α	$(\hat{x}_\alpha, \hat{y}_\alpha)$	w_α
1	$(0, 0)$	$\frac{1}{27}$	2	$(1, 0)$	$\frac{1}{27}$
3	$(0, 1)$	$\frac{1}{27}$	4	$(\frac{1}{2}, 0)$	$\frac{4}{27}$
5	$(\frac{1}{2}, \frac{1}{2})$	$\frac{4}{27}$	6	$(0, \frac{1}{2})$	$\frac{4}{27}$
7	$(\frac{1}{4}, \frac{1}{2})$	$\frac{4}{27}$	8	$(\frac{1}{2}, \frac{1}{4})$	$\frac{4}{27}$
9	$(\frac{1}{4}, \frac{1}{4})$	$\frac{4}{27}$			

Table 11
The quadrature points and corresponding weights for the case of $k = 3$.

α	$(\hat{x}_\alpha, \hat{y}_\alpha)$	w_α	α	$(\hat{x}_\alpha, \hat{y}_\alpha)$	w_α
1	$(0, 0)$	$\frac{1}{108}$	2	$(1, 0)$	$\frac{1}{108}$
3	$(0, 1)$	$\frac{1}{108}$	4	$(\frac{5-\sqrt{5}}{10}, 0)$	$\frac{5}{108}$
5	$(\frac{5+\sqrt{5}}{10}, 0)$	$\frac{5}{108}$	6	$(\frac{5+\sqrt{5}}{10}, \frac{5-\sqrt{5}}{10})$	$\frac{5}{108}$
7	$(\frac{5-\sqrt{5}}{10}, \frac{5+\sqrt{5}}{10})$	$\frac{5}{108}$	8	$(0, \frac{5+\sqrt{5}}{10})$	$\frac{5}{108}$
9	$(0, \frac{5-\sqrt{5}}{10})$	$\frac{5}{108}$	10	$(\frac{3-\sqrt{5}}{10}, \frac{5+\sqrt{5}}{10})$	$\frac{25-5\sqrt{5}}{432}$
11	$(\frac{1}{5}, \frac{5+\sqrt{5}}{10})$	$\frac{25-5\sqrt{5}}{432}$	12	$(\frac{1}{5}, \frac{5-\sqrt{5}}{10})$	$\frac{25+5\sqrt{5}}{432}$
13	$(\frac{3+\sqrt{5}}{10}, \frac{5-\sqrt{5}}{10})$	$\frac{25+5\sqrt{5}}{432}$	14	$(\frac{5+\sqrt{5}}{10}, \frac{1}{5})$	$\frac{25-5\sqrt{5}}{432}$
15	$(\frac{5+\sqrt{5}}{10}, \frac{3-\sqrt{5}}{10})$	$\frac{25-5\sqrt{5}}{432}$	16	$(\frac{5-\sqrt{5}}{10}, \frac{3+\sqrt{5}}{10})$	$\frac{25+5\sqrt{5}}{432}$
17	$(\frac{5-\sqrt{5}}{10}, \frac{1}{5})$	$\frac{25+5\sqrt{5}}{432}$	18	$(\frac{1}{5}, \frac{3-\sqrt{5}}{10})$	$\frac{25-5\sqrt{5}}{432}$
19	$(\frac{3-\sqrt{5}}{10}, \frac{1}{5})$	$\frac{25-5\sqrt{5}}{432}$	20	$(\frac{3+\sqrt{5}}{10}, \frac{1}{5})$	$\frac{25+5\sqrt{5}}{432}$
21	$(\frac{1}{5}, \frac{3+\sqrt{5}}{10})$	$\frac{25+5\sqrt{5}}{432}$			

Table 12
The quadrature points and corresponding weights for the case of $k = 4$.

α	$(\hat{x}_\alpha, \hat{y}_\alpha)$	w_α	α	$(\hat{x}_\alpha, \hat{y}_\alpha)$	w_α
1	$(0, 0)$	$\frac{1}{300}$	2	$(1, 0)$	$\frac{1}{300}$
3	$(0, 1)$	$\frac{1}{300}$	4	$(\frac{7-\sqrt{21}}{14}, 0)$	$\frac{49}{2700}$
5	$(\frac{1}{2}, 0)$	$\frac{16}{675}$	6	$(\frac{7+\sqrt{21}}{14}, 0)$	$\frac{49}{2700}$
7	$(\frac{7+\sqrt{21}}{14}, \frac{7-\sqrt{21}}{14})$	$\frac{49}{2700}$	8	$(\frac{1}{2}, \frac{1}{2})$	$\frac{16}{675}$
9	$(\frac{7-\sqrt{21}}{14}, \frac{7+\sqrt{21}}{14})$	$\frac{49}{2700}$	10	$(0, \frac{7+\sqrt{21}}{14})$	$\frac{49}{2700}$
11	$(0, \frac{1}{2})$	$\frac{16}{675}$	12	$(0, \frac{7-\sqrt{21}}{14})$	$\frac{49}{2700}$
13	$(\frac{5-\sqrt{21}}{14}, \frac{7+\sqrt{21}}{14})$	$\frac{2401-343\sqrt{21}}{97200}$	14	$(\frac{7-\sqrt{21}}{28}, \frac{7+\sqrt{21}}{14})$	$\frac{196-28\sqrt{21}}{6075}$
15	$(\frac{1}{7}, \frac{7+\sqrt{21}}{14})$	$\frac{2401-343\sqrt{21}}{97200}$	16	$(\frac{7-\sqrt{21}}{28}, \frac{1}{2})$	$\frac{196}{6075}$
17	$(\frac{1}{4}, \frac{1}{2})$	$\frac{256}{6075}$	18	$(\frac{7+\sqrt{21}}{28}, \frac{1}{2})$	$\frac{196}{6075}$
19	$(\frac{1}{7}, \frac{7-\sqrt{21}}{14})$	$\frac{2401+343\sqrt{21}}{97200}$	20	$(\frac{7+\sqrt{21}}{28}, \frac{7-\sqrt{21}}{14})$	$\frac{196+28\sqrt{21}}{6075}$
21	$(\frac{5+\sqrt{21}}{14}, \frac{7-\sqrt{21}}{14})$	$\frac{2401+343\sqrt{21}}{97200}$	22	$(\frac{7+\sqrt{21}}{14}, \frac{1}{7})$	$\frac{2401-343\sqrt{21}}{97200}$
23	$(\frac{7+\sqrt{21}}{14}, \frac{7-\sqrt{21}}{28})$	$\frac{196-28\sqrt{21}}{6075}$	24	$(\frac{7+\sqrt{21}}{14}, \frac{5-\sqrt{21}}{14})$	$\frac{2401-343\sqrt{21}}{97200}$
25	$(\frac{1}{2}, \frac{7+\sqrt{21}}{28})$	$\frac{196}{6075}$	26	$(\frac{1}{2}, \frac{1}{4})$	$\frac{256}{6075}$
27	$(\frac{1}{2}, \frac{7-\sqrt{21}}{28})$	$\frac{196}{6075}$	28	$(\frac{7-\sqrt{21}}{14}, \frac{5+\sqrt{21}}{14})$	$\frac{2401+343\sqrt{21}}{97200}$
29	$(\frac{7-\sqrt{21}}{14}, \frac{7+\sqrt{21}}{28})$	$\frac{196+28\sqrt{21}}{6075}$	30	$(\frac{7-\sqrt{21}}{14}, \frac{1}{7})$	$\frac{2401+343\sqrt{21}}{97200}$
31	$(\frac{1}{7}, \frac{5-\sqrt{21}}{14})$	$\frac{2401-343\sqrt{21}}{97200}$	32	$(\frac{7-\sqrt{21}}{28}, \frac{7-\sqrt{21}}{28})$	$\frac{196-28\sqrt{21}}{6075}$
33	$(\frac{5-\sqrt{21}}{14}, \frac{1}{7})$	$\frac{2401-343\sqrt{21}}{97200}$	34	$(\frac{7+\sqrt{21}}{28}, \frac{7-\sqrt{21}}{28})$	$\frac{196}{6075}$
35	$(\frac{1}{4}, \frac{1}{4})$	$\frac{256}{6075}$	36	$(\frac{7-\sqrt{21}}{28}, \frac{7+\sqrt{21}}{28})$	$\frac{196}{6075}$
37	$(\frac{5+\sqrt{21}}{14}, \frac{1}{7})$	$\frac{2401+343\sqrt{21}}{97200}$	38	$(\frac{7+\sqrt{21}}{28}, \frac{7+\sqrt{21}}{28})$	$\frac{196+28\sqrt{21}}{6075}$
39	$(\frac{1}{7}, \frac{5+\sqrt{21}}{14})$	$\frac{2401+343\sqrt{21}}{97200}$			

Appendix C. The specific $f_\alpha^{(K)}(x, y)$ for the case of P^k

In this appendix, we give the expression of the functions $f_\alpha^{(K)}(x, y)$ for case of P^k on the arbitrary triangular element K. Firstly we give the $f_\alpha(\hat{x}, \hat{y})$ on the reference triangular element $\hat{K}$, then we can get $f_\alpha^{(K)}(x, y)$ by the affine transformation (2.17) and its inverse transformation (2.18) between the reference triangular element $\hat{K}$ and the arbitrary triangular element K.

For $k = 1$:

$$
\begin{aligned}
&f_1(\hat{x}, \hat{y}) = \frac{103}{189} - \frac{16}{21}\hat{x} - \frac{16}{21}\hat{y}, \quad f_2(\hat{x}, \hat{y}) = -\frac{41}{189} + \frac{16}{21}\hat{x}, \quad f_3(\hat{x}, \hat{y}) = -\frac{41}{189} + \frac{16}{21}\hat{y}, \\
&f_4(\hat{x}, \hat{y}) = \frac{52}{189} - \frac{8}{21}\hat{y}, \quad f_5(\hat{x}, \hat{y}) = -\frac{20}{189} + \frac{8}{21}\hat{x} + \frac{8}{21}\hat{y}, \quad f_6(\hat{x}, \hat{y}) = \frac{52}{189} - \frac{8}{21}\hat{x}, \\
&f_7(\hat{x}, \hat{y}) = \frac{16}{189} + \frac{4}{21}\hat{y}, \quad f_8(\hat{x}, \hat{y}) = \frac{16}{189} + \frac{4}{21}\hat{x}, \quad f_9(\hat{x}, \hat{y}) = \frac{52}{189} - \frac{4}{21}\hat{x} - \frac{4}{21}\hat{y}.
\end{aligned}
\tag{C.1}
$$

For $k = 2$:

$$
\begin{aligned}
f_1(\hat{x}, \hat{y}) &= \frac{6496}{3519}\hat{x}^2 + \frac{6496}{3519}\hat{y}^2 + \frac{13840}{3519}\hat{x}\hat{y} - \frac{9964}{3519}\hat{x} - \frac{9964}{3519}\hat{y} + \frac{10363}{10557}, \\
f_2(\hat{x}, \hat{y}) &= \frac{6496}{3519}\hat{x}^2 - \frac{848}{3519}\hat{y}^2 - \frac{848}{3519}\hat{x}\hat{y} - \frac{3028}{3519}\hat{x} + \frac{848}{3519}\hat{y} - \frac{41}{10557}, \\
f_3(\hat{x}, \hat{y}) &= -\frac{848}{3519}\hat{x}^2 + \frac{6496}{3519}\hat{y}^2 - \frac{848}{3519}\hat{x}\hat{y} + \frac{848}{3519}\hat{x} - \frac{3028}{3519}\hat{y} - \frac{41}{10557}, \\
f_4(\hat{x}, \hat{y}) &= -\frac{10448}{3519}\hat{x}^2 + \frac{3016}{3519}\hat{y}^2 - \frac{10448}{3519}\hat{x}\hat{y} + \frac{10448}{3519}\hat{x} - \frac{2914}{3519}\hat{y} + \frac{358}{10557}, \\
f_5(\hat{x}, \hat{y}) &= \frac{1544}{3519}\hat{x}^2 + \frac{1544}{3519}\hat{y}^2 + \frac{15008}{3519}\hat{x}\hat{y} - \frac{1646}{3519}\hat{x} - \frac{1646}{3519}\hat{y} - \frac{440}{10557}, \\
f_6(\hat{x}, \hat{y}) &= \frac{88}{69}\hat{x}^2 - \frac{176}{69}\hat{y}^2 - \frac{176}{69}\hat{x}\hat{y} - \frac{86}{69}\hat{x} + \frac{176}{69}\hat{y} + \frac{86}{621}, \\
f_7(\hat{x}, \hat{y}) &= -\frac{944}{3519}\hat{x}^2 - \frac{3392}{3519}\hat{y}^2 - \frac{944}{3519}\hat{x}\hat{y} + \frac{944}{3519}\hat{x} + \frac{3800}{3519}\hat{y} - \frac{776}{10557}, \\
f_8(\hat{x}, \hat{y}) &= -\frac{3392}{3519}\hat{x}^2 - \frac{944}{3519}\hat{y}^2 - \frac{944}{3519}\hat{x}\hat{y} + \frac{3800}{3519}\hat{x} + \frac{944}{3519}\hat{y} - \frac{776}{10557}, \\
f_9(\hat{x}, \hat{y}) &= -\frac{3392}{3519}\hat{x}^2 - \frac{3392}{3519}\hat{y}^2 - \frac{5840}{3519}\hat{x}\hat{y} + \frac{2984}{3519}\hat{x} + \frac{2984}{3519}\hat{y} + \frac{448}{10557}.
\end{aligned}
\tag{C.2}
$$

For $k = 3$:

$$
\begin{aligned}
f_1(\hat{x}, \hat{y}) = &-\frac{243625}{57357}\hat{x}^3 - \frac{243625}{57357}\hat{y}^3 - \frac{4023677750}{271470681}\hat{x}^2\hat{y} - \frac{4023677750}{271470681}\hat{x}\hat{y}^2 + \frac{265893050}{30163409}\hat{x}^2 \\
&+ \frac{265893050}{30163409}\hat{y}^2 + \frac{5300318825}{271470681}\hat{x}\hat{y} - \frac{1503138790}{271470681}\hat{x} - \frac{1503138790}{271470681}\hat{y} + \frac{264094367}{271470681},
\end{aligned}
$$

$$
\begin{aligned}
f_2(\hat{x}, \hat{y}) = &\frac{243625}{57357}\hat{x}^3 - \frac{564446375}{271470681}\hat{x}^2\hat{y} - \frac{564446375}{271470681}u\hat{y}^2 - \frac{355397975}{90490227}\hat{x}^2 + \frac{5578050}{30163409}\hat{y}^2 \\
&+ \frac{614648825}{271470681}\hat{x}\hat{y} + \frac{176295265}{271470681}\hat{x} - \frac{5578050}{30163409}\hat{y} + \frac{915902}{271470681}
\end{aligned}
$$

$$
\begin{aligned}
f_3(\hat{x}, \hat{y}) = &\frac{243625}{57357}\hat{y}^3 - \frac{564446375}{271470681}\hat{x}^2\hat{y} - \frac{564446375}{271470681}\hat{x}\hat{y}^2 + \frac{5578050}{30163409}\hat{x}^2 - \frac{355397975}{90490227}\hat{y}^2 \\
&+ \frac{614648825}{271470681}\hat{x}\hat{y} - \frac{5578050}{30163409}\hat{x} + \frac{176295265}{271470681}\hat{y} + \frac{915902}{271470681}
\end{aligned}
$$

$$
\begin{aligned}
f_4(\hat{x}, \hat{y}) = &\frac{286325}{108341}\sqrt{5}\hat{x}^3 + \left(-\frac{24250}{19119} - \frac{703100}{975069}\sqrt{5}\right)\hat{y}^3 \\
&+ \left(\frac{3752532875}{542941362} + \frac{858975}{216682}\sqrt{5}\right)\hat{x}^2\hat{y} + \left(\frac{3752532875}{542941362} - \frac{235475}{1950138}\sqrt{5}\right)\hat{x}\hat{y}^2 \\
&+ \left(-\frac{1075798625}{542941362} - \frac{858975}{216682}\sqrt{5}\right)\hat{x}^2 + \left(\frac{465792500}{271470681} + \frac{1191500}{975069}\sqrt{5}\right)\hat{y}^2 \\
&+ \left(-\frac{2414165750}{271470681} - \frac{31375}{19119}\sqrt{5}\right)\hat{x}\hat{y} + \left(\frac{1075798625}{542941362} + \frac{2530141}{1950138}\sqrt{5}\right)\hat{x}
\end{aligned}
$$

$$+ \left(-\frac{130412120}{271470681} - \frac{500096}{975069}\sqrt{5} \right)\hat{y} - \frac{714550}{271470681} + \frac{688}{57357}\sqrt{5}$$

$$f_5(\hat{x},\hat{y}) = -\frac{286325}{108341}\sqrt{5}\hat{x}^3 + \left(-\frac{24250}{19119} + \frac{703100}{975069}\sqrt{5} \right)\hat{y}^3$$
$$+ \left(\frac{3752532875}{542941362} - \frac{858975}{216682}\sqrt{5} \right)\hat{x}^2\hat{y} + \left(\frac{3752532875}{542941362} + \frac{235475}{1950138}\sqrt{5} \right)\hat{x}\hat{y}^2$$
$$+ \left(-\frac{1075798625}{542941362} + \frac{858975}{216682}\sqrt{5} \right)\hat{x}^2 + \left(\frac{465792500}{271470681} - \frac{1191500}{975069}\sqrt{5} \right)\hat{y}^2$$
$$+ \left(-\frac{2414165750}{271470681} + \frac{31375}{19119}\sqrt{5} \right)\hat{x}\hat{y} + \left(\frac{1075798625}{542941362} - \frac{2530141}{1950138}\sqrt{5} \right)\hat{x}$$
$$+ \left(-\frac{130412120}{271470681} + \frac{500096}{975069}\sqrt{5} \right)\hat{y} - \frac{714550}{271470681} - \frac{688}{57357}\sqrt{5},$$

$$f_6(\hat{x},\hat{y}) = \left(\frac{24250}{19119} + \frac{703100}{975069}\sqrt{5} \right)\hat{x}^3 + \left(\frac{24250}{19119} - \frac{703100}{975069}\sqrt{5} \right)\hat{y}^3$$
$$+ \left(\frac{5818487375}{542941362} + \frac{625}{306}\sqrt{5} \right)\hat{x}^2\hat{y} + \left(\frac{5818487375}{542941362} - \frac{625}{306}\sqrt{5} \right)\hat{x}\hat{y}^2$$
$$+ \left(-\frac{567184750}{271470681} - \frac{917800}{975069}\sqrt{5} \right)\hat{x}^2 + \left(-\frac{567184750}{271470681} + \frac{917800}{975069}\sqrt{5} \right)\hat{y}^2$$
$$- \frac{2472736625}{271470681}\hat{x}\hat{y} + \left(\frac{231804370}{271470681} + \frac{226396}{975069}\sqrt{5} \right)\hat{x}$$
$$+ \left(\frac{231804370}{271470681} - \frac{226396}{975069}\sqrt{5} \right)\hat{y} - \frac{9659920}{271470681},$$

$$f_7(\hat{x},\hat{y}) = \left(\frac{24250}{19119} - \frac{703100}{975069}\sqrt{5} \right)\hat{x}^3 + \left(\frac{24250}{19119} + \frac{703100}{975069}\sqrt{5} \right)\hat{y}^3$$
$$+ \left(\frac{5818487375}{542941362} - \frac{625}{306}\sqrt{5} \right)\hat{x}^2\hat{y} + \left(\frac{5818487375}{542941362} + \frac{625}{306}\sqrt{5} \right)\hat{x}\hat{y}^2$$
$$+ \left(-\frac{567184750}{271470681} + \frac{917800}{975069}\sqrt{5} \right)\hat{x}^2 + \left(-\frac{567184750}{271470681} - \frac{917800}{975069}\sqrt{5} \right)\hat{y}^2$$
$$- \frac{2472736625}{271470681}\hat{x}\hat{y} + \left(\frac{231804370}{271470681} - \frac{226396}{975069}\sqrt{5} \right)\hat{x}$$
$$+ \left(\frac{231804370}{271470681} + \frac{226396}{975069}\sqrt{5} \right)\hat{y} - \frac{9659920}{271470681},$$

$$f_8(\hat{x},\hat{y}) = \left(\frac{703100}{975069}\sqrt{5} - \frac{24250}{19119} \right)\hat{x}^3 - \frac{286325}{108341}\sqrt{5}\hat{y}^3$$
$$+ \left(\frac{3752532875}{542941362} + \frac{235475}{1950138}\sqrt{5} \right)\hat{x}^2\hat{y} + \left(\frac{3752532875}{542941362} - \frac{858975}{216682}\sqrt{5} \right)\hat{x}\hat{y}^2$$
$$+ \left(\frac{465792500}{271470681} - \frac{1191500}{975069}\sqrt{5} \right)\hat{x}^2 + \left(-\frac{1075798625}{542941362} + \frac{858975}{216682}\sqrt{5} \right)\hat{y}^2$$
$$+ \left(-\frac{2414165750}{271470681} + \frac{31375}{19119}\sqrt{5} \right)\hat{x}\hat{y} + \left(-\frac{130412120}{271470681} + \frac{500096}{975069}\sqrt{5} \right)\hat{x}$$
$$+ \left(\frac{1075798625}{542941362} - \frac{2530141}{1950138}\sqrt{5} \right)\hat{y} - \frac{714550}{271470681} - \frac{688}{57357}\sqrt{5},$$

$$f_9(\hat{x},\hat{y}) = \left(-\frac{24250}{19119} - \frac{703100}{975069}\sqrt{5} \right)\hat{x}^3 + \frac{286325}{108341}\sqrt{5}\hat{y}^3$$
$$+ \left(\frac{3752532875}{542941362} - \frac{235475}{1950138}\sqrt{5} \right)\hat{x}^2\hat{y} + \left(\frac{3752532875}{542941362} + \frac{858975}{216682}\sqrt{5} \right)\hat{x}\hat{y}^2$$
$$+ \left(\frac{465792500}{271470681} + \frac{1191500}{975069}\sqrt{5} \right)\hat{x}^2 + \left(-\frac{1075798625}{542941362} - \frac{858975}{216682}\sqrt{5} \right)\hat{y}^2$$
$$+ \left(-\frac{2414165750}{271470681} - \frac{31375}{19119}\sqrt{5} \right)\hat{x}\hat{y} + \left(-\frac{130412120}{271470681} - \frac{500096}{975069}\sqrt{5} \right)\hat{x}$$
$$+ \left(\frac{1075798625}{542941362} + \frac{2530141}{1950138}\sqrt{5} \right)\hat{y} - \frac{714550}{271470681} + \frac{688}{57357}\sqrt{5},$$

$$f_{10}(\hat{x}, \hat{y}) = \left(-\frac{659000}{975069} + \frac{433700}{975069}\sqrt{5}\right)\hat{x}^3 + \left(-\frac{246000}{108341} - \frac{890150}{975069}\sqrt{5}\right)\hat{y}^3$$
$$+ \left(-\frac{26023771375}{6153335436} + \frac{9837932975}{6153335436}\sqrt{5}\right)\hat{x}^2\hat{y} + \left(-\frac{41105475875}{6153335436} + \frac{14432094425}{18460006308}\sqrt{5}\right)\hat{x}\hat{y}^2$$
$$+ \left(\frac{9991395275}{9230003154} - \frac{6091102075}{9230003154}\sqrt{5}\right)\hat{x}^2 + \left(\frac{30369090125}{9230003154} + \frac{1152541675}{1025555906}\sqrt{5}\right)\hat{y}^2$$
$$+ \left(\frac{5919692525}{1085882724} - \frac{1711560025}{1085882724}\sqrt{5}\right)\hat{x}\hat{y} + \left(-\frac{1423286965}{3076667718} + \frac{746168779}{3076667718}\sqrt{5}\right)\hat{x}$$
$$+ \left(-\frac{9442745915}{9230003154} - \frac{1836000839}{9230003154}\sqrt{5}\right)\hat{y} + \frac{5121445}{180980454} - \frac{2507473}{542941362}\sqrt{5},$$

$$f_{11}(\hat{x}, \hat{y}) = \left(\frac{659000}{975069} - \frac{433700}{975069}\sqrt{5}\right)\hat{x}^3 + \left(\frac{834875}{975069} - \frac{527225}{975069}\sqrt{5}\right)\hat{y}^3$$
$$+ \left(-\frac{4515861125}{2051111812} + \frac{1627124575}{6153335436}\sqrt{5}\right)\hat{x}^2\hat{y} + \left(\frac{1534121125}{6153335436} + \frac{19963078225}{18460006308}\sqrt{5}\right)\hat{x}\hat{y}^2$$
$$+ \left(-\frac{8722886725}{9230003154} + \frac{6225110525}{9230003154}\sqrt{5}\right)\hat{x}^2 + \left(-\frac{6129041375}{4615001577} + \frac{4424247050}{4615001577}\sqrt{5}\right)\hat{y}^2$$
$$+ \left(\frac{1212724025}{1085882724} - \frac{295919725}{1085882724}\sqrt{5}\right)\hat{x}\hat{y} + \left(\frac{3001352345}{9230003154} - \frac{2372514787}{9230003154}\sqrt{5}\right)\hat{x}$$
$$+ \left(\frac{2420167915}{4615001577} - \frac{1999938188}{4615001577}\sqrt{5}\right)\hat{y} - \frac{5007175}{180980454} + \frac{12363613}{542941362}\sqrt{5},$$

$$f_{12}(\hat{x}, \hat{y}) = \left(\frac{659000}{975069} + \frac{433700}{975069}\sqrt{5}\right)\hat{x}^3 + \left(\frac{834875}{975069} + \frac{527225}{975069}\sqrt{5}\right)\hat{y}^3$$
$$+ \left(-\frac{4515861125}{2051111812} - \frac{1627124575}{6153335436}\sqrt{5}\right)\hat{x}^2\hat{y} + \left(\frac{1534121125}{6153335436} - \frac{19963078225}{18460006308}\sqrt{5}\right)\hat{x}\hat{y}^2$$
$$+ \left(-\frac{8722886725}{9230003154} - \frac{6225110525}{9230003154}\sqrt{5}\right)\hat{x}^2 + \left(-\frac{6129041375}{4615001577} - \frac{4424247050}{4615001577}\sqrt{5}\right)\hat{y}^2$$
$$+ \left(\frac{1212724025}{1085882724} + \frac{295919725}{1085882724}\sqrt{5}\right)\hat{x}\hat{y} + \left(\frac{3001352345}{9230003154} + \frac{2372514787}{9230003154}\sqrt{5}\right)\hat{x}$$
$$+ \left(\frac{2420167915}{4615001577} + \frac{1999938188}{4615001577}\sqrt{5}\right)\hat{y} - \frac{5007175}{180980454} - \frac{12363613}{542941362}\sqrt{5},$$

$$f_{13}(\hat{x}, \hat{y}) = \left(-\frac{659000}{975069} - \frac{433700}{975069}\sqrt{5}\right)\hat{x}^3 + \left(-\frac{246000}{108341} + \frac{890150}{975069}\sqrt{5}\right)\hat{y}^3$$
$$+ \left(-\frac{26023771375}{6153335436} - \frac{9837932975}{6153335436}\sqrt{5}\right)\hat{x}^2\hat{y} + \left(-\frac{41105475875}{6153335436} - \frac{14432094425}{18460006308}\sqrt{5}\right)\hat{x}\hat{y}^2$$
$$+ \left(\frac{9991395275}{9230003154} + \frac{6091102075}{9230003154}\sqrt{5}\right)\hat{x}^2 + \left(\frac{30369090125}{9230003154} - \frac{1152541675}{1025555906}\sqrt{5}\right)\hat{y}^2$$
$$+ \left(\frac{5919692525}{1085882724} + \frac{1711560025}{1085882724}\sqrt{5}\right)\hat{x}\hat{y} + \left(-\frac{1423286965}{3076667718} - \frac{746168779}{3076667718}\sqrt{5}\right)\hat{x}$$
$$+ \left(-\frac{9442745915}{9230003154} + \frac{1836000839}{9230003154}\sqrt{5}\right)\hat{y} + \frac{5121445}{180980454} + \frac{2507473}{542941362}\sqrt{5},$$

$$f_{14}(\hat{x}, \hat{y}) = \left(\frac{834875}{975069} - \frac{527225}{975069}\sqrt{5}\right)\hat{x}^3 + \left(\frac{659000}{975069} - \frac{433700}{975069}\sqrt{5}\right)\hat{y}^3$$
$$+ \left(\frac{1534121125}{6153335436} + \frac{19963078225}{18460006308}\sqrt{5}\right)\hat{x}^2\hat{y} + \left(-\frac{4515861125}{2051111812} + \frac{1627124575}{6153335436}\sqrt{5}\right)\hat{x}\hat{y}^2$$
$$+ \left(-\frac{6129041375}{4615001577} + \frac{4424247050}{4615001577}\sqrt{5}\right)\hat{x}^2 + \left(-\frac{8722886725}{9230003154} + \frac{6225110525}{9230003154}\sqrt{5}\right)\hat{y}^2$$
$$+ \left(\frac{1212724025}{1085882724} - \frac{295919725}{1085882724}\sqrt{5}\right)\hat{x}\hat{y} + \left(\frac{2420167915}{4615001577} - \frac{1999938188}{4615001577}\sqrt{5}\right)\hat{x}$$
$$+ \left(\frac{3001352345}{9230003154} - \frac{2372514787}{9230003154}\sqrt{5}\right)\hat{y} - \frac{5007175}{180980454} + \frac{12363613}{542941362}\sqrt{5},$$

$$f_{15}(\hat{x}, \hat{y}) = \Big(-\frac{246000}{108341} - \frac{890150}{975069}\sqrt{5}\Big)\hat{x}^3 + \Big(-\frac{659000}{975069} + \frac{433700}{975069}\sqrt{5}\Big)\hat{y}^3$$
$$+ \Big(-\frac{41105475875}{6153335436} + \frac{14432094425}{18460006308}\sqrt{5}\Big)\hat{x}^2\hat{y} + \Big(-\frac{26023771375}{6153335436} + \frac{9837932975}{6153335436}\sqrt{5}\Big)\hat{x}\hat{y}^2$$
$$+ \Big(\frac{30369090125}{9230003154} + \frac{1152541675}{1025555906}\sqrt{5}\Big)\hat{x}^2 + \Big(\frac{9991395275}{9230003154} - \frac{6091102075}{9230003154}\sqrt{5}\Big)\hat{y}^2$$
$$+ \Big(\frac{5919692525}{1085882724} - \frac{1711560025}{1085882724}\sqrt{5}\Big)\hat{x}\hat{y} + \Big(-\frac{9442745915}{9230003154} - \frac{1836000839}{9230003154}\sqrt{5}\Big)\hat{x}$$
$$+ \Big(-\frac{1423286965}{3076667718} + \frac{746168779}{3076667718}\sqrt{5}\Big)\hat{y} + \frac{5121445}{180980454} - \frac{2507473}{542941362}\sqrt{5},$$

$$f_{16}(\hat{x}, \hat{y}) = \Big(-\frac{246000}{108341} + \frac{890150}{975069}\sqrt{5}\Big)\hat{x}^3 + \Big(-\frac{659000}{975069} - \frac{433700}{975069}\sqrt{5}\Big)\hat{y}^3$$
$$+ \Big(-\frac{41105475875}{6153335436} - \frac{14432094425}{18460006308}\sqrt{5}\Big)\hat{x}^2\hat{y} + \Big(-\frac{26023771375}{6153335436} - \frac{9837932975}{6153335436}\sqrt{5}\Big)\hat{x}\hat{y}^2$$
$$+ \Big(\frac{30369090125}{9230003154} - \frac{1152541675}{1025555906}\sqrt{5}\Big)\hat{x}^2 + \Big(\frac{9991395275}{9230003154} + \frac{6091102075}{9230003154}\sqrt{5}\Big)\hat{y}^2$$
$$+ \Big(\frac{5919692525}{1085882724} + \frac{1711560025}{1085882724}\sqrt{5}\Big)\hat{x}\hat{y} + \Big(-\frac{9442745915}{9230003154} + \frac{1836000839}{9230003154}\sqrt{5}\Big)\hat{x}$$
$$+ \Big(-\frac{1423286965}{3076667718} - \frac{746168779}{3076667718}\sqrt{5}\Big)\hat{y} + \frac{5121445}{180980454} + \frac{2507473}{542941362}\sqrt{5},$$

$$f_{17}(\hat{x}, \hat{y}) = \Big(\frac{834875}{975069} + \frac{527225\sqrt{5}}{975069}\Big)\hat{x}^3 + \Big(\frac{659000}{975069} + \frac{433700\sqrt{5}}{975069}\Big)\hat{y}^3$$
$$+ \Big(\frac{1534121125}{6153335436} - \frac{19963078225\sqrt{5}}{18460006308}\Big)\hat{x}^2\hat{y} + \Big(-\frac{4515861125}{2051111812} - \frac{1627124575\sqrt{5}}{6153335436}\Big)\hat{x}\hat{y}^2$$
$$+ \Big(-\frac{6129041375}{4615001577} - \frac{4424247050\sqrt{5}}{4615001577}\Big)\hat{x}^2 + \Big(-\frac{8722886725}{9230003154} - \frac{6225110525\sqrt{5}}{9230003154}\Big)\hat{y}^2$$
$$+ \Big(\frac{1212724025}{1085882724} + \frac{295919725\sqrt{5}}{1085882724}\Big)\hat{x}\hat{y} + \Big(\frac{2420167915}{4615001577} + \frac{1999938188\sqrt{5}}{4615001577}\Big)\hat{x}$$
$$+ \Big(\frac{3001352345}{9230003154} + \frac{2372514787\sqrt{5}}{9230003154}\Big)\hat{y} - \frac{5007175}{180980454} - \frac{12363613\sqrt{5}}{542941362},$$

$$f_{18}(\hat{x}, \hat{y}) = \Big(\frac{246000}{108341} + \frac{890150}{975069}\sqrt{5}\Big)\hat{x}^3 + \Big(-\frac{834875}{975069} + \frac{527225}{975069}\sqrt{5}\Big)\hat{y}^3$$
$$+ \Big(-\frac{5725637125}{9230003154} + \frac{11294215325}{3076667718}\sqrt{5}\Big)\hat{x}^2\hat{y} + \Big(-\frac{26341793725}{9230003154} + \frac{28348193875}{9230003154}\sqrt{5}\Big)\hat{x}\hat{y}^2$$
$$+ \Big(-\frac{3777085625}{1025555906} - \frac{14607666875}{9230003154}\sqrt{5}\Big)\hat{x}^2 + \Big(\frac{553389375}{512777953} - \frac{2912851850}{4615001577}\sqrt{5}\Big)\hat{y}^2$$
$$+ \Big(\frac{790693175}{542941362} - \frac{1810895575}{542941362}\sqrt{5}\Big)\hat{x}\hat{y} + \Big(\frac{4355808805}{3076667718} + \frac{6070792639}{9230003154}\sqrt{5}\Big)\hat{x}$$
$$+ \Big(-\frac{1271630915}{4615001577} + \frac{488542988}{4615001577}\sqrt{5}\Big)\hat{y} + \frac{8113495}{271470681} + \frac{1731715}{271470681}\sqrt{5}$$

$$f_{19}(\hat{x}, \hat{y}) = \Big(-\frac{834875}{975069} + \frac{527225}{975069}\sqrt{5}\Big)\hat{x}^3 + \Big(\frac{246000}{108341} + \frac{890150}{975069}\sqrt{5}\Big)\hat{y}^3,$$
$$+ \Big(-\frac{7233501625}{4615001577} + \frac{3927592600}{1538333859}\sqrt{5}\Big)\hat{x}^2\hat{y} + \Big(\frac{4077776750}{4615001577} + \frac{15553203925}{4615001577}\sqrt{5}\Big)\hat{x}\hat{y}^2$$
$$+ \Big(\frac{6470193125}{4615001577} - \frac{356754400}{512777953}\sqrt{5}\Big)\hat{x}^2 + \Big(-\frac{31014393125}{9230003154} - \frac{15203542375}{9230003154}\sqrt{5}\Big)\hat{y}^2$$
$$+ \Big(\frac{24901675}{90490227} - \frac{280439825}{90490227}\sqrt{5}\Big)\hat{x}\hat{y} + \Big(-\frac{2761319665}{4615001577} + \frac{262160246}{1538333859}\sqrt{5}\Big)\hat{x}$$
$$+ \Big(\frac{10088048915}{9230003154} + \frac{2222222713}{3076667718}\sqrt{5}\Big)\hat{y} + \frac{5404970}{271470681} + \frac{2273420}{271470681}\sqrt{5}$$

$$f_{20}(\hat{x},\hat{y}) = \left(-\frac{834875}{975069} - \frac{527225}{975069}\sqrt{5}\right)\hat{x}^3 + \left(\frac{246000}{108341} - \frac{890150}{975069}\sqrt{5}\right)\hat{y}^3$$

$$+\left(-\frac{4757244125}{2051111812} - \frac{49907349325}{18460006308}\sqrt{5}\right)\hat{x}^2\hat{y} + \left(\frac{809972125}{6153335436} - \frac{64989053825}{18460006308}\sqrt{5}\right)\hat{x}\hat{y}^2$$

$$+\left(\frac{5725348750}{4615001577} + \frac{3061820725}{4615001577}\sqrt{5}\right)\hat{x}^2 + \left(-\frac{32504081875}{9230003154} + \frac{4968534875}{3076667718}\sqrt{5}\right)\hat{y}^2$$

$$+\left(\frac{940103225}{1085882724} + \frac{3493534525}{1085882724}\sqrt{5}\right)\hat{x}\hat{y} + \left(-\frac{224052810}{512777953} - \frac{637511863}{4615001577}\sqrt{5}\right)\hat{x}$$

$$+\left(\frac{11577737665}{9230003154} - \frac{6368730389}{9230003154}\sqrt{5}\right)\hat{y} + \frac{4506155}{180980454} - \frac{445015}{60326818}\sqrt{5},$$

$$f_{21}(\hat{x},\hat{y}) = \left(\frac{246000}{108341} - \frac{890150\sqrt{5}}{975069}\right)\hat{x}^3 + \left(-\frac{834875}{975069} - \frac{527225\sqrt{5}}{975069}\right)\hat{y}^3$$

$$+\left(\frac{809972125}{6153335436} - \frac{64989053825\sqrt{5}}{18460006308}\right)\hat{x}^2\hat{y} + \left(-\frac{4757244125}{2051111812} - \frac{49907349325\sqrt{5}}{18460006308}\right)\hat{x}\hat{y}^2$$

$$+\left(-\frac{32504081875}{9230003154} + \frac{4968534875\sqrt{5}}{3076667718}\right)\hat{x}^2 + \left(\frac{5725348750}{4615001577} + \frac{3061820725\sqrt{5}}{4615001577}\right)\hat{y}^2$$

$$+\left(\frac{940103225}{1085882724} + \frac{3493534525\sqrt{5}}{1085882724}\right)\hat{x}\hat{y} + \left(\frac{11577737665}{9230003154} - \frac{6368730389\sqrt{5}}{9230003154}\right)\hat{x}$$

$$+\left(-\frac{224052810}{512777953} - \frac{637511863\sqrt{5}}{4615001577}\right)\hat{y} + \frac{4506155}{180980454} - \frac{445015\sqrt{5}}{60326818}.$$

Because the expression is too tedious for case of $k = 4$, we are not going to list it here.

References

[1] B. Cockburn, C.-W. Shu, TVB Runge-Kutta local projection discontinuous Galerkin finite element method for conservation laws II: general framework, Math. Comput. 52 (1989) 411–435.

[2] B. Cockburn, S.-Y. Lin, C.-W. Shu, TVB Runge-Kutta local projection discontinuous Galerkin finite element method for conservation laws III: one dimensional systems, J. Comput. Phys. 84 (1989) 90–113.

[3] B. Cockburn, S. Hou, C.-W. Shu, The Runge-Kutta local projection discontinuous Galerkin finite element method for conservation laws IV: the multidimensional case, Math. Comput. 54 (1990) 545–581.

[4] B. Cockburn, C.-W. Shu, The Runge-Kutta discontinuous Galerkin method for conservation laws V: multidimensional systems, J. Comput. Phys. 141 (1998) 199–224.

[5] S. Chandrasekhar, Radiative Transfer, Clarendon Press, Oxford, 1950.

[6] J.C. Chai, S.V. Patankar, H.S. Lee, Evaluation of spatial differencing practices for the discrete-ordinates method, J. Thermophys. Heat Transf. 8 (1994) 140–144.

[7] G. Colomer, R. Borrell, F.X. Trias, I. Rodriguez, Parallel algorithms for Sn transport sweeps on unstructured meshes, J. Comput. Phys. 232 (2013) 118–135.

[8] E.M. Gelbard, Simplifed Spherical Harmonics Equations and Their Use in Shielding Problems, Technical Report WAPD-T-1182, Bettis Atomic Power Laboratory, 1961.

[9] J.R. Howell, M. Perlmutter, Monte Carlo solution of thermal transfer through radiant media between gray walls, J. Heat Transf. 86 (1964) 116–122.

[10] A.S. Jamaluddin, P.J. Smith, Predicting radiative heat transfer in rectangular enclosures using the discrete-ordinate method, Combust. Sci. Technol. 59 (1988) 321–340.

[11] M. Krook, On the solution of equations of transfer, Astrophys. J. 122 (1955) 488.

[12] P. LeSaint, P.-A. Raviart, On a finite element method for solving the neutron transport equation, in: C. de Boor (Ed.), Mathematical Aspects of Finite Elements in Partial Differential Equations, Academic Press, New York, 1974, pp. 89–123.

[13] D. Ling, J. Cheng, C.-W. Shu, Conservative high order positivity-preserving discontinuous Galerkin methods for linear hyperbolic and radiative transfer equations, J. Sci. Comput. 77 (2018) 1801–1831.

[14] E.E. Lewis, W.F. Miller Jr., Computational Methods of Neutron Transport, Wiley Interscience, New York, 1984.

[15] E.W. Larsen, R.E. Alcouffe, The linear characteristic method for spatially discretizing the discrete-ordinates equations in (x, y)-geometry, in: Proceedings of the ANS/ENS Joint Topical Meeting, Mathematical Methods in Nuclear Engineering, Munich, FRG, 1981.

[16] K.D. Lathrop, Spatial differencing of the transport equation: positivity vs. accuracy, J. Comput. Phys. 4 (1969) 475–498.

[17] P.G. Maginot, J.E. Morel, J.C. Ragusa, A non-negative moment-preserving spatial discretization scheme for the linearized Boltzmann transport equation in 1-D and 2-D Cartesian geometries, J. Comput. Phys. 231 (2012) 6801–6826.

[18] K.A. Mathews, Adaptive characteristic spatial quadratures for discrete ordinates neutral particle transport-the slab geometry case, Transp. Theory Stat. Phys. 19 (1990) 419–458.

[19] N.K. Madsen, Convergent centered difference schemes for the discrete ordinate neutron transport equations, SIAM J. Numer. Anal. 12 (1975) 164–176.

[20] M.F. Modest, Radiative Heat Transfer, McGraw-Hill, New York, 1993.

[21] G.C. Pomraning, The Equations of Radiation Hydrodynamics, 1973.

[22] W.H. Reed, T.R. Hill, Triangular Mesh Methods for the Neutron Transport Equation, Report LA-UR-73-479, Los Alamos Scientific Laboratory, Los Alamos, NM, 1973.

[23] G.D. Raithby, E.H. Chui, A finite volume method for predicting radiant heat transfer in enclosures with participating media, J. Heat Transf. 112 (1990) 415–423.

[24] M.M. Razzaque, D.E. Klein, J.R. Howell, Finite element solution of radiative heat transfer in a two-dimensional rectangular enclosure with gray participating media, J. Heat Transf. 105 (1983) 933–936.

[25] T.A. Wareing, An exponential discontinuous scheme for discrete-ordinate calculations in Cartesian geometries, in: Proceedings of the Joint International Conference on Mathematical Methods and Supercomputing for Nuclear Applications, Saratoga Springs, NY, 1997.

[26] D. Yuan, J. Cheng, C.-W. Shu, High order positivity-preserving discontinuous Galerkin methods for radiative transfer equations, SIAM J. Sci. Comput. 38 (2016) A2987–A3019.

[27] X. Zhang, C.-W. Shu, On maximum-principle-satisfying high order schemes for scalar conservation laws, J. Comput. Phys. 229 (2010) 3091–3120.

[28] X. Zhang, C.-W. Shu, On positivity preserving high order discontinuous Galerkin methods for compressible Euler equations on rectangular meshes, J. Comput. Phys. 229 (2010) 8918–8934.

[29] X. Zhang, Y. Xia, C.-W. Shu, Maximum-principle-satisfying and positivity-preserving high order discontinuous Galerkin schemes for conservation laws on triangular meshes, J. Sci. Comput. 50 (2012) 29–62.

[30] J. Zhao, L. Liu, Least-squares spectral element method for radiative heat transfer in semitransparent media, Numer. Heat Transf., Part A, Appl. 50 (2006) 473–489.

[31] J. Zhu, J. Qiu, C.-W. Shu, M. Dumbser, Runge-Kutta discontinuous Galerkin method using WENO limiters II: unstructured meshes, J. Comput. Phys. 227 (2008) 4330–4353.

[32] J. Zhu, J. Qiu, Hermite WENO schemes and their application as limiters for Runge-Kutta discontinuous Galerkin method III: unstructured meshes, J. Sci. Comput. 39 (2009) 293–321.